Physics – Uspekhi **56** (4) 347 – 394 (2013)

REVIEWS OF TOPICAL PROBLEMS PACS numbers: 52.20.Dq, 52.40.Kh, **94.05. – a**

Quasiadiabatic dynamics of charged particles in a space plasma

L M Zelenyi, A I Neishtadt, A V Artemyev, D L Vainchtein, H V Malova

DOI: 10.3367/UFNe.0183.201304b.0365

Contents

L M Zelenyi
Space Research Institute, Russian Academy of Sciences,
ul. Profsoyuznaya 83/32, 117997 Moscow, Russian Federation
E-mail: lzelenyi@iki.rssi.ru
Moscow Institute of Physics and Technology (State University)
Institutskii per. 9, 141700 Dolgoprudnyi, Moscow region,
Russian Federation
A I Neishtadt
Space Research Institute, Russian Academy of Sciences,
ul. Profsoyuznaya 83/32, 117997 Moscow, Russian Federation
E-mail: aneishta@iki.rssi.ru
Department of Mathematical Sciences, Loughborough University,
Loughborough, Leicestershire, LE11 3TU, UK
A V Artemyev Space Research Institute, Russian Academy of Sciences,
ul. Profsoyuznaya 83/32, 117997 Moscow, Russian Federation
E-mail: ante0226@gmail.com
D L Vainchtein
Space Research Institute, Russian Academy of Sciences,
ul. Profsoyuznaya 83/32, 117997 Moscow, Russian Federation;
Department of Mechanical Engineering, Temple University,
1947 N. 12th St, Philadelphia, PA 19122, USA
E-mail: dmitri@temple.edu
H V Malova
Space Research Institute, Russian Academy of Sciences,
ul. Profsoyuznaya 83/32, 117997 Moscow, Russian Federation;
Skobel'tsyn Institute of Nuclear Physics,
Lomonosov Moscow State University,
Leninskie gory 1, str. 2, 119991 Moscow, Russian Frderation

Received 5 May 2012
Uspekhi Fizicheskikh Nauk **183** (4) 365 – 415 (2013)
DOI: 10.3367/UFNr.0183.201304b.0365
Translated by G Pontecorvo; edited by A M Semikhatov

Abstract. In many space plasma systems, especially when the magnetic field is weak, characteristic scales of the magnetic field inhomogeneity are much smaller than the Larmor radius of the ions. Over the last two decades, quasiadiabatic models of the dynamics of charged particles in such systems have been actively developed. In this paper, we systematically review the quasiadiabatic approximation and illustrate how it can be used to describe various phenomena in Earth's magnetosphere and to explain many effects observed by satellites.

Seek not the unity in the totality
but rather segregation in uniformity
Koz'ma Prutkov

1. Introduction

The theory of adiabatic invariants has a long history (the original work, published by Paul Ehrenfest in 1910–1920, is collected in book [1] (see also the article ''On one of Boltzmann's mechanical theorems and its relationship with the theory of quanta'' in [2, p. 51])).

In the classic textbook by Landau and Lifshitz, *Mechanics* [3], adiabatic invariants are introduced for systems characterized by fast and slow time scales. In solving such a problem, a small parameter emerges, which immediately permits obtaining a simplified solution by the introduction of a quantity that is nearly conserved, namely, an adiabatic invariant representing the action integral over the fast variables, with the slow variables 'frozen'.

Adiabatic theories are used in solving many problems in physics and mechanics, but in this review we concentrate on the dynamics of charged particles in magnetic fields of complex geometry (for simplicity, we restrict ourselves to considering nonrelativistic theory). The issue of energetic charged particles moving in the magnetic field of Earth's dipole was considered in detail by Störmer [4] in order to explain penetration into Earth's atmosphere of cosmic rays accelerated by the Sun or other stars of our Galaxy. No general solution of this problem has yet been found, but many important particular solutions have been successfully constructed.

In the 1930s, the future Nobel prize winner Hans Alfvén set about to solve the problem, as applied to cosmic physics issues, of electrons and ions moving in inhomogeneous magnetic fields. He constructed an approximate theory of the motion of charged particles in a dipole magnetic field based on three adiabatic invariants that he introduced, which corresponded to three different-scale periods of the motion of charged particles (see Ref. [5] and the references to original work in book [6] and review [7]).

The first invariant coincides precisely with the particle magnetic moment. This invariant corresponds to the rapid periodic rotation of a particle about the magnetic field vector. We note that the proof that this quantity is conserved and is indeed an invariant of motion was obtained independently of Alfvén by Bogoliubov and Zubarev (see Ref. [8] and the references to original work presented in book [9]).

The second invariant, $\oint v_{\|}\,\mathrm{d}r_{\|}$, corresponds to averaging over periodic longitudinal oscillations of a particle between two magnetic mirrors (here, $v_{\|}$ and $r_{\|}$ are the velocity and coordinate components parallel to the magnetic field). The third invariant, $\oint v_{\varphi}\,\mathrm{d}\varphi$, corresponds to averaging over the azimuthal drift of particles around Earth.

For each of these invariants to be conserved, conditions must be satisfied restricting variations of the magnetic field in time and space. The characteristic period of quasiperiodic motions must be much smaller than the characteristic time of magnetic field variations, while the scale of magnetic field variations in space must be much larger than the spatial scale related to periodic motion.

The 1950s turned out to be a 'golden age' for the development of the theory of charged particle motion in magnetic fields. This was due to two events: the discovery of Earth's radiation belts by Van Allen [10] and Vernov [11] and the beginning of work on controlled nuclear fusion, i.e., on magnetic confinement of hot collisionless plasma. Several groups in the USSR and the USA were simultaneously involved in the development of the theory. 'Thermonuclear' work turned out to have much in common with work in space physics. By the mid-1960s, construction of the theory of charged particle motion in laboratory and space conditions was, on the whole, completed (reviews written in those times on problems of particle dynamics can be found in books [12, 13]). An important role in developing this theory in the USSR was played by groups at the Kurchatov Institute, the Institute of Nuclear Physics of the Siberian Branch of the Academy of Sciences, and the Skobel'tsyn Institute of Nuclear Physics of Moscow State University (SINP MSU).

Besides constructing theories of the motion of charged particles based on the conservation of adiabatic invariants, it was also very important to reveal the physical consequences of the violation of such conservation, i.e., of the violation of adiabaticity. Here, once again, an essential role was played by the Soviet plasma school (see reviews Refs [14, 15]). It turned out that adiabatic invariants are conserved with exponential precision in a small parameter, which ensures reliability in using adiabatic invariants for integrating equations of charged particle motion in slowly varying magnetic fields with large spatial inhomogeneity scales. Violation of the conservation of adiabatic invariants results in particle diffusion in the velocity space. As a rule, this process turns out to be weaker than diffusion caused by the scattering of particles on fluctuations of the electromagnetic field, which are excited in plasma because the system is not in thermodynamic equilibrium. In such cases, collective effects dominate over single-particle ones.

The theories mentioned above have become classical; they are expounded in a number of monographs [12, 13, 16] and are relevant to the case of charged particles moving in quite a strong magnetic field, when the spatial scales of its variations are much greater than the spatial scales of quasiperiodic particle motions. But, as it turned out, another, entirely opposite case is possible. In 1965, the 'tail' of Earth's magnetosphere was discovered, with a neutral layer at its center [17]. The magnetic field in this region is extremely small (several nT) because the main component of the magnetic field is 'drawn out' by the solar wind from Earth's dipole field, changing sign in the neutral layer.

In laboratory plasma, in devices for confining plasma in Z- and Θ-pinch configurations, a similar situation arises: there is quite a narrow region within which the magnetic field reversal occurs [18–21]. In this limit, both space and laboratory problems have been actively investigated in the literature; however, the problem turned out to be much more complex than the preceding one: in this case, the magnetic field does not fully control the motion of particles and the theory of adiabatic invariants is no longer applicable. After a

series of useful, but empirical, studies based on numerical integration of the equations of motion of particles, it became clear that the description of motion in weak magnetic fields required an alternative to the theory of a guiding center.

To construct such an alternative theory, it turned out to be necessary to change the small parameter of the problem: instead of the ratio of the Larmor radius and the scale of the magnetic field spatial variation, the inverse ratio must be used. In this case, success was achieved in constructing a seemingly 'mirror' theory compared with the guiding center theory. The theory is based on two adiabatic invariants that result from averaging the momenta over fast oscillations in the field, vanishing in the neutral layer and in the field perpendicular to that layer. Everywhere below, we call these invariants quasiadiabatic. This term is used not only for stressing the difference of these invariants from the adiabatic invariants introduced in the guiding center theory; the motion of particles in the theory based on the quasiadiabatic approximation differs strongly from their motion in classical theory: instead of Larmor helixes, we obtain complex loop-like trajectories.

The quasiadiabatic approximation allows representing the motion of charged particles as piecewise-regular: at the boundaries between regions of regular motion, where the quasiadiabatic invariant is conserved, a jump in the quasiadiabatic invariant occurs. The magnitudes of such jumps are determined by the relations derived in Appendices A and B. The magnitude of a jump depends on the small parameter and the phase of fast motion in passing from one regular region to another. The jump amplitudes can be calculated in many problems for any given trajectories. However, the jumps are extremely sensitive to the fast phase, which leads to stochastization of individual trajectories and of the corresponding systems consisting of particle ensembles, i.e., trajectories with close initial conditions diverge in phase space. Therefore, deterministic chaos arises in the system at long times. Thus, the theory of jumps of a quasiadiabatic invariant also permits examining the diffusion limit imposed on the description of particle motion.

Taking the approximate conservation of the quasiadiabatic invariant into account yields an additional integral of motion and permits integrating the equations of motion of two-dimensional problems on the basis of energy conservation and of conservation of the generalized momentum and the quasiadiabatic invariant. This is crucial for the construction of an equilibrium model in the case of weakly two-dimensional plasma configurations with current sheets.

Having set the charged particle distribution function in plasma sources at the boundary of the system under consideration, we can use the Liouville theorem and project this function along the regular phase trajectories to any point in space and calculate moments of the distribution function at that point. The assumption that quasiadiabatic invariants are conserved is also very useful in resolving problems of particle acceleration in plasma.

It is interesting to compare possible consequences of the conservation of adiabatic and quasiadiabatic invariants. The motion of particles in these two cases exhibits essentially different symmetries. In the adiabatic case, there is a cylindrical symmetry of an anisotropic (but gyrotropic) system, but in the quasiadiabatic case this symmetry vanishes and the system turns out to be nongyrotropic (the directions perpendicular to the magnetic field are no longer equivalent).

This review presents results of the theory based on the quasiadiabatic approximation that have been obtained in recent decades. We believe that the methods of nonlinear dynamics and the solutions of plasma problems found with their aid may be of interest to both the physical and astrophysical communities.

2. General equations

The present review is devoted to problems of the dynamics of charged particles in configurations involving the plane of magnetic field reversal. One of the simplest examples of such configurations is represented by a current sheet (see reviews on current sheets in space [22, 23] and laboratory [18, 19, 24] plasma). We mainly consider the current sheet of Earth's magnetotail [23, 25], which has been well studied owing to numerous satellite measurements. In this section, we define the geometry of the system: the main component of the magnetic field B_x changes sign in the $z = 0$ plane, the component B_z is perpendicular to the given plane, and a nonzero component B_y can also exist (Fig. 1).

The components of the magnetic field in the current sheet, $B_x(x, z)$, $B_z(x, z)$, and $B_y(x, z)$, are independent of the y coordinate and are related by the divergence-free condition $\partial B_x/\partial x + \partial B_z/\partial z = 0$. Then the corresponding configuration has two components of the vector potential: $A_y(x, z) = \int^x B_z(x', z)\,\mathrm{d}x' - \int^z B_x(x, z')\,\mathrm{d}z'$ and $A_x = \int^z B_y(x, z')\,\mathrm{d}z'$. The Hamiltonian of a particle of charge q and mass m in such a field has the form

$$H = \frac{1}{2m}\left(p_x - \frac{q}{c}A_x(x, z)\right)^2 + \frac{1}{2m}p_z^2 + \frac{1}{2m}\left(p_y - \frac{q}{c}A_y(x, z)\right)^2, \quad (1)$$

where $\mathbf{p}$ is the generalized momentum of the particle. In most problems, it is possible to consider configurations with $B_z(x) = B_z(x/L_x)$, $B_y = \text{const}$, and $B_x(z) = B_0 b_x(z/L_z)$, where $b_x(z/L_z)$ is a certain dimensionless function of the z coordinate, L_z is the thickness of the current sheet, L_x is a characteristic scale of the variation of B_z, and the parameter B_0 is determined from the condition $b_x(1) = 1$. Moreover, the problem can often be simplified by setting $B_y = 0$ and $B_z = \text{const}$.

We introduce the dimensionless variables $\mathbf{p} \to \mathbf{p}/mv_0$, $H \to H/mv_0^2$, $\mathbf{r} \to \mathbf{r}/l_0$, and $t \to tv_0/l_0$, where v_0 is a char-

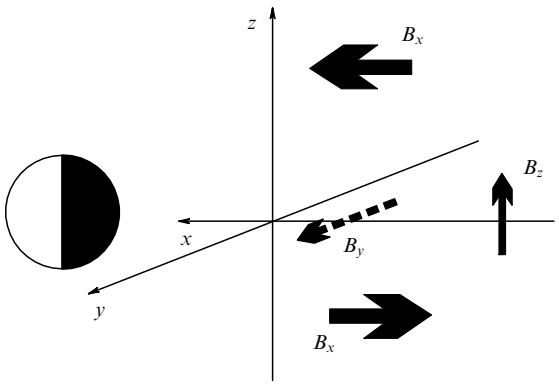

Figure 1. Geometry of the system considered in the review.

acteristic particle velocity and l_0 is a spatial scale to be defined below. We also introduce the functions

$$a_y(x,z) = \int_{x_0 l_0/L_z}^{x l_0/L_z} \frac{B_z(x')}{B_0}\,\mathrm{d}x' - \int_0^{z l_0/L_z} b_x(z')\,\mathrm{d}z'\,,$$

$$a_x(z) = \int_0^{z l_0/L_z} \frac{B_y}{B_0}\,\mathrm{d}z' = \frac{B_y}{B_0}\,\frac{z l_0}{L_z}\,,$$

corresponding to components of the dimensionless vector potential. The parameter x_0 is determined from the condition that $a_y(x,z)$ vanishes at the point $x = x_0$ in the neutral plane $z = 0$. Then the Hamiltonian assumes the form

$$H = \frac{1}{2}\left(p_x - \frac{L_z}{\rho_0}\,a_x(z)\right)^2 + \frac{1}{2}\,p_z^2 + \frac{1}{2}\left(p_y - \frac{L_z}{\rho_0}\,a_y(x,z)\right)^2, \qquad (2)$$

where $\rho_0 = (mcv_0)/(qB_0)$ is the particle gyroradius in the field B_0.

In typical conditions of Earth's magnetotail, the energies of ions are in the range 1–10 keV, while the amplitude of the magnetic field $B_0 \sim 10-40$ nT. The ratio B_z/B_0 depends essentially on the conditions in which the current sheet forms, and in the case of thin current sheets observed at distances between 10 and 30 Earth radii on the night side, it is in the range $10^{-2} < B_z/B_0 < 1$ [26–28], and $|B_y|$ then varies from 0 to $10B_0$ [29]. As a result, the thickness of the current sheet, L_z, turns out to be of the order of the Larmor radius of ions, ρ_0, [30, 31]. The curvature radius of the field line at the center of the current sheet for $B_y = 0$ can be estimated as $\sim B_z L_z/B_0$; consequently, $B_z L_z/(\rho_0 B_0) \ll 1$ (a system with a nonzero component B_y has the curvature radius $\sim (B_z L_z/B_0)(1 + B_y^2/B_z^2)^{3/2}$ [32]). Therefore, the guiding center theory cannot be applied to describing the system with Hamiltonian (2) (the scale of the magnetic field inhomogeneity is much less than the scale of Larmor radii of the particles), and investigating the dynamics of charged particles requires finding an alternative approach.

The Hamiltonian equations $\dot{\mathbf{r}} = \partial H/\partial \mathbf{p}$, $\dot{\mathbf{p}} = -\partial H/\partial \mathbf{r}$ describe the dynamics of charged particles in the current sheet. In what follows, we successively examine solutions of these equations for various functions $a_x(z)$ and $a_y(x,z)$, investigate the system in the presence of electric fields, and discuss the behavior of ensembles of particle trajectories described by Hamiltonian (2).

3. Dynamics of charged particles in simple configurations

This section is devoted to problems of particle dynamics in systems without the B_y-component of the magnetic field under the simplest assumption of homogeneity along x, with $B_z = \text{const}$. We introduce the quasiadiabatic invariant for a system with Hamiltonian (2) and consider its description in the framework of the quasiadiabatic approximation corresponding to the exact conservation of this invariant. We also determine the deviation of the system behavior from that dictated by the quasiadiabatic approximation, and discuss the consequences of violation of the invariant conservation.

3.1 Charged particle motion in one-dimensional current sheets

The dynamics of charged particles in a one-dimensional current sheet depend on the value of the parameter $\kappa = (B_z L_z/B_0 l_0)$ and on the form of the function $b_x(z)$. Because $b_x(0) = 0$, we can use the approximation $b_x(z) = z$, whence $a_y(x,z) = \kappa x - 1/2(z l_0/L_z)^2$. The case where this approximation is inapplicable, i.e., $\partial b_x/\partial z = 0$ for $z = 0$, is discussed in Section 4.3. Taking into account that Hamiltonian (2) is independent of y ($p_y = \text{const}$), we now introduce a change in notation: $\kappa x \to \kappa x + p_y$. Then Eqn (2) becomes

$$H = \frac{1}{2}\,p_x^2 + \frac{1}{2}\,p_z^2 + \frac{1}{2}\left(\kappa x - \frac{1}{2}\,\frac{l_0^2}{L_z\rho_0}\,z^2\right)^2. \qquad (3)$$

We set $l_0 = \sqrt{L_z\rho_0}$ and represent Hamiltonian (3) as

$$H = \frac{1}{2}\,p_x^2 + \frac{1}{2}\,p_z^2 + \frac{1}{2}\left(\kappa x - \frac{1}{2}\,z^2\right)^2, \qquad (4)$$

where $\kappa = (B_z/B_0)\sqrt{L_z/\rho_0}$. The parameter κ thus introduced is nothing but the square root of the ratio of the smallest curvature radius of a magnetic field line and the largest particle Larmor radius $\rho_0 B_0/B_z$ in the system. That is, the scale of magnetic field inhomogeneities — the curvature radius of field lines $\sim L_z B_z/B_0 \sim \rho_0 B_z/B_0$ — is much smaller than the scale of the Larmor radius of particles $\rho_0 B_0/B_z$ determined in the plane where the field B_x vanishes.

A numerical solution of the Hamiltonian equations for the system considered here was first obtained in Ref. [33]. The author showed that while particles are far from the $z = 0$ plane, they oscillate across the magnetic field lines and travel along them. The solution of the equation for the field lines ($\mathrm{d}x/B_x = \mathrm{d}z/B_z$) in the configuration considered here is represented by the parabolas $z^2 = 2\kappa x + \text{const}$. After crossing the $z = 0$ plane, a particle makes a half-turn in the field B_z, its motion being composed of two motions: gyrorotation in the constant field B_z and nonlinear oscillations in the field $B_x \sim z$ (Fig. 2) [33, 34].

Having made a half-turn in the field B_z, the particle leaves the $z = 0$ plane and once again starts to move along a field line, oscillating across it. Therefore, such a particle can be found near the $z = 0$ plane only for a limited period of

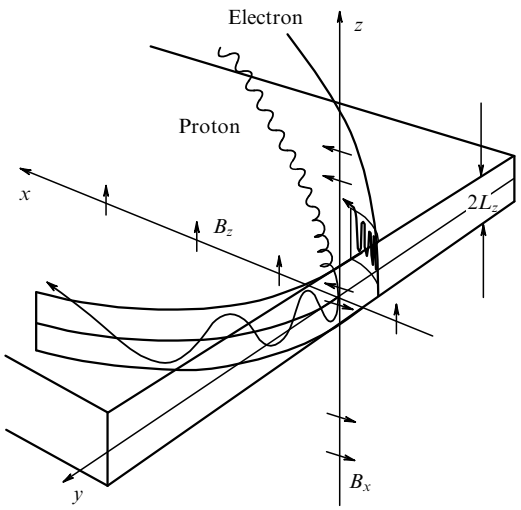

Figure 2. Trajectories of an ion and an electron obtained by numerical integration of the system with Hamiltonians (4). (From Ref. [33].)

time [35]. But the energy distributions of the particle over the two degrees of freedom (p_x, p_z) can be very different when the particle approaches the $z = 0$ plane and after it leaves this plane. Attempts to classify particle trajectories by values of the magnetic moment $\mu = mv_\perp^2/2B$ for the system with Hamiltonian (4) have not met with success because μ experiences a jump of the order of its own magnitude when a particle interacts with the current sheet [36]. Current sheets of zero thickness with the magnetic field $B_x = \pm B_0$ [37] represent an exception here.

The geometry of a real current sheet implies the presence of not only a central region in which $B_x \sim z$ but also current sheet boundaries at which the field is spatially homogeneous ($B_x \sim B_0 \operatorname{sign} z$). Particles arriving in these regions from the current sheet never return to it. These particles, which belong to the class of transient particles with open trajectories, follow their paths toward infinity ($z \to \pm\infty$). In the system with Hamiltonian (4), the magnetic field $b_x = z$ increases at infinity, and all the particles eventually return to the $z = 0$ plane (with the exception of particles with zero components of the momentum across the field line). Nevertheless, the system with Hamiltonian (4) effectively describes the conditions of particle interaction with the current sheet, and it is actively used in analytic theory. In considering systems with Hamiltonian (2), the function $b_x = \tanh(z)$ from the well-known Harris model of the current sheet [38] is often used. In this case, the main difference between the general system with Hamiltonian (2) and the simplified system with Hamiltonian (4) is that the first system involves transient trajectories.

The fact that it is not possible to construct an exact analytic solution of the Hamiltonian equations for (2) and to classify the trajectories hindered investigation of the dynamics of charged particles in current sheets for a long time. However, it turned out to be possible to perform such a classification on the basis of the Poincaré technique for constructing cross sections [39]. The solutions of Hamiltonian equations for (2) and (4) are curves in the four-dimensional space (z, p_z, κx, p_x). Because of the energy conservation, the trajectories fill up a certain three-dimensional manifold. Then, if one of the coordinates is fixed (for example, $z = 0$), the whole set of trajectories is represented by a set in the $(\kappa x, p_x)$ plane. The following approach is used for constructing this set: the Hamiltonian equations of motion are integrated numerically and, when the particle crosses the $z = 0$ plane, its position in the $(\kappa x, p_x)$ plane is recorded. The initial coordinate of the particle here is a point in the $z = 0$ plane. Thus, if the particle in its further motion never crosses the $z = 0$ plane again, it is not included in the Poincaré section. An example of such a section from Ref. [39] is presented in Fig. 3. In the system with Hamiltonian (2), the y coordinate obviously varies as $\mathrm{d}y/\mathrm{d}t = p_y - (L_z/\rho_0)\, a_y(x, z)$. As a consequence, $\mathrm{d}p_x/\mathrm{d}t \sim \mathrm{d}y/\mathrm{d}t$, and Fig. 3 can be considered a set of intersections of particle trajectories and the (x, y) plane at $z = 0$. In the figure, different regions can be identified, which allows classifying trajectories in the system. Regions not occupied by points correspond to transient particles. The regions containing closed curves correspond to particles that are 'trapped' inside the current sheet and never leave the vicinity of the $z = 0$ plane. During their motion, these particles constantly cross the $z = 0$ plane. Such trajectories are called regular (as is shown below, these trajectories do not take part in the chaos, and motion along them is quasiperiodic). The regions filled up with points correspond

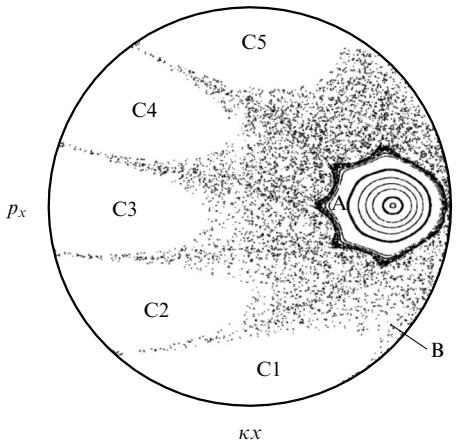

Figure 3. The Poincaré section for a system with Hamiltonian (2). C1–C5 are regions with transient particles, B is a region of quasi-trapped particles, and A is the region of regular trajectories. (From Ref. [39].)

to chaotic trajectories. After having experienced interaction with the current sheet, the particles on these trajectories do not depart toward infinity, but return to the current sheet, turning back at a certain distance from the $z = 0$ plane. As a result of multiple interaction with the current sheet, their motion becomes chaotic.

For a more complete description of the dynamics of the system with Hamiltonian (4), an analytic approach is generally used that is based on the introduction of different time scales for the variation of the variables (z, p_z) and (κx, p_x). The existence of different scales allows introducing a quasiadiabatic invariant. Because $\kappa \ll 1$, in the system with Hamiltonian (4), the variables κx, p_x can be considered slow, and the variables z, p_z fast. This approximation allows considering the dynamics in the (z, p_z) plane with 'frozen' κx and p_x. We now introduce the Hamiltonian of fast motion,

$$h_z = H - \frac{1}{2}\, p_x^2 = \frac{1}{2}\, p_z^2 + \frac{1}{2}\left(\kappa x - \frac{1}{2}\, z^2\right)^2 ,$$

which depends on the parameter κx. The potential energy

$$U = \frac{1}{2}\left(\kappa x - \frac{1}{2}\, z^2\right)^2$$

corresponding to this Hamiltonian is presented in Fig. 4a for different values of κx. As can be seen from the figure, particles can oscillate either in one of the 'small' wells (for $s > 1$, $s = \kappa x/\sqrt{2h_z}$) or within a single 'large' well (for $1 > s > 0$). When $\kappa x < 0$, there is only a single potential well in the system. Motions with and without intersections of the $z = 0$ plane correspond to trajectories of two types in the (z, p_z) phase plane (Fig. 4b, c). Trajectories of these two types are separated by a separatrix. When $\kappa x > 0$ (Fig. 4b), the particle can be found either in one of the loops of the separatrix or in the external region. When $\kappa x < 0$, the particle is trapped at the center of the current sheet.

The periodicity of the fast motion of a particle in the (z, p_z) plane at a constant value of κx permits introducing the action variable as the area bounded by a closed trajectory and normalized to 2π: $\hat{I}_z = (2\pi)^{-1} \oint p_z\, \mathrm{d}z$ [3]. For the system with Hamiltonian (4), $\hat{I}_z$ has the form

$$\hat{I}_z = \frac{1}{\pi} \int_{z_-}^{z_+} \sqrt{2h_z - \left(\kappa x - \frac{1}{2}\, z^2\right)^2}\, \mathrm{d}z\,. \qquad (5)$$

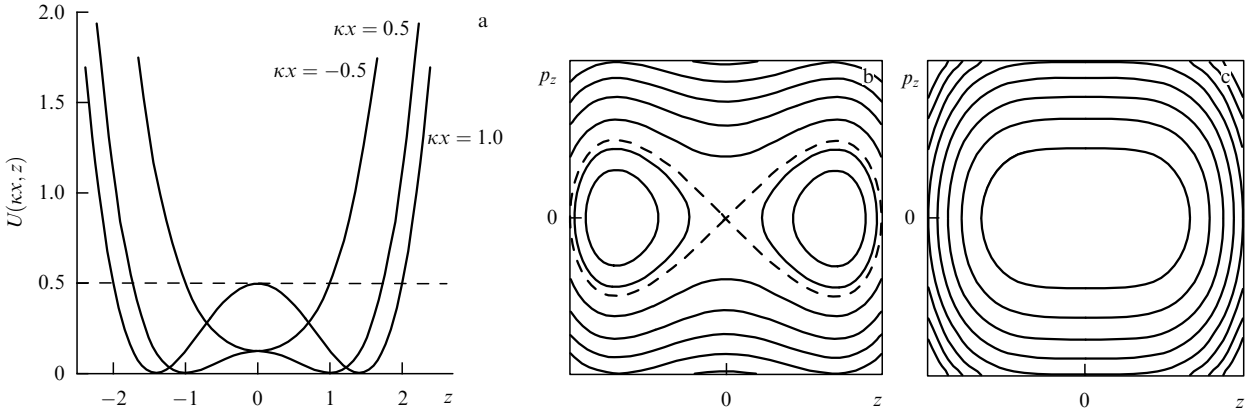

Figure 4. (a) Potential energy $U(\kappa x, z) = 1/2(\kappa x - (1/2)\, z^2)^2$ for different values of κx. Level lines of the Hamiltonian $p_z^2/2 + (\kappa x - (1/2)\, z^2)^2/2$ (b) for $\kappa x > 0$ and (c) for $\kappa x < 0$. The dashed curve shows the separatrix.

The integration limits $z_\pm$ are determined from the equation $2h_z = (\kappa x - (1/2)\, z_\pm^2)^2$. We can introduce the quasiadiabatic invariant $I_z = (\alpha/2)\, \hat{I}_z = (2\pi)^{-1}(2h_z)^{3/4} f(s)$, where $s = \kappa x/\sqrt{2h_z}$ and

$$f(s) = \alpha \int_{z'_-}^{z'_+} \sqrt{1 - \left(s - \frac{1}{2}\, z'^2\right)^2}\, \mathrm{d}z' .$$

The coefficient is $\alpha = 1$ if the particle oscillates in a single potential well and $\alpha = 2$ if the particle is in one of the small wells.

The quantity I_z depends on the slow variables κx and p_x just as on parameters, and its conservation is a consequence of the separation of time scales for z, p_z and κx, p_x.

Here and hereafter, as mentioned in the Introduction, we use the term 'quasiadiabatic' invariant to underline the difference between the invariant that we consider (and of the approximation within which its conservation is assumed) and the classical adiabatic invariant of this problem, namely, the magnetic moment.

The quasiadiabatic invariant thus introduced is equal to half the area inside the trajectory divided by 2π in the external region, and to the total area inside the trajectory divided by 2π in the internal region (inside the loop of the separatrix). Consequently, in the framework of the quasiadiabatic approximation, I_z has the same value inside both the internal and the external regions, i.e., $f(s)$ is a continuous function.

The function $f(s)$ can be expressed in terms of the complete elliptic integrals of the first (K) and second (E) kinds [40]:

$$\begin{aligned} f(s) &= \frac{8}{3}\left[2(1-k^2)\, K(k) + 2(2k^2-1)\, E(k)\right], \quad k < 1, \\ f(s) &= \frac{8}{3}\left[2(1-k^2)\, kK\left(\frac{1}{k}\right) + (2k^2-1)\, kE\left(\frac{1}{k}\right)\right], \quad k > 1, \\ k &= \sqrt{\frac{1}{2}(1+s)}\,. \end{aligned} \tag{6}$$

From Fig. 5a, $f(s)$ can be seen to increase from zero for s varying from $s = -1$ up to $s = 1$, reaching its maximum $f_{\max} \approx 1.6$, after which it decreases, as s increases, as $\sim s^{-1/2}$.

The value of the invariant I_z depends on κx and $h_z = H - (1/2)\, p_x^2$. For a fixed energy H, the value of I_z determines the trajectory in the plane of slow variables (κx, p_x), i.e., each value of I_z corresponds to its own trajectory in the (κx, p_x) plane. For the system with Hamiltonian (4), trajectories in the (κx, p_x) plane were first constructed as lines of constant $I_z = I_z(\kappa x, p_x)$ in Ref. [40] on the basis of previous studies [33, 41]. The trajectories from Ref. [40] are presented in Fig. 5b (the curves are symmetric with respect to the axis $p_x = 0$).

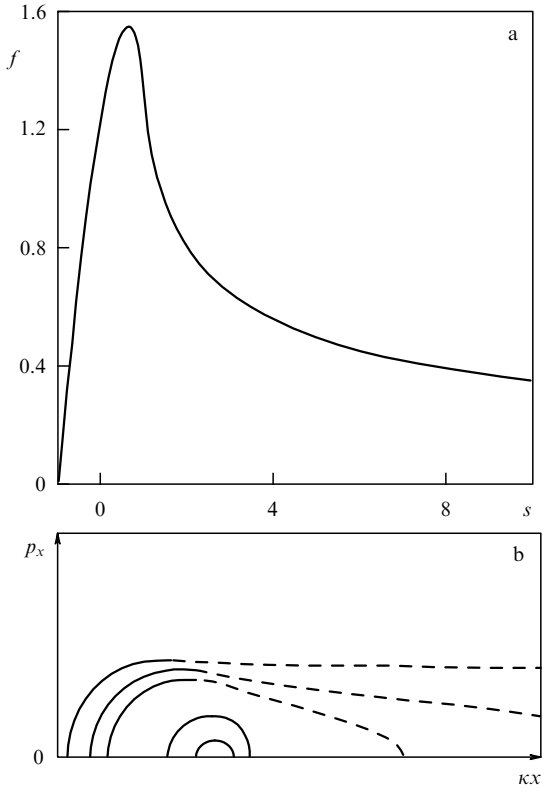

Figure 5. (a) The function $f(s)$. (b) Trajectories in the (κx, p_x) phase plane for a system with Hamiltonian (4). (From Ref. [40].)

Each point in the (κx, p_x) plane corresponds to a certain trajectory in the (z, p_z) plane. In Fig. 5b, solid curves indicate the trajectories in the (κx, p_x) plane that correspond to trajectories in the (z, p_z) plane in the external region. The dashed curves show segments of trajectories in the (κx, p_x) plane that correspond to one of the internal regions in the (z, p_z) plane. Certain trajectories do not have segments

marked by dashed lines. The particles on these trajectories never cross over to internal regions of the (z, p_z) plane.

We note that during the motion of a particle in the plane of slow variables $(\kappa x,\ p_x)$, the potential U, in which the particle oscillates in the plane of fast variables undergoes changes. Then, in the case of transition from one of the loops to the external region, the area inside the trajectory doubles, and, consequently, $\hat{I}_z$ also doubles. This effect is called a geometric jump of the invariant. If the loops of the separatrix are symmetric, as in the case considered here, and their areas have the same value as the trajectory passes to the external region and returns to one of the loops, then the geometric jump can be excluded from consideration, with I_z set to be half $\hat{I}_z$ in the external region. A system with nonsymmetric separatrix loops is discussed in Section 4.4 and in Appendix A.

The quasiadiabatic invariant I_z is conserved in the system away from the separatrix with a linear accuracy in the small parameter κ at times $\sim 1/\kappa$ [3]. However, it is always possible to introduce the so-called improved quasiadiabatic invariant, which is conserved far from the separatrix with an accuracy $\sim \kappa^2$ [42]. We use I_z everywhere in what follows, unless stipulated otherwise. We only need the improved quasiadiabatic invariant in dealing with a particle crossing the separatrix (see Appendix A). Using I_z corresponds to considering a system in the leading approximation in κ.

3.2 Dynamics of particles and diffusion of the quasiadiabatic invariant

In this section, we consider effects related to jumps of the quasiadiabatic invariant I_z. These jumps occur when a particle crosses the separatrix in the plane of fast variables (z, p_z). The level lines of I_z in the plane $(\kappa x/\sqrt{2H},\ p_x/\sqrt{2H})$ determine the entire set of trajectories in the quasiadiabatic approximation (i.e., for $I_z = \text{const}$). Trajectories for Hamiltonian (4) are presented in Fig. 5b and, in a more complete form, in Fig. 6a, in which half of the big circle (depicted by the thick light line) for $\kappa x > 0$ indicates the *uncertainty curve* ($\kappa x > 0$ and $p_x^2 + (\kappa x)^2 = 2H$). Each point on this curve corresponds to the particle motion along the separatrix in the (z, p_z) plane. Therefore, the trajectories that do not cross the uncertainty curve in Fig. 6a never cross the separatrix in the (z, p_z) plane. As a consequence, no jumps exist for these trajectories, and they form closed curves on the Poincaré section (see Fig. 3).

Trajectories crossing the uncertainty curve in the plane of slow variables cross the separatrix in the (z, p_z) plane. When leaving the external region, the particle is inside one of the loops. An example of numerical simulation of a particle trajectory is presented in Fig. 6b, c: it shows particle trajectories in the plane of slow variables and the value of the adiabatic invariant as a function of time. In Fig. 6c, two jumps of the invariant are seen, which correspond to crossing the uncertainty curve (and to crossing the separatrix in the plane of fast variables). Because of the existence of these jumps, the trajectory is open, even though its general shape is similar to the shape of trajectories constructed in the adiabatic approximation with $I_z(\kappa x,\ p_x) = \text{const}$.

In the three-dimensional $(\kappa x,\ p_x, z)$ space, the surface swept by the trajectory in the quasiadiabatic approximation (for $I_z = \text{const}$) looks like a split deformed torus (Fig. 7).

The adiabaticity of motion is violated in the vicinity of the separatrix because the period of particle oscillations in the plane of fast variables depends singularly on the particle

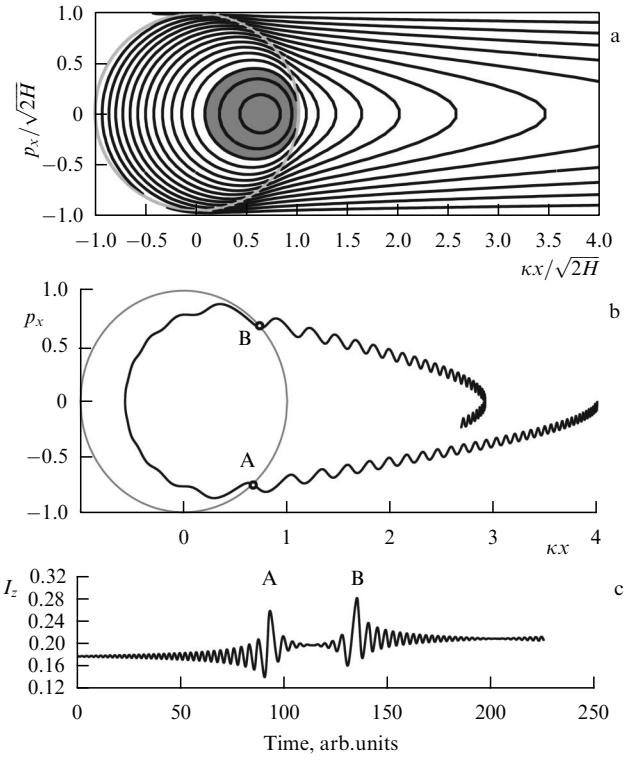

Figure 6. (a) Level lines of the quasiadiabatic invariant $I_z(\kappa x,\ p_x)$, (b) projection of numerically calculated trajectory in plane of slow variables, and (c) dependence of invariant I_z on time for Hamiltonian system (4).

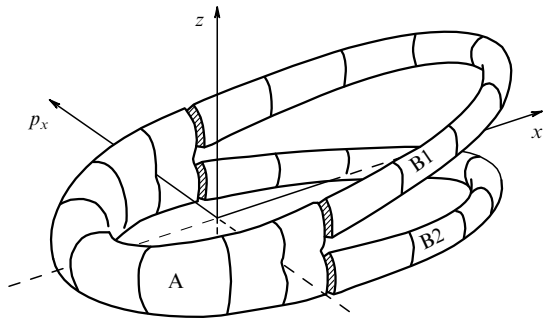

Figure 7. Invariant torus in the quasiadiabatic approximation in the $(\kappa x,\ p_x,\ z)$ space. Region A corresponds to the external region $(\kappa x/\sqrt{2H} < 1)$, and B1 and B2 are regions bounded by two loops of the separatrix $(\kappa x/\sqrt{2H} > 1)$. Shading indicates regions of intersection with the separatrix. (From Ref. [43].)

energy [44]. Thus, in the course of approaching the separatrix, crossing it, and receding from it, changes in the quasiadiabatic invariant accumulate (small changes in I_z occur at each oscillation period in the plane of fast variables). The sum of these changes, called the jump of the invariant, is determined (see Appendix A) as

$$\Delta I_z = -\frac{2}{\pi}\,\kappa p_x^*\,\ln\left(2\sin\pi\xi\right), \tag{7}$$

where p_x^* is the momentum p_x at the crossing of the separatrix and $\xi \in (0, 1)$ is a variable characterizing the point at which the crossing occurs. We note that ξ is very sensitive to initial values of the fast variables (a change in the initial position of a point in the (z, p_z) plane by a quantity $\sim \kappa$ leads to a change in ξ of the order of unity). Hence, ξ can be considered a random

quantity, and jumps ΔI_z can be regarded as random changes in the invariant I_z occurring at crossings of the separatrix.

As a result of such jumps, trajectories in the $(\kappa x, p_x)$ plane are open (Fig. 6b). Multiple crossing of the separatrix (multiple interaction of the particle with the current sheet) leads to stochasticization of the system at times much longer than the period of slow motion ($\gg 1/\kappa$) [45].

Consecutive jumps of the quasiadiabatic invariant can be considered random, independent quantities for most particles (see Appendix A). As a result, the quasiadiabatic invariant varies with time in accordance with the law of random walk with a random step ΔI_z and the time interval between the jumps $\sim 1/\kappa$. This process can be described in terms of random walk in the space of invariants for a single trajectory or in terms of diffusion, if we consider a certain distribution over I_z. If a certain particle distribution over the quasiadiabatic invariants exists in the system at the initial instant, then the accumulation of jumps ΔI_z with time leads to diffusion in the space of invariants and to evolution of this distribution [46, 47].

The value of the jump averaged over ξ and determined by formula (7), $\langle \Delta I_z \rangle_\xi$, can be shown to be exactly zero:

$$\int_0^1 \ln(2\sin\pi\xi)\,\mathrm{d}\xi = 0\,.$$

But the average of the square of the jump magnitude $\langle (\Delta I_z)^2 \rangle_\xi$ is not equal to zero:

$$\left\langle (\Delta I_z)^2 \right\rangle = \int_0^1 (\Delta I_z)^2\,\mathrm{d}\xi = \frac{4(\kappa p_x^*)^2}{\pi^3}\int_0^\pi \ln^2(2\sin x')\,\mathrm{d}x' = \frac{1}{3}\,(\kappa p_x^*)^2\,. \quad (8)$$

Here, we use the tabulated integral [48, p. 544]

$$\int_0^{\pi/2} \ln^2(2\sin x)\,\mathrm{d}x = \frac{\pi^3}{24}\,.$$

Therefore, the variance of ΔI_z depends on the small parameter κ quadratically. Hence, for the change of I_z to be of the order of unity, $1/\kappa^2$ crossings of the separatrix must occur. The characteristic time for a change in I_z to occur is determined by the ratio of the slow motion period $\sim 1/\kappa$ and a value $\sim \kappa^2$, and therefore the time required for a significant change in the quasiadiabatic invariant to occur is of the order of $1/\kappa^3$.

It is possible to express p_x^* as a function of the quasiadiabatic invariant itself. For this, we consider equality (5) at the point $p_x = p_x^*$:

$$2H = p_x^2 + (\kappa x)^2\,,$$

$$s = \frac{\kappa x}{\sqrt{2H - p_x^2}} = 1\,,$$

$$I_z = \frac{1}{2\pi}\,(2H - p_x^2)^{3/4} f(1) = \frac{8}{3\pi}\,(2H - p_x^2)^{3/4}\,.$$

As a result, $p_x^*/\sqrt{2H} = 1 - I^{4/3}$, where $I = 3\pi I_z/8(2H)^{3/4}$. The diffusion coefficient in the space of quasiadiabatic invariants assumes the form

$$D_{II} = \frac{\left\langle (\Delta I_z)^2 \right\rangle}{\tau_c} = \frac{2}{3}\,\frac{H\kappa^2(1 - I^{4/3})}{\tau_c}\,,$$

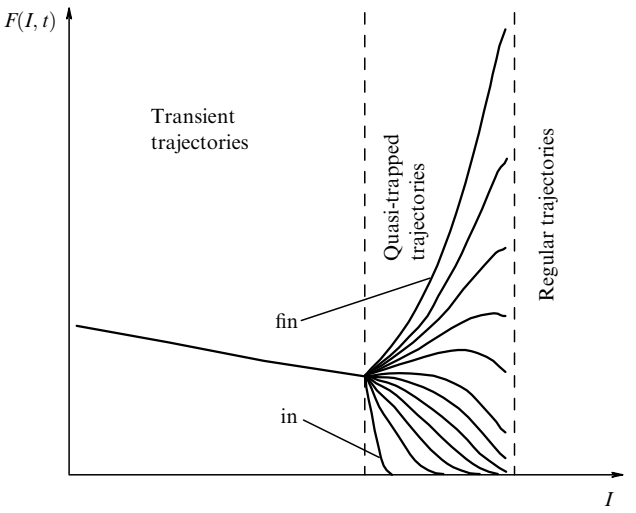

Figure 8. Distribution function $F(I, t)$ at different moments of time. The initial moment is indicated by 'in', and the final moment by 'fin'. (From Ref. [46].)

where τ_c is the period of particle motion in the plane of slow variables [46].

If we introduce an ensemble of particles with different values of the invariant I in terms of a distribution function $F(I, t)$, then the evolution of $F(I, t)$ is described by the equation

$$\frac{\partial F}{\partial t} = \frac{\partial}{\partial I}\left(D_{II}\,\frac{\partial F}{\partial I}\right)\,. \quad (9)$$

The solution of Eqn (9) yields the distribution function in the space of quasiadiabatic invariants in systems that are not subject to the action of external forces capable of changing the distribution $F(I, t)$. The function $F(I, t)$ was computed numerically in Refs [46, 47]. Figure 8 presents the phase density $F(I, t)$ for several time moments, obtained by numerical solution of the diffusion equation. It was assumed that in a current sheet with a magnetic field reaching its limit values $b_x = \pm 1$, sources of particles exist at the boundary of the system, $|z| = 1$ ($b_x = \tanh z$). Due to these sources, the population of particles in the sheet that move along transient trajectories is maintained constant. These particles cross the whole sheet either because the jump of I_z is small or because of a particular resonance effect (see Section 3.3). However, these transient particles are only a part of all the particles landing in the current sheet per unit time. Because of the jumps ΔI_z of the quasiadiabatic invariant, the remaining particle population undergoes transition from the initially transient orbits to quasi-trapped orbits and remains within the current sheet. With time, the phase density related to this population increases. The primary reason is that the initial particle distribution over I_z corresponds to quite a narrow maximum of the function $F(I, t)$ in the vicinity of small I_z values (i.e., all the particles move along transient trajectories at the initial moment). Subsequently, although the jump is a random quantity and a particle has the possibility of both increasing and decreasing the value of I_z, the number of particles with large I_z values (particles on quasi-trapped trajectories) on the average increases due to diffusion of the quasiadiabatic invariant. From Fig. 8, the results of numerical simulation are seen to be consistent with the above ideas: with time, the phase density of particles moving along quasi-trapped (chaotic) trajectories increases. The increase in the number

of particles on these trajectories is responsible for the so-called ageing process of current sheets (see Refs [46, 49, 50] and Section 6.4).

3.3 Resonance effect and correlation of jumps of the quasiadiabatic invariant

In Section 3.2, we discussed problems related to diffusion in the space of invariants due to jumps ΔI_z. However, among the multitude of trajectories in the system, there are two separate groups for which scattering processes play no significant role. The first group includes trajectories that do not cross the separatrix, i.e., regular trajectories. The second group consists of trajectories of the so-called resonance particles.

In the case of a single interaction with the current sheet, a particle crosses the separatrix twice (when leaving one of the loops and landing in the external region and then when returning and falling into some loop). Hence, two jumps of the quasiadiabatic invariant occur:

$$\Delta I_{z,1} = -\frac{2}{\pi}\,\kappa p_x^* \ln\left(2\sin\pi\xi\right),$$
$$\Delta I_{z,2} = \frac{2}{\pi}\,\kappa p_x^* \ln\left[2\sin\left(\pi\xi + \pi\delta\xi\right)\right],$$

where $\delta\xi$ is the change in ξ between the separatrix crossings. Here, $\xi + \delta\xi \in (0, 1)$, i.e., the integer part is subtracted from $\xi + \delta\xi$. The sum of two jumps (the resultant jump in the invariant) is given by

$$\Delta I_z^{\text{sum}} = \frac{2}{\pi}\,\kappa p_x^* \ln\left[\cos\left(\pi\delta\xi\right) + \frac{\cos\left(\pi\xi\right)}{\sin\left(\pi\xi\right)}\sin\left(\pi\delta\xi\right)\right],$$

and hence the equation $\Delta I_z^{\text{sum}}(\delta\xi) = 0$ has two solutions: $\delta\xi = 0$ and $\delta\xi = 1 - 2\xi$. The second root depends on ξ, and the corresponding condition for the total jump to be zero is not valid for all the particles. For this reason, we only consider the first root, $\delta\xi = 0$, which is independent of ξ.

The quantity $2\pi\delta\xi$ is given by the integral of the frequency of fast motion $\Omega_z(\kappa x, h_z) = \partial H/\partial I_z$ over time, taken with the minus sign and modulo unity [45]. Then the condition for ΔI_z^{sum} to be zero takes the form

$$2\pi N = \int \Omega_z\,\mathrm{d}t = \frac{1}{\kappa}\int \frac{\Omega_z}{p_x}\,\mathrm{d}\kappa x,$$

where N is an integer. Hamiltonian (4) can be expressed in terms of the variables I_z and κx:

$$H = \frac{1}{2}\,p_x^2 + h_z(I_z, \kappa x).$$

Consequently, $\Omega_z = \partial h_z/\partial I_z$. Here, $\kappa x = \sqrt{2h_z}s$ and $2\pi I_z = (2h_z)^{3/4} f(s)$, i.e.,

$$2h_z = \left(\frac{2\pi I_z}{f(s)}\right)^{4/3},$$
$$p_x = \sqrt{2H - 2h_z} = \sqrt{2H - \left(\frac{2\pi I_z}{f(s)}\right)^{4/3}},$$
$$\mathrm{d}\kappa x = \mathrm{d}s\left(\frac{2\pi I_z}{f(s)}\right)^{2/3}\left(1 - \frac{2sf'(s)}{3f(s)}\right).$$

As a result, we obtain the following condition for the total jump of the invariant to be zero:

$$\pi N = \frac{2I_z}{3\kappa}\int_0^{\hat{s}} \frac{1 - 2sf'(s)/3f(s)}{f^2(s)\sqrt{2H - \left(2\pi I_z/f(s)\right)^{4/3}}}\,\mathrm{d}s.$$

The integration limit $\hat{s}$ is determined from the equation $f(\hat{s}) = 2\pi I_z/(2H)^{3/4}$. We note that the trajectories of transient particles correspond to small I_z values. To obtain an analytic expression in this region, we expand the integral in a Taylor series in the vicinity of $I_z = 0$:

$$N = (2H)^{1/4}\kappa^{-1}C_0, \tag{10}$$

where $C_0 = \Gamma(3/4)/\sqrt{\pi}\,\Gamma(1/4) \approx 0.76$ [45]. Hence, the phase increment for particles of the energy $2H = (N\kappa/C_0)^4$ is equal to an integer and $I_z^{\text{sum}} = 0$. As a result, the scattering effect turns out to be insignificant for such particles [51].

If we consider the dynamics of particles with thermal energies v_0, then $2H = 1$, and from the equation $N = C_0/\kappa$ we obtain a relation for the resonance values of κ [52]; for a system with fixed κ, particles of the energy H are therefore not scattered.

In Earth's magnetotail, $\kappa \sim B_z$ decreases with the distance from Earth according to a power law: $\kappa \sim (-x)^{-h}$, $0 < h < 1$ [53]. This implies that a number of regions with coordinates x_N exists that correspond to resonance values $\kappa_N = C_0/N$. The existence in space of such particular regions, in which no particle scattering occurs, is manifested in the effects of resonance acceleration discussed in Section 5.2.

In the case of an ensemble of particles with velocities exhibiting a thermal spread, the obtained relation $(N\kappa = (2H)^{1/4}C_0)$ determines the energies of particles that do not experience stochastic scattering: $(2H)^{1/4} \sim N$. This effect was revealed numerically in Ref. [51].

The formulation of the problem in Ref. [51] can be explained as follows. We consider a current sheet with a population of transient particles ($b_x = \tanh z$), and a source of particles preset on one of the boundaries of the current sheet. The distribution of particles that have crossed the current sheet is investigated. At the beginning, all trajectories at the boundary of the system can be considered transient. But because of the jumps of the quasiadiabatic invariant, ΔI_z, some of the particles increase the value of I_z and undergo transition to quasi-trapped orbits. This effect is not felt only by the particles that from the very beginning had resonance energies $H \sim N^4$. To confirm this assumption, the authors of Ref. [51] analyzed how the distribution function of particles after they cross the current sheet depends on the thermal energy $V = \sqrt{2H}$ of the particles. The phase density of particles with certain values of $H^{1/4}$ can be seen from Fig. 9 to have characteristic maxima. Each such maximum is explained by particles with resonance energies remaining on transient trajectories, i.e., no scattering occurring at these energies (all particles with these energies cross the current sheet).

Other manifestations of the resonance effect were revealed numerically in Refs [32, 54]. The concept of lifetime on the current sheet, i.e., of the time interval spent in crossing the current sheet, can be introduced for particles. In the case of particles moving along transient trajectories, this time is small compared to the same time for particles on quasi-trapped trajectories. In the case of nonresonance energies, as a result of jumps of the quasiadiabatic invariant, ΔI_z, particles on quasi-trapped trajectories possibly reduce the value of the quasiadiabatic invariant I_z and leave the current sheet in a finite time (particles on transient orbits can either traverse the current sheet or undergo transition to a quasi-trapped trajectory and remain inside the current sheet). In the case of resonance energies, compensation of the jumps ΔI_z results in

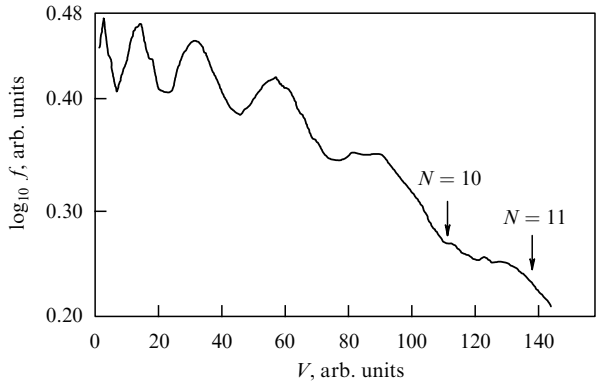

Figure 9. Distribution function of particles that have crossed the current sheet. (From Ref. [51].)

particles preserving the values of the quasiadiabatic invariant in the current sheet and remaining on the initial trajectories. As a result, if a transient particle rapidly leaves the current sheet, while a particle on a quasi-trapped trajectory remains in the current sheet for a long time (from a formal standpoint, this particle should never leave the current sheet, but the jumps no longer compensate each other in the next order in κ, and particles actually do leave the current sheet; the only exception is a special class of stable quasi-trapped trajectories with the total jump $\Delta I_z = 0$ [see Refs [55, 56]]).

The following simulation procedure is used for demonstration of the above effect: particles are introduced in the neutral plane ($z = 0$) from the region bounded by the circle $(\kappa x)^2 + p_x^2 = 2H$. Particle trajectories are then calculated for quite a long period of time, and a map is constructed of the distribution of lifetimes: in the $(\kappa x, p_x)$ plane, a particle lifetime is marked by an appropriate color on the trajectory, starting from the given point. For any values of H, it is possible to single out three principal regions in the $(\kappa x, p_x)$ plane (Fig. 10): the region of transient particles, from which particles do not return to the current sheet (shown in white in the figure); the region of regular trajectories, such that the particles belonging to it do not leave the current sheet (shown in black); and the region of quasi-trapped particles, whose the lifetime in the current sheet is finite (shown in grey in Fig. 10a). In the case of resonance energies, particles on quasi-trapped trajectories become nearly regular: their lifetime increases significantly (Fig. 10b).

A relatively large (≈ 0.4) value of κ was chosen for the calculations whose results are presented in Figs 10a, b. The lifetime map for the system with $\kappa = 0.2$ is presented in Fig. 10c, from which the lifetime in the current sheet of particles on quasi-trapped trajectories is seen to increase significantly at resonance energies.

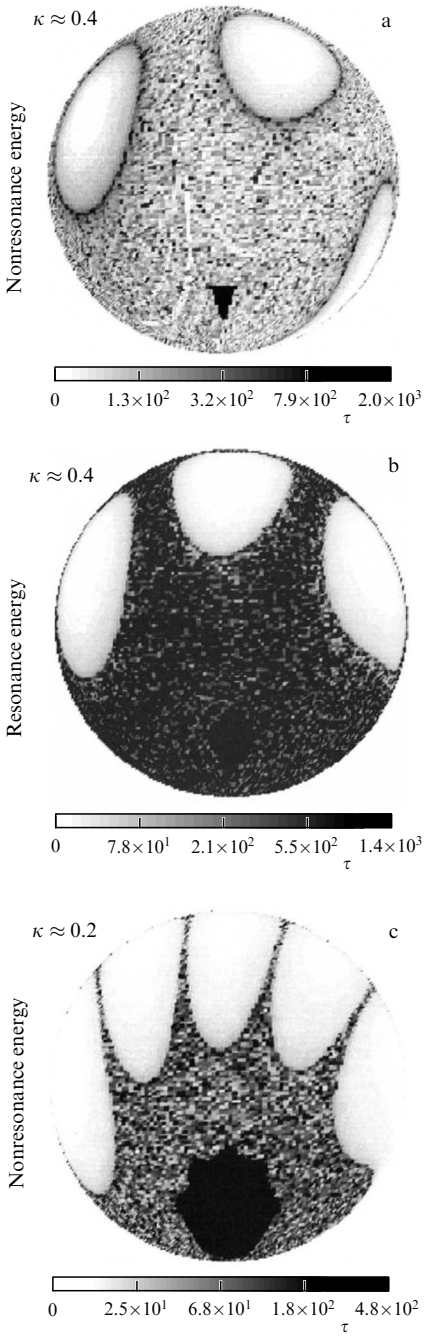

Figure 10. Lifetime τ normalized to the gyrofrequency in the field B_0 for (a) nonresonance and (b) resonance energies in the case $\kappa \approx 0.4$ and (c) for nonresonance energy in the case $\kappa \approx 0.2$. (From Ref. [54].)

4. Dynamics of charged particles in systems with a complex geometry

In Section 3, we showed how the charged particle dynamics in the simplest magnetic configuration $\mathbf{B} = B_0(z/L_z)\,\mathbf{e}_x + B_z\,\mathbf{e}_z$ can be described using quasiadiabatic invariants. However, the geometry of current sheets observed in Earth's magnetotail, in the magnetospheres of other planets of the Solar System, and in the solar wind are certainly much richer (see reviews [22, 23]). For example, a characteristic feature of magnetospheric current sheets consists in the presence of a nonzero gradient $\partial B_z/\partial x$ [53, 57], which, although significantly less than the gradient $\partial B_x/\partial z$, can also play an important role in charged particle dynamics.

The development of tearing instability in current sheets leads to the formation of configurations with X- and O-lines, in which $B_z(x)$ represents not just a variable but an alternating-sign quantity, $B_z \sim x$ [58–62]. Particle dynamics in the configurations indicated can also be described using the theory based on the conservation of quasiadiabatic invariants.

Certain current sheets exhibit a complex internal structure, bifurcation of the transverse current. Current sheets with such a structure are observed in Earth's magnetosphere

[63, 64], in the magnetospheres of other planets of the Solar System [65], and in the solar wind [66]. In this case, the derivative of the magnetic field component $\partial B_x/\partial z$ has a local minimum at the center of the current sheet. In Section 4.3, we examine characteristic features of particle dynamics in such a configuration and obtain an expression for jumps of the quasiadiabatic invariant.

Furthermore, in the current sheets of Earth's magnetotail [67, 68] and of the magnetopause [69–71], a nonzero component of the magnetic field B_y directed along the current is often present. The existence of $B_y \neq 0$ in Earth's magnetotail can be due to both internal current systems and processes of the interplanetary magnetic field penetrating the magnetosphere [29]. In Section 4.4, we consider a current sheet in the case of a nonzero component directed along the current ($B_y \neq 0$) [72]. This configuration differs from those discussed in Section 3 in the asymmetry of separatrix loops in the phase plane of fast variables, which leads to an essential change in the particle dynamics already in the quasiadiabatic approximation (i.e., even without taking the dynamic jump of the quasiadiabatic invariant ΔI_z into account).

4.1 Particle dynamics in two-dimensional current sheets

In this subsection, we consider charged particle dynamics in a current sheet with an inhomogeneous magnetic field $B_z(x/L_x)$, where L_x is the B_z inhomogeneity scale. We assume that the field $B_z(x/L_x)$ is nonvanishing everywhere in a region $x \in [x_1, x_0]$ considered. The parameters x_1 and x_0 satisfy the inequalities $x_1 < x_0 < 0$, which corresponds to the current sheet on the night side of Earth's magnetosphere and also to the choice of a coordinate system with its origin at the point corresponding to the coordinate of Earth and the x axis directed from Earth toward the Sun (see Fig. 1). The magnetic field lines are shown in Fig. 11 (for comparison, field lines for a system with $B_z = \text{const}$ are also shown). We see from the figure that the field lines in the system with $\partial B_z/\partial x \neq 0$, unlike the ones in a current sheet with $B_z = \text{const}$, are no longer equidistant along the x axis.

Particle trajectories for the above problem were obtained for different dependences of B_z on x in Refs [75, 76] by numerical integration of the Hamiltonian equations of motion. The analytic description of particle motion considered in this section is based on Refs [77, 78].

The Hamiltonian of the system in the dimensionless variables introduced in Section 3.1 has the form

$$H = \frac{1}{2}\,p_x^2 + \frac{1}{2}\,p_z^2 + \frac{1}{2}\left(p_y + \frac{1}{2}\,z^2 - \kappa\int_{x_0}^{x}\frac{B_z(vx')}{\bar{B}_z}\,\mathrm{d}x'\right)^2,$$

where $\kappa = \bar{B}_z/B_0\sqrt{L_z/\rho_0}$, $v = \sqrt{L_z\rho_0}/L_x \ll 1$, and $\bar{B}_z$ is a certain characteristic value of B_z within the interval $x \in [x_1, x_0]$. We now introduce a new coordinate

$$\chi = -\frac{p_y}{\kappa} + \int_{x_0}^{x}\frac{B_z(vx')}{\bar{B}_z}\,\mathrm{d}x'.$$

Then $p_x = p_\chi\beta(v\chi)$, where $\beta = B_z(vx)/\bar{B}_z$. In the new variables, the Hamiltonian takes the form

$$H = \frac{1}{2}\,p_\chi^2\,\beta^2(v\chi) + \frac{1}{2}\,p_z^2 + \frac{1}{2}\left(\kappa\chi - \frac{1}{2}\,z^2\right)^2. \qquad (11)$$

As in Section 3.1, the variables z and p_z are fast, while the variables $\kappa\chi$ and p_χ are slow. We note that it is possible to separate the Hamiltonian of fast motion, h_z, from Hamiltonian (11) and to compute its quasiadiabatic invariant $I_z = (1/2\pi)(2h_z)^{3/4}f(s)$, where $s = \kappa\chi/\sqrt{2h_z}$. We can then write

$$h_z = \frac{1}{2}\,p_z^2 + \frac{1}{2}\left(\kappa\chi - \frac{1}{2}\,z^2\right)^2,$$

$$I_z = I_z\bigl(v\chi\,,\, h_z(H, p_\chi\beta)\bigr) = I_z\left(\kappa\chi\,,\, H - \frac{1}{2}\,p_x^2\right).$$

Therefore, motion in the (z, p_z) is identical to the one considered in Section 3.1 (see Fig. 4). For the slow motion, we obtain the Hamiltonian

$$H = \frac{1}{2}\,p_\chi^2\,\beta^2(v\chi) + h_z(I_z, \kappa\chi)\,, \qquad (12)$$

where h_z is expressed in terms of the invariant I_z in accordance with a formula given in Section 3.1.

The phase portrait of the Hamiltonian of system (12) in the variables $\kappa\chi$ and $p_\chi\beta$ looks similar to the one shown in Fig. 6a. Hence, the above change of variables has reduced the problem to the one discussed in Section 3.1. But the original variables of the system, in which it is necessary to plot phase portraits, are κx and p_x. To represent the phase portrait, shown in the variables $\kappa\chi$ and $p_\chi\beta$ in Fig. 6a, using the variables κx and p_x, we must fix the form of the function $\beta(vx)$. We consider two possible choices of β, corresponding to the two characteristic magnetospheric configurations shown in Figs 11b, c.

The magnetic field $B_z(x/L_x)$ in Earth's magnetotail is formed as a result of the magnetic field of Earth's dipole being

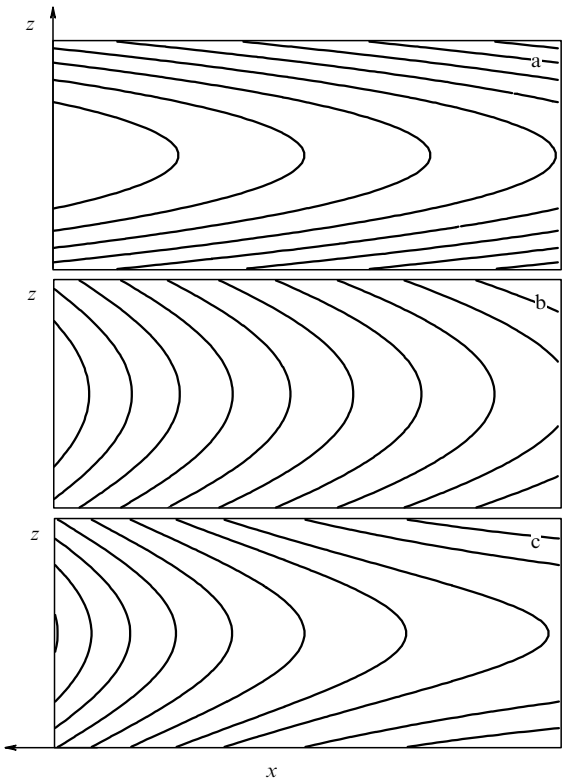

Figure 11. Field lines for a system with $B_x \sim z$ and with different profiles of $B_z(x/L_x)$: (a) $B_z = \text{const}$; (b) $B_z \sim (-x/L_x)^{-1/2}$ [73]; (c) $B_z \sim \exp(x/L_x)$ [74].

screened by currents of the current sheet. A good approximation for the dependence of B_z on x in this case is the power law $\beta = (-vx)^{-1/2}$ (Fig. 11b), considered in Refs [57, 73, 79]. Here,

$$\chi = -\frac{p_y}{\kappa} - 2\left(\sqrt{\frac{-x}{v}} - \sqrt{\frac{-x_0}{v}}\right).$$

We now introduce the notation

$$p_y' = \frac{p_y - 2\kappa\sqrt{-x_0/v}}{\sqrt{2H}} = \text{const},$$

where

$$\frac{-x}{\sqrt{2H}} = \frac{1}{4}\, v\sqrt{2H}\left(\frac{\chi}{\sqrt{2H}} + \frac{p_y'}{\kappa}\right)^2,$$

or

$$-vx = \left(\frac{v}{\kappa}\right)^2 \frac{H}{2}\left(\frac{\kappa\chi}{\sqrt{2H}} + p_y'\right)^2.$$

The phase portraits in the plane of slow variables are presented in Fig. 12 for several values of p_y'. The parameter p_y' contains information on the particle momentum along the y axis and on the particle position on the x axis at the initial moment. The larger p_y' is, the deeper the particle can penetrate the tail of the magnetosphere when moving along the trajectory in the plane of slow variables, which corresponds to larger values of the coordinate $-x_0$. Here, regions with larger values of $-x_0$ correspond to smaller values of the field gradient $B_z(x/L_x)$ because $\mathrm{d}B_z/\mathrm{d}x \sim \bar{B}_z/x$. As a result, the phase portrait at large values of p_y' is, more than others, similar to the phase portrait presented in Fig. 6a and obtained at a zero gradient $B_z(x/L_x)$.

An exponential dependence of the magnetic field on the coordinate, $\beta = \exp(vx)$, is also frequently used in models of current sheets (see Refs [80, 81]). Such an approximation corresponds to the magnetosphere in the quiet condition. In this case,

$$\chi = -\frac{p_y}{\kappa} + \frac{\exp(vx) - \exp(vx_0)}{v},$$

$$-vx = -\ln\left[\frac{v}{\kappa}\sqrt{2H}\left(\frac{\kappa\chi}{\sqrt{2H}} + p_y'\right)\right],$$

$$p_y' = \frac{p_y}{\sqrt{2H}} + \frac{(\kappa/v)\exp(vx_0)}{\sqrt{2H}}.$$

The phase portraits for this system are presented in Fig. 13. In this case, as $-x_0$ increases, the field gradient $B_z(x/L_x)$ decreases exponentially. As a result, already for $p_y' = 2, 3$, the phase portrait is similar in structure to the portrait of the system with a zero gradient (Fig. 6a).

The shaded regions in Figs 12 and 13 correspond to the region filled with trajectories that do not cross the separatrix in the $(\kappa\chi, p_\chi\beta)$ plane (Fig. 6a). From Figs 12 and 13, the area occupied by these trajectories can be seen to depend on the value of the parameter p_y'. Because larger values of p_y' correspond to smaller values of $\mathrm{d}B_z/\mathrm{d}x$, we conclude that in systems with strong magnetic field gradients, fewer particles move along regular trajectories.

As in the case of the system with a constant field B_z, a trajectory crossing the separatrix in the case discussed here leads to a jump ΔI_z of the quasiadiabatic invariant. Because the substitution of the variables $\kappa\chi$ and $p_\chi\beta$ for the slow variables reduces the system with Hamiltonian (11) to the

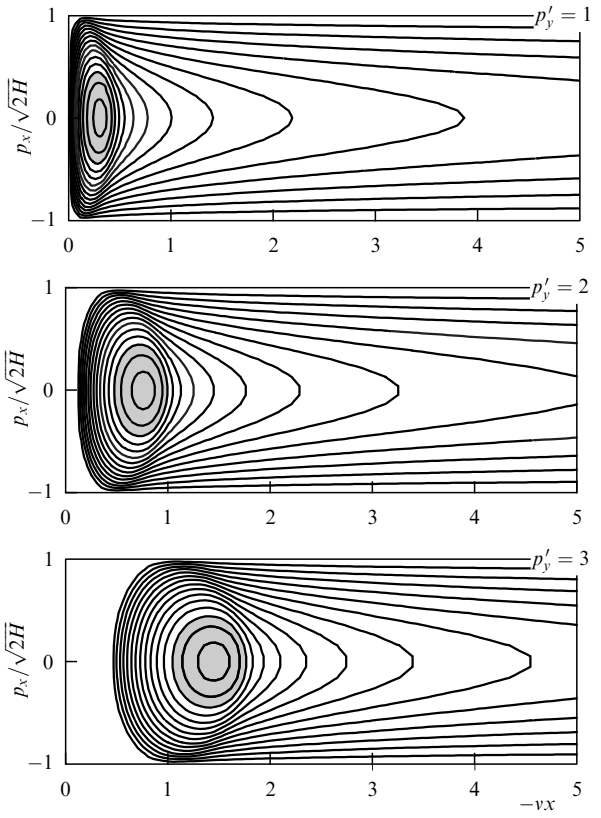

Figure 12. Phase portraits in the $(-vx, p_x)$ plane for the system with $\beta = (-vx)^{-1/2}$ and three values of p_y'. The parameters of the system are $H = 1$ and $v/\kappa = 0.5$.

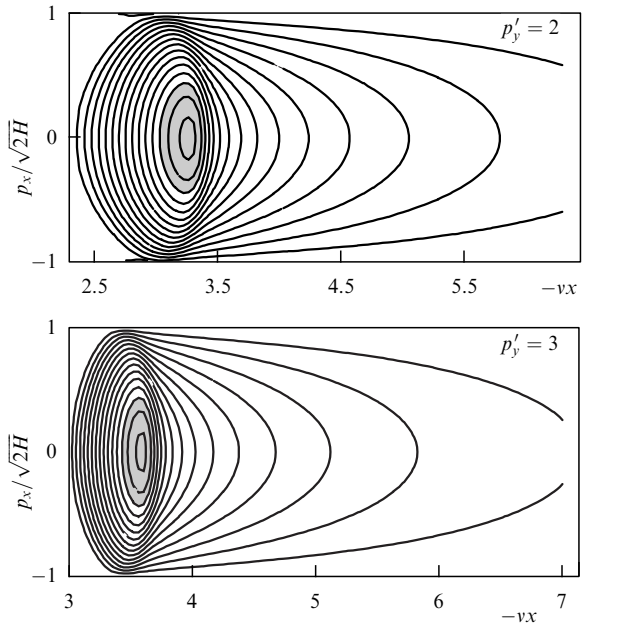

Figure 13. Phase portraits in the $(-vx, p_x)$ plane for the system with $\beta = \exp(vx)$ and two values of p_y'. The parameters of the system are $H = 1$ and $\kappa = 0.1$.

system with Hamiltonian (4), the jump of the invariant can be written as

$$\Delta I_z = -\frac{2}{\pi}\,\kappa p_\chi^* \beta^2 (v\chi^*)\,\ln(2\sin\pi\xi)\,.$$

Such jumps, as noted in Section 3.2, result in diffusion of the quasiadiabatic invariant, and in time periods of the order of κ^{-3}, the invariant changes by a value of the order of unity.

4.2 Particle dynamics in the vicinity of X- and O-lines

The X- and O-line geometry is determined by the magnetic field components $B_x = B_0(z/L_z)$ and $B_z = \pm B_0(x/L_x)$, where the plus sign corresponds to an X-line and the minus sign corresponds to an O-line. The respective configurations of magnetic field lines are shown in Fig. 14.

The theoretical treatment of particle dynamics in the vicinity of an X-line, presented below, is based on the theory of quasiadiabatic invariants [40, 78, 82].

The Hamiltonian of a system with an X-line can be written in dimensionless variables as

$$H = \frac{1}{2}\,p_x^2 + \frac{1}{2}\,p_z^2 + \frac{1}{2}\left(p_y + \frac{1}{2}\,\lambda^2 x^2 - \frac{1}{2}\,z^2\right)^2, \qquad (13)$$

where $\lambda^2 = L_z/L_x$. In a system with $\lambda^2 \ll 1$, as previously, z and p_z are fast variables for which the Hamiltonian is

$$h_z = \frac{1}{2}\,p_z^2 + \frac{1}{2}\left(p_y + \frac{1}{2}\,\lambda^2 x^2 - \frac{1}{2}\,z^2\right)^2.$$

As in Section 3.1, we can introduce the invariant $I_z = (1/2\pi)\,(2h_z)^{3/4} f(s)$, where $s = \chi/\sqrt{2h_z}$ and $\chi = p_y + (1/2)\,\lambda^2 x^2$. Here, the phase portrait of fast motion corresponds to the one shown in Figs 4b, c.

The slow variables of the system are λx and p_x, in terms of which the Hamiltonian has the form $H = p_x^2/2 + h_z(\chi, I_z)$. The phase portrait in the plane of slow variables can be constructed as a family of level lines of the invariant $I_z\bigl(\chi, H - (1/2)\,p_x^2\bigr)$. The phase portrait of slow motion in the coordinates χ and p_x is then fully identical to the phase portrait presented in Fig. 6a, but not all values of χ correspond to real values of x for a given p_y.

We introduce the constant $p_y' = p_y/\sqrt{2H}$. Then, expressing x in terms of χ for different values of p_y' ($\lambda x = \pm(8H)^{1/4}(\chi/\sqrt{2H} - p_y')^{1/2}$), we can obtain different phase portraits in the $(\lambda x, p_x)$ plane.

If $p_y' < -1$, then $\chi/\sqrt{2H} - p_y' > 0$ for all $\chi/\sqrt{2H} > -1$. Hence, the entire $(\kappa\chi, p_x)$ space represented in Fig. 6a transforms into the $(\lambda x, p_x)$ space, but no trajectories in the $(\lambda x, p_x)$ space cross the vertical straight line $x = 0$, because $x \sim \chi/\sqrt{2H} - p_y'$ is never equal to zero. The phase portrait shown in Fig. 15a corresponds to these trajectories. Particles moving along these trajectories land in the neutral plane ($z \sim 0$) even before reaching the X-line ($x \sim 0$); therefore, their motion resembles that of particles in the two-dimensional current sheet with an inhomogeneous magnetic field $B_z(x/L_x)$ (see Figs 12 and 13).

If $p_y' = -1$, then $\chi/\sqrt{2H}$ ranges within the limits $1 > \chi/\sqrt{2H} \geqslant p_y'$. Hence, the point $x = 0$ corresponds to $\chi/\sqrt{2H} = p_y'$ and is in the range of $\chi/\sqrt{2H}$ values. In this case, there is a single trajectory in Fig. 6a with $\chi/\sqrt{2H} = -1$, such that its corresponding trajectory in the $(\lambda x, p_x)$ phase portrait passes from the region of negative λx to the region of positive λx (or vice versa) across the X-line ($x \sim 0$). But all the other trajectories of the system still do not cross the X-line. The corresponding phase portrait in the plane of slow motion is shown in Fig. 15b.

If $-1 < p_y' < 1$, the condition $\chi/\sqrt{2H} - p_y' > 0$ is satisfied for $\chi/\sqrt{2H} > -1$. Consequently, only part of the phase portrait presented in Fig. 6a is projected onto the $(\lambda x, p_x)$ plane. The phase portrait in the $(\lambda x, p_x)$ plane is shown in Fig. 15c. Trajectories passing from the half-space of positive λx into the half-space of negative λx already exist in the system.

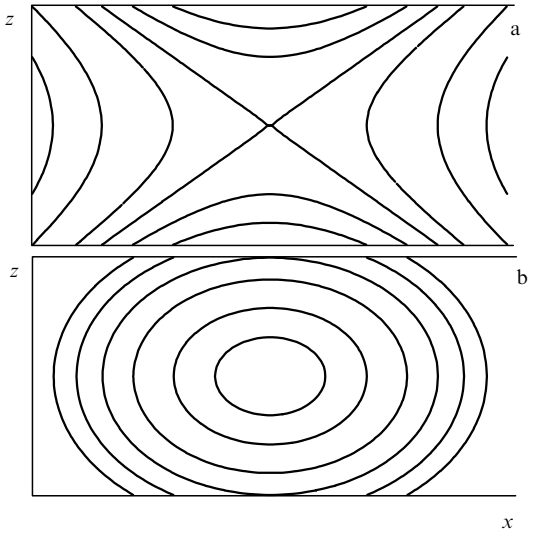

Figure 14. Magnetic field lines (a) in the X-line geometry and (b) in the O-line geometry.

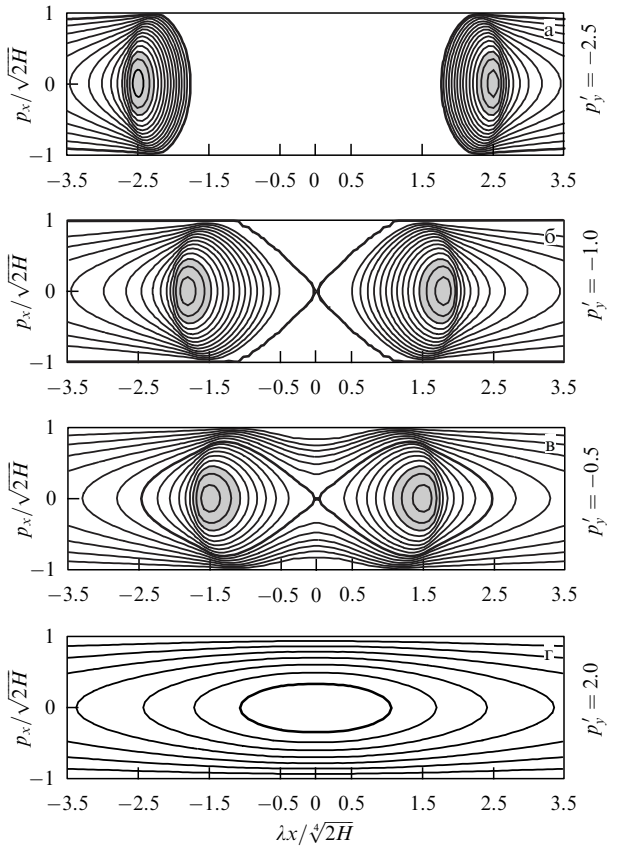

Figure 15. Phase portrait in the plane of slow variables for four values of the momentum p_y' for the system with Hamiltonian (13).

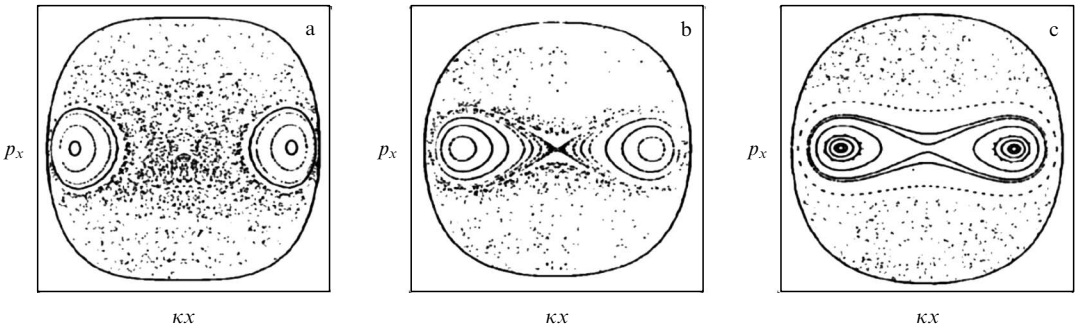

Figure 16. Poincaré sections for three values of the momentum p_y' for the system with Hamiltonian (13). (From Ref. [83].)

If $p_y' > 1$, then the condition $\chi/\sqrt{2H} - p_y' > 0$ is satisfied for $\chi/\sqrt{2H} > 1$. As a result, only those parts of trajectories that correspond to $\chi/\sqrt{2H} > 1$ are projected onto the $(\lambda x, p_x)$ phase plane. These trajectories no longer cross the uncertainty curve, and no separatrix is present in the $(\lambda x, p_x)$ plane (Fig. 15d).

The uncertainty curve corresponding to particle motion along the separatrix in the (z, p_z) plane can also be projected onto the $(\lambda x, p_x)$ plane from the $(\kappa x, p_x)$ plane, where the uncertainty curve is represented by the semicircle $(\kappa x)^2 + p_x^2 = 2H$, $\kappa x > 0$. In this case, the uncertainty curve in the $(\lambda x, p_x)$ plane is represented by two arcs of circles touching two regions with regular trajectories (indicated by dark lines). As a result, the trajectories that are inside the region around $x = 0$ bounded by these arcs do not cross the separatrix in the (z, p_z) plane.

For the system under consideration, Poincaré sections were constructed in Ref. [83] for three values of p_y'. For this, an ensemble of trajectories is calculated and, when a trajectory crosses the $z = 0$ plane, the position of the particle in the $(\lambda x, p_x)$ plane is marked. Figure 16a corresponds to the case where no trajectories crossing the straight line $x = 0$ and not crossing the uncertainty curve are present in the plane of slow variables. As a result, the region with $x \sim 0$ is filled with points scattered about chaotically. Figure 16c corresponds to a system with trajectories that do not cross the uncertainty curve but pass through $x = 0$ (in the plane of slow variables, undestroyed trajectories are seen passing from the half-space $x > 0$ into the half-space $x < 0$). In all the Poincaré sections, we can clearly see the region of regular motion (closed curves) indicated in Fig. 15 by dark lines. We can also see the region of stochastic motion filled with isolated points in space. The formation of this region is related to the existence of jumps of the quasiadiabatic invariant I_z. The particles on open orbits fill the space around the regular region chaotically because of the random nature of the jump ΔI_z (see Section 3.2 and Appendix A).

The dynamics of a particle in the vicinity of an O-line are described by the Hamiltonian obtained from (13) by replacing the minus sign with the plus sign in front of the summand $(1/2)\lambda^2 x^2$:

$$H = \frac{1}{2}\,p_x^2 + \frac{1}{2}\,p_z^2 + \frac{1}{2}\left(p_y - \frac{1}{2}\,\lambda^2 x^2 - \frac{1}{2}\,z^2\right)^2. \qquad (14)$$

Motion in the plane of fast variables in this case differs in no way from motion of the system considered above. But we now have $\lambda x = \pm(8H)^{1/4} \times (p_y' - \chi/\sqrt{2H})^{1/2}$, and the phase portrait in the plane of slow motion looks different (Fig. 17): all

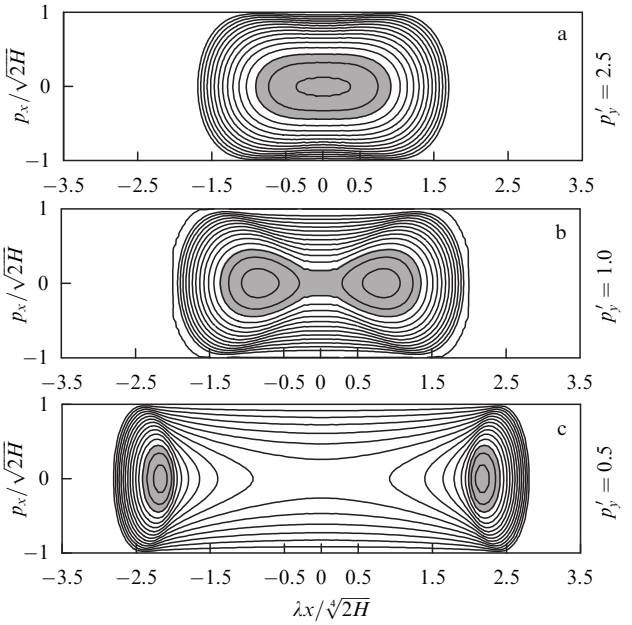

Figure 17. Phase portrait in plane of slow variables for three values of the momentum p_y' for the system with Hamiltonian (14).

the trajectories cross the vertical straight line $x = 0$ at quite large values of p_y'.

Thus, the problems with both the X-lines and the O-lines can be treated analytically based on the quasiadiabatic description if the configuration remains elongated ($\lambda \ll 1$).

4.3 Particle dynamics in a bifurcated current sheet

This section is devoted to charged particle dynamics in a bifurcated current sheet. We consider the case of total bifurcation, when not only the magnetic field component B_x but also the current density $j_y \sim \partial B_x/\partial z$ vanishes in the $z = 0$ plane. In this case, $b_x = (z/L_z)^3$ and $a_y = \kappa x - (1/4)\,z^4/L_z^3$. We introduce the spatial scale $l_0 = (L_z^3 \rho_0)^{1/4}$ and represent Hamiltonian (2) in the form

$$H = \frac{1}{2}\,p_x^2 + \frac{1}{2}\,p_z^2 + \frac{1}{2}\left(\kappa_{\rm bif}\,x - \frac{1}{4}\,z^4\right)^2. \qquad (15)$$

In this case, $\kappa_{\rm bif} = (B_z/B_0) \times (L/\rho_0)^{3/4}$ and, as before, this parameter can be considered the small parameter of our problem, $\kappa_{\rm bif} \ll 1$.

The level lines of the Hamiltonian $h_z = H - (1/2)\,p_x^2$ in the plane of fast motion are shown for $\kappa_{\rm bif} x > 0$ in Fig. 18. We see from the figure that the singular point (0, 0), unlike the

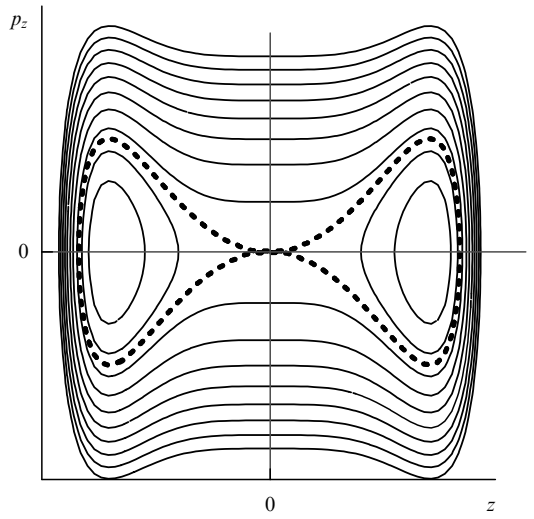

Figure 18. Phase portrait of fast motion for the system with the Hamiltonian $h_z = (1/2)\,p_z^2 + (1/2)\,(\kappa_{\rm bif}\,x - (1/4)\,z^4)^2$.

point (0, 0) in the problem considered in Section 3.1 (Figs 4b, c), is degenerate, i.e., the separatrices approach this point at a zero angle. In the case of such a system, the formulas obtained in Sections 4.1 and 4.2 for the invariant I_z and the jump ΔI_z are no longer valid.

We consider the quasiadiabatic approximation for the system with a degenerate singular point. We can define I_z as $(1/2\pi)(2h_z)^{5/8} f_{\rm bif}(s)$, where $s = \kappa_{\rm bif}\,x/\sqrt{2h_z} > 1$ and

$$f_{\rm bif}(s) = \alpha \int_{z_-}^{z_+} \sqrt{1 - \left(s - \frac{1}{4}\,z'^4\right)^2}\,{\rm d}z' .$$

Here, $z_\pm$ are roots of the equation $(s - z_\pm^4/4)^2 = 1$. The coefficient is $\alpha = 2$ if the particle is in one of the closed loops of the separatrix and $\alpha = 1$ if the particle is in a region that is external with respect to the separatrix. As we can see from the plots of the functions $f_{\rm bif}(s)$ and $f(s)$ taken from Section 3.1 and presented in Fig. 19a, as s increases, $f_{\rm bif}(s)$ decreases faster than $f(s)$, and the maximum value of $f_{\rm bif}(s)$ is smaller than the maximum value of $f(s)$.

Particle trajectories in the plane of slow variables $(\kappa_{\rm bif}x, p_x)$, defined as level lines of $I_z = I_z(\kappa_{\rm bif}x, p_x)$ (Fig. 19b), have a structure similar to the structure of trajectories in the system with Hamiltonian (4), depicted in Fig. 6a.

Comparison of Figs 6a and 19b permits noting that the region occupied by regular trajectories (shown by dark lines) is larger in the case of the system with the degenerate singular point. To verify this, we find the areas $S^{\rm reg}$ and $S^{\rm reg}_{\rm bif}$ of the regions occupied by the relevant trajectories in the respective planes $(\kappa_{\rm bif}x, p_x)$ and $(\kappa x, p_x)$. The boundary of the region with regular trajectories is the curve $I_z^{\rm reg} = {\rm const}$ that touches the uncertainty curve $2H = p_x^2 + (\kappa_{\rm bif}x)^2$ at the point $\kappa_{\rm bif}x = \sqrt{2H}$ (similarly to the case of a classical current sheet with κ). The respective values of the quasiadiabatic invariant are $I_z^{\rm reg} = S^*_{\rm bif}/2\pi$ and $I_z^{\rm reg} = S^*/2\pi$, where $S^*_{\rm bif} = (2H)^{5/8} f_{\rm bif}(1)$ and $S^* = (2H)^{3/4} f(1)$. Calculations yield $S^*_{\rm bif} = 2^{-1/4}(2H)^{5/8} B(3/4, 3/2)$ and $S^* = (2^{5/2}/3)(2H)^{3/4}$, where B is the beta-function. Hence, the area $S^{\rm reg}_{\rm bif}$ can be defined as the integral $\oint p_x\,{\rm d}\kappa_{\rm bif}x$, where $p_x(\kappa_{\rm bif}x)$ is defined by the relations

$$\begin{aligned} &(2H - p_x^2)^{5/8} f_{\rm bif}\left(\frac{\kappa_{\rm bif}\,x}{\sqrt{2H - p_x^2}}\right) = S^*_{\rm bif}\,, \\ &(2H - p_x^2)^{3/4} f\left(\frac{\kappa x}{\sqrt{2H - p_x^2}}\right) = S^*\,. \end{aligned} \qquad (16)$$

(and similarly for $S^{\rm reg}$). Finding $p_x(\kappa_{\rm bif}x)$ and calculating the integrals, we obtain $S^{\rm reg}_{\rm bif} \approx 0.64\pi$ and $S^{\rm reg} \approx 0.19\pi$. Hence, the phase space occupied by regular trajectories is more than three times larger in the system with a degenerate singular point than in the system with Hamiltonian (4).

The following asymptotic formula for a jump in the quasiadiabatic invariant in the system with a degenerate singular point was obtained in Ref. [84] (see also Ref. [85] and Appendix B):

$$\Delta I_z = -(\kappa_{\rm bif}\,p_x^*)^{3/4}(\kappa_{\rm bif}x^*)^{-1/16} C(\xi)\,.$$

Here, p_x^* and $\kappa_{\rm bif}x^*$ are values of the momentum and coordinate at a separatrix crossing point, ξ is a variable that has the same meaning as for a current sheet without bifurcation (see Appendix A), and $C(\xi) = C_1(\xi) + (1/\sqrt{2})\,C_1(1 - \xi)$, where $C_1(\xi)$ is given by the formula (see Appendix B)

$$C_1(\xi) = \frac{2^{-11/16}}{\pi^{5/8}\sqrt{\Gamma(1/4)}} \int_0^\infty \left[\frac{1}{t} - \frac{\exp(-\xi t)}{1 - \exp(-t)}\right] \frac{{\rm d}t}{t^{3/4}}\,.$$

As in the case of the system with Hamiltonian (4), the mean value $\langle \Delta I_z \rangle_\xi = 0$.

If we introduce the dimensionless quasiadiabatic invariant $I = \tilde{C} I_z / H^{5/8}$, where $\tilde{C} = 2^{3/8}\pi B^{-1}(3/4, 3/2)$, the expression for the jump of the invariant can be rewritten as

$$\Delta I = -\kappa^{3/4}(1 - I^{8/5})^{3/8}\, I^{-1/20} C'(\xi)\,.$$

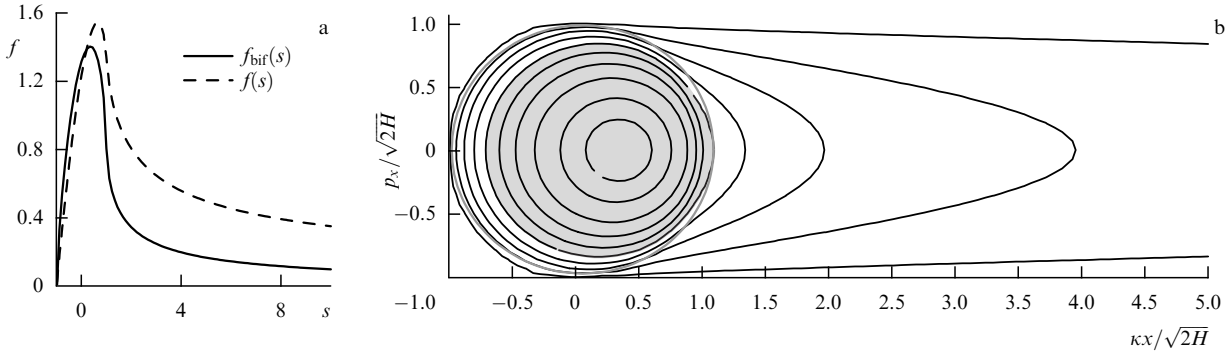

Figure 19. (a) The functions $f_{\rm bif}(s)$ and $f(s)$. (b) Trajectories of particles in the plane of slow variables $(\kappa_{\rm bif}x, p_x)$ for the system with Hamiltonian (15).

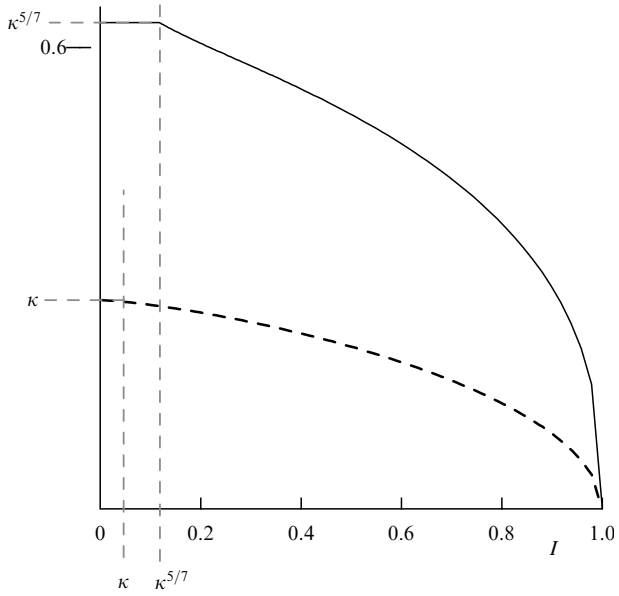

Figure 20. Dependences of the jump in the invariant, ΔI, on the value of the invariant I for the system with Hamiltonian (15) (solid curve) and the system with Hamiltonian (4) (dashed curve).

Here, $C'(\xi)$ differs from $C(\xi)$ by the presence of a constant factor (see Appendix B). If $I < \kappa_{\text{bif}}^{5/7}$, the last formula is no longer applicable and it is only possible to obtain the scaling $\Delta I \sim \kappa_{\text{bif}}^{5/7}$ (see Ref. [84]). The dependences of ΔI for the system with Hamiltonian (4) and for the system with a degenerate singular point with Hamiltonian (15) are presented in Fig. 20.

As can be seen from Fig. 20, jumps of the quasiadiabatic invariant in a current sheet with a degenerate singular point are larger, $\Delta I_z \sim \kappa_{\text{bif}}^{3/4}$, than in an ordinary current sheet, $\Delta I_z \sim \kappa$. Hence, the particle scattering rate in bifurcated sheets should be higher. This result is confirmed by numerical simulations [86, 87].

4.4 Particle dynamics in a sheet with a guiding magnetic field component

In this section, we consider particle dynamics in a current sheet with $B_y = \text{const} \neq 0$, i.e., with a magnetic field $\mathbf{B} = B_0(z/L)\,\mathbf{e}_x + B_y\mathbf{e}_y + B_z\mathbf{e}_z$. The vector potential corresponding to the magnetic field of such a current sheet has two components: $\mathbf{A}/B_0 l_0 = (\kappa x - z^2/2)\,\mathbf{e}_y + b_s z\mathbf{e}_x$, where $b_s = (B_y/B_0)\sqrt{L/\rho_0}$. For current sheets of Earth's magnetotail, $b_s \leqslant 1$, while for current sheets of the magnetopause, the cases where $b_s > 1$ are possible. The Hamiltonian of a charged particle in such a system is given by

$$H = \frac{1}{2}\,p_z^2 + U(p_x, \kappa x, z)\,,$$
$$U = \frac{1}{2}\,(p_x - b_s z)^2 + \frac{1}{2}\left(\kappa x - \frac{1}{2}\,z^2\right)^2. \qquad (17)$$

It follows from (17) that the system under consideration, unlike the system with Hamiltonian (4), does not have the symmetry $z \to -z$. However, Hamiltonian (17) preserves its form under the transformation $z \to -z$, $p_x \to -p_x$.

The potential energy U in (17) now depends on three parameters: κx, b_s, and p_x. As seen from Fig. 21, the two potential wells that originate in the system, unlike such wells in the case of the system with Hamiltonian (4), can differ in shape. That is, the loops of the separatrix of such a system are asymmetric. Therefore, in passing from the external region to one of the loops, the quasiadiabatic invariant experiences so-called geometric jumps, related to a change in the area bounded by the trajectory. For the system with Hamiltonian (4), we could redefine $\hat{I}_z$ so as to avoid geometric jumps (because the loops were symmetric and the total area bounded by the separatrix was always twice the area of one of the loops), but this can no longer be done because of the difference between the areas of the right and left loops.

We next consider the system in the quasiadiabatic approximation: we neglect dynamic jumps of the invariant related to transitions across the separatrix (see Appendix A), and discuss the role of geometric jumps.

In a transition between the wells, a particle can change the value of the quasiadiabatic invariant by a quantity of the order of unity (a quantity independent of κ). Geometric jumps of $\hat{I}_z$, like dynamic ones, occur when a particle crosses the uncertainty curve. Precisely at this moment the particle can change the potential well in which it oscillates (can undergo a transition from a loop of the separatrix to the external region or to another loop or from the external region to one of the separatrix loops). In the problem with $b_s = 0$, only transitions from the external region to one of the separatrix loops and from a separatrix loop to the external region are possible, but now, because of the asymmetry of the loops and to the asynchronicity in their evolution, transitions are possible with the change of slow variables from one separatrix loop to another. These transitions proceed as follows: at one period of fast motion, particle crosses the separatrix twice: the first time when it leaves the loop and passes to the external region, and the second time when it undergoes a transition from the external region to another loop.

In this case, a geometric jump occurs, which implies a change in the invariant $\hat{I}_z$. As a result, the trajectory on the uncertainty curve 'splits' into two, and several such bifurcation points can exist. This means that in the plane of slow variables $(\kappa x, p_x)$, the same trajectory can have several values of the quasiadiabatic invariant corresponding to it. But because the Hamiltonian is invariant under the transformation $z \to -z$, $p_x \to -p_x$, the number of bifurcation points for each value of b_s is finite.

When speaking of bifurcation of a trajectory, we do not mean that the trajectory of a real particle actually splits into two. We mean that at each bifurcation point, the particle can move along one of the two possible trajectories. The choice of a concrete trajectory among the set of possible versions is a probabilistic problem. This means that the probability of transition to one of the two possible loops (or one loop and the external region) on the uncertainty curve can be determined in terms of the rates at which the areas of the given loops undergo changes (in the case of the external region, this rate equals the total rate with which areas of both loops change, taken with the opposite sign) (see Ref. [42]). The probability of transition to one loop or another is defined as the ratio of the change rate of the area of this loop and the total change rate of the area of both loops. If this rate is negative, the particle cannot undergo the transition to the loop considered. If a particle is in a loop with a negative rate (negative probability), it must leave the loop on the uncertainty curve.

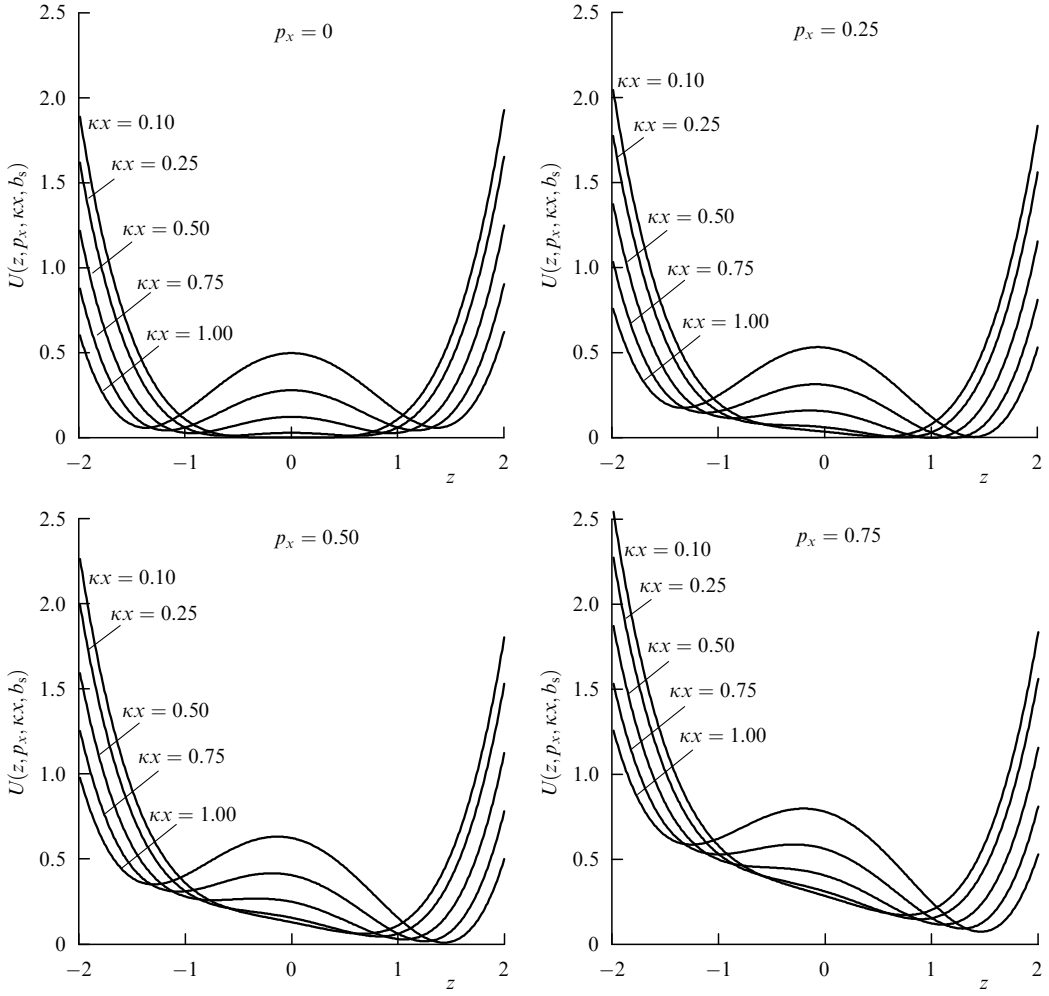

Figure 21. Potential energy U for $b_s = 0.25$ and different values of κx and p_x.

Examples of adiabatic trajectories in the $(\kappa x, p_x)$ plane are shown for different b_s values in Fig. 22. The trajectories were determined as follows. The trajectory of a particle that started from a certain point in the plane of slow variables was calculated numerically in accordance with the equation $I_z(\kappa x, p_x) = \text{const}$. Then, when the particle reached the uncertainty curve, the calculation was stopped, provisionally. For this point on the uncertainty curve, the change rates were calculated for the areas bounded by the separatrix loops and, thus, the trajectories (loops) along which the particle could continue motion were established. Then, in each loop with an increasing area, a new trajectory $I_z(\kappa x, p_x) = \text{const}$ was launched.

In Fig. 22, regions S, R, L, B, and N are indicated in which the potential energy U has different forms and the particle of a given energy H can undergo oscillations of appropriate types:

- S: either a single potential well exists that occupies the region $z = 0$ or there are two potential wells below the energy level of the particle. As a result, the particle oscillates in the external region about the separatrix in the plane of fast variables, crossing $z = 0$ twice at each turn;
- R and L: the particle can only oscillate in a single potential well, whose bottom is situated to the right or to the left of $z = 0$. No R or L regions are present in the system with $b_s = 0$;
- B: two potential wells exist, in each of which the particle can oscillate;
- N: no solution exists.

We see from Fig. 22 that the trajectory bifurcates on the uncertainty curve. The figure demonstrates all possible trajectories for a particle that at a certain instant occupied a position on the trajectory shown. As can be seen from the figure, the uncertainty curve in the system does not reach the boundaries of the region of motion in the $(\kappa x, p_x)$ plane, unlike the uncertainty curves in Figs 6a and 19b, which are semicircles. As a result, some of the trajectories traverse region $\kappa x < 0$ without crossing the uncertainty curve (i.e., without crossing the separatrix). This new effect is due to the introduction of the field B_y into the system. When B_y is sufficiently large (if $b_s > 1$), the uncertainty curve completely disappears and the system passes to the dynamics without any jumps of $\hat{I}_z$. There is no separatrix in the plane of fast variables in such a system. This means that the system corresponds to the case where the curvature radius of magnetic field lines (in other words, the magnetic field inhomogeneity scale) is greater than the gyroradius of the particle. The limit of such a system, as b_s increases, is a system that can be described in the standard approximation of a guiding center, where the role of the quasiadiabatic invariant is taken by the magnetic moment.

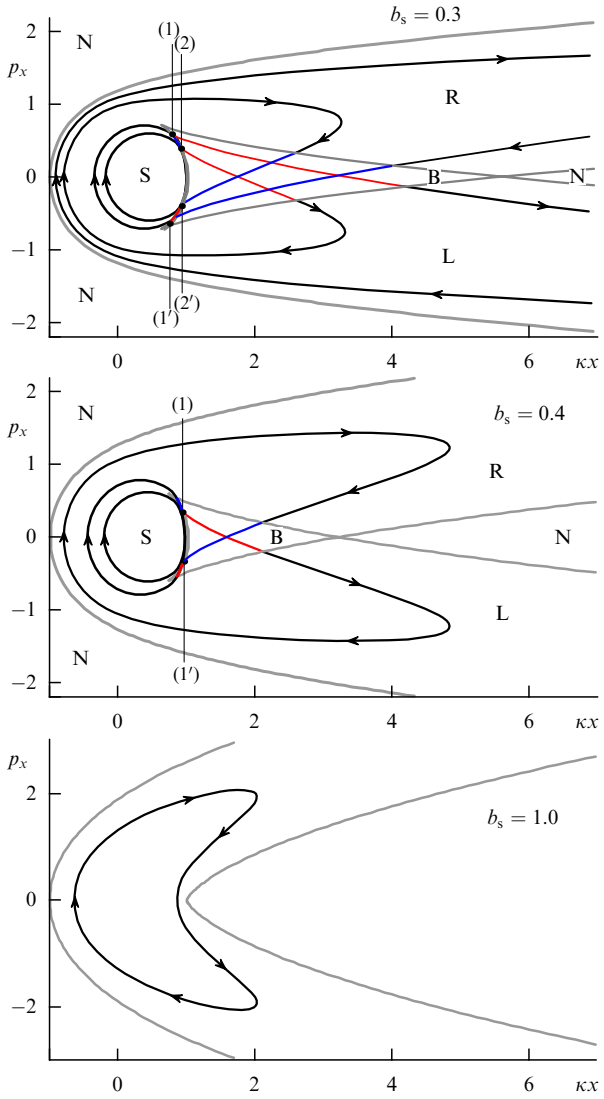

Figure 22. Trajectory of a particle in the $(\kappa x, p_x)$ plane for three b_s values. Light thin curves indicate boundaries of regions with different geometries. The light thick arc is the uncertainty curve. Dark curves show particle trajectories.

Because a real particle chooses one of the two versions of further motion on the uncertainty curve, each trajectory in Fig. 22 for different b_s actually represents a set of trajectories. As a result, in numerical simulations of Hamiltonian equations, we should obtain a trajectory corresponding to only a part of the trajectory shown in Fig. 22. In Fig. 23, the trajectory of a particle in three-dimensional space is presented, which was obtained by straightforward integration of the Hamiltonian equations for (17). In this computation, the value of κ was chosen to be sufficiently small for the trajectory to seem closed (the dynamic jump effect is insignificant). As can be seen from Fig. 23, the particle indeed moves along a part of the quasiadiabatic trajectory shown in Fig. 22.

We note that the actual geometric jumps of the quasiadiabatic invariant that are related to the asymmetry of the loops of the separatrix (owing to the existence of $B_y \neq 0$) are independent of the small parameter κ and therefore give rise to a very rapid change in the invariant [8].

The presence of the field B_y leads to the disappearance of resonance trajectories with jumps, reducing the quasiadiabatic invariant during the first and second crossings of the

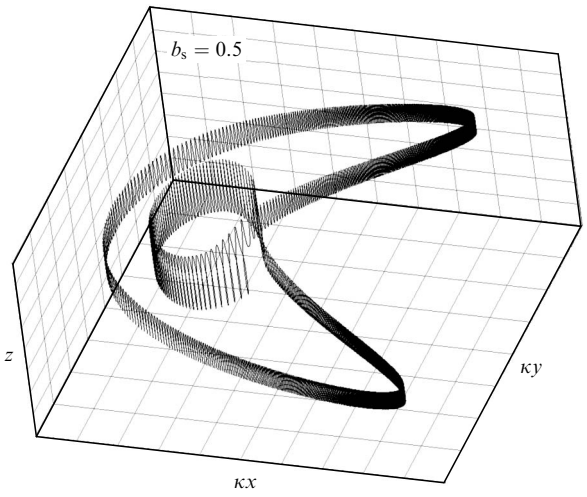

Figure 23. Results of numerical simulations of the trajectory of a particle with Hamiltonian (17).

separatrix. This effect was revealed numerically in Ref. [89]. Furthermore, it can be shown that in the case of a system with asymmetric loops, no stable resonance quasi-trapped trajectories exist [90].

5. Acceleration of charged particles

Quasistationary acceleration of charged particles in current sheets of the tail of Earth's magnetoshpere is primarily related to the presence of a large-scale electric field E_y. We define this field by introducing a vector potential, i.e., consider a curl electric field with $A_y \sim E_y t$. From a formal standpoint, E_y in Earth's magnetotail can be considered an electric field related to interaction of the magnetic field of Earth's dipole with the solar wind flux [23]. But when $E_y = \text{const}$ is substituted in the Hamiltonian, we can use either of the two possible methods for its definition: via the vector potential A_y or via the scalar potential φ, owing to the gauge invariance of A_y and φ [91]. We note that if the field is introduced by means of the scalar potential $\varphi \sim E_y y$, the p_y momentum conservation is violated in the system, but the system remains stationary ($H = \text{const}$). If we use the relation $A_y \sim E_y t$, then $p_y = \text{const}$, but stationarity is violated.

5.1 Quasiadiabatic acceleration with conservation of invariants

In this section, particle acceleration is considered in a system with a magnetic field B_z depending on the coordinate x and in the presence of a constant electric field $E_y = \text{const}$. Here, we assume B_z to be everywhere greater than zero. This problem was discussed in Refs [77, 78, 92]. It must be noted that due to the existence of a gradient $\partial B_z/\partial x$, charged particles drift slowly along y, which leads to an increase in energy in the constant field E_y. Therefore, this acceleration mechanism is an analog of adiabatic acceleration (the betatron mechanism and the Fermi mechanism), for which the existence of the inhomogeneity $\partial B_z/\partial x$ is essential.

The motion of quasiadiabatic ions in two-dimensional geometry is shown schematically in Fig. 24. Because of the presence of a transverse electric field E_y, particles drift slowly toward Earth (this drift, related to the open-endedness of trajectories in the plane of slow motion, is manifested in averaging over the slow motion), arriving to the region of

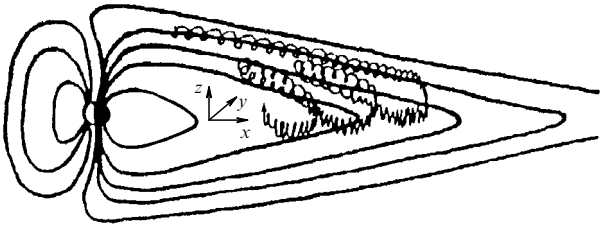

Figure 24. Schematic view of an ion trajectory in the two-dimensional configuration of a current sheet. (From Ref. [93].)

large $B_z(x)$ values. The particles drift in the y direction due to the inhomogeneity of the magnetic field, and their orbits become open-ended.

The Hamiltonian of the system can be obtained by adding the term $-\varepsilon\kappa t$ to $\kappa\chi$ in Hamiltonian (11), where $\varepsilon = cE_y/v_0\bar{B}_z$:

$$H = \frac{1}{2}\,p_\chi^2\beta^2(v\chi) + \frac{1}{2}\,p_z^2 + \frac{1}{2}\left(\kappa\chi - \frac{1}{2}\,z^2 - \varepsilon\kappa t\right)^2 .$$

We make the following change of variables: we consider the quantity $\chi - \varepsilon t$ to be a new variable, keeping the notation χ for it:

$$H = \frac{1}{2}\,p_\chi^2\beta^2\big(v(\chi+\varepsilon t)\big) + \frac{1}{2}\,p_z^2 + \frac{1}{2}\left(\kappa\chi - \frac{1}{2}\,z^2\right)^2 - \varepsilon p_\chi .$$

We also introduce the variable $p_\chi - \varepsilon/\beta^2$ and continue using the notation p_χ for it. This change of variables allows isolating a complete square in the Hamiltonian H and obtaining the following expression for the new Hamiltonian:

$$H = \frac{1}{2}\,p_\chi^2\beta^2\big(v(\chi+\varepsilon t)\big) + \frac{1}{2}\,p_z^2 + \frac{1}{2}\left(\kappa\chi - \frac{1}{2}\,z^2\right)^2 + \frac{1}{2}\,\frac{\varepsilon^2}{\beta^2} . \tag{18}$$

We note that both changes of variables preserve the Hamiltonian form of the equations (see Refs [77, 78]).

We now find the relations between the parameters entering Hamiltonian (18). The parameters κ and v being small allows separating the variables into fast (z, p_z) and slow $(\kappa\chi, p_\chi)$ ones (as in Section 4.1). The electric field E_y determines the evolution time of the system (or the convection time of charged particles toward Earth in the magnetotail). For realistic values of E_y ($E_y < 0.1\,\text{mV m}^{-1}$ (see Ref. [94]), this time significantly exceeds the particle oscillation period in the phase plane of slow variables, and we can assume that $\varepsilon \ll \kappa$. In this case, we obtain a time hierarchy of processes: a particle moves with a velocity ~ 1 in the (z, p_z) plane and with a velocity $\sim \kappa$ in the $(\kappa\chi, p_\chi)$ plane, and the trajectory of the particle with a velocity $\sim v\varepsilon$ undergoes evolution in the $(\kappa\chi, p_\chi)$ plane. In the first approximation in ε, we can therefore neglect the term $\sim \varepsilon^2$ in Hamiltonian (18).

For this system, similarly to how this was done in Section 4.1, we can introduce a quasiadiabatic invariant, when I_z is 'frozen' (and at a 'frozen' time εt), by the formulas given in Section 3.1. The Hamiltonian of fast motion, h_z, in this system has the form

$$h_z = \frac{1}{2}\,p_z^2 + \frac{1}{2}\left(\kappa\chi - \frac{1}{2}\,z^2\right)^2 .$$

Correspondingly, $I_z = I_z(h_z, \kappa\chi) = (1/2\pi)(2h_z)^{3/4} f(s)$, where $s = \kappa\chi/\sqrt{2h_z}$. Hence, the quasiadiabatic invariant and the phase portrait in the (z, p_z) plane for the system are similar to the those discussed in Section 4.1. The Hamiltonian of slow motion then takes the form

$$H = \frac{1}{2}\,p_\chi^2\beta^2\big(v(\chi+\varepsilon t)\big) + h_z(I_z, \kappa\chi) .$$

This Hamiltonian describes a system with 1.5 degrees of freedom. This means that in the case of a frozen time εt, the problem is integrable. The corresponding results in the case of $\varepsilon t = \text{const}$ are presented in Section 4.1.

We investigate the slow evolution of the system related to a change in the time εt. In the $(\kappa\chi, p_\chi\beta)$ plane (and in its corresponding $(\kappa x, p_x)$ plane [see Figs 11, 12]), the trajectories of the system can be considered closed at time scales of $1/\kappa$ and their evolution is slow, and we can therefore introduce one more quasiadiabatic invariant

$$I_\chi = \frac{1}{2\pi}\oint p_\chi\,\mathrm{d}\chi .$$

We note that I_χ is an analog of the second (longitudinal) adiabatic invariant in the classical theory of motion of a guiding center. We describe the evolution of the system taking the conservation of I_z and I_χ into account. For this, we divide the trajectories in the $(\kappa\chi, p_\chi)$ plane into two groups: trajectories that do not cross the uncertainty curve (the region occupied by these trajectories is shown by dark lines in Figs 6a, 11, 12) and trajectories crossing the uncertainty curve and, consequently, the separatrix in the (z, p_z) plane.

5.1.1 Acceleration of particles not crossing the separatrix. For the group of particles whose trajectories do not cross the separatrix, $I_z = I_z(h_z, \kappa\chi)$ and $I_\chi = I_\chi(H, \varepsilon t, I_z)$ are conserved with a high precision. Therefore, motion in the $(H, \varepsilon t)$ plane is determined by the equation $I_\chi = \text{const}$, and a particle moves in the $(\kappa\chi, p_\chi)$ plane along phase curves $I_z = \text{const}$, which undergo deformation with time. To illustrate this assertion, we consider the phase portrait of the system constructed for a fixed value of I_z (Fig. 25). In the case of a fixed value of I_z, the uncertainty curve that at a fixed energy H was a semicircle in the plane of slow variables is now determined by the equation of the straight line $\kappa x = \kappa x^* = (3\pi I_z/8)^{2/3}$ [77]. As the energy H increases, the trajectory approaches the uncertainty curve closer and closer (such a typical trajectory is shown in Fig. 25 for $H = H_2$).

This motion in the plane of physical variables $(\kappa x, p_x)$ corresponds to the situation where a particle undergoes transition from one trajectory to another, i.e., a drift over the phase portrait occurs, corresponding to a drift over energy:

$$\frac{\partial H}{\partial t} = \left\langle p_\chi^2\beta\big(v(\chi+\varepsilon t)\big)\,\frac{\partial\beta}{\partial t}\right\rangle = \varepsilon v\left\langle p_\chi^2\beta\,\frac{\partial\beta}{\partial v\chi}\right\rangle .$$

Here, the operator $\langle\ldots\rangle$ stands for time averaging over the period of slow particle motion in the $(\kappa\chi, p_\chi\beta)$ plane. Because $\partial\beta/\partial v\chi > 0$ (which follows from the positivity of the gradient $\partial B_z/\partial x$), the particle energy increases with time. At a certain instant, the particle therefore acquires a sufficiently high energy for its trajectory to cross the uncertainty curve.

We obtain the expression describing the increase in the energy of a particle with time until the moment it arrives at the

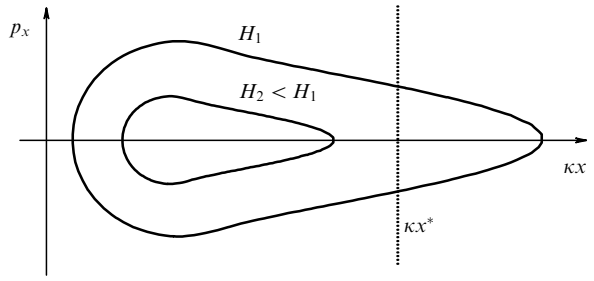

Figure 25. Phase portrait of a system with a constant value of the invariant I_z for different values of the energy H. The vertical straight line represents the uncertainty curve.

uncertainty curve. For this, we write

$$I_\chi = \frac{1}{2\pi}\oint \frac{\sqrt{2H-2h_z}}{\beta\bigl(v(\chi+\varepsilon t)\bigr)}\,\mathrm{d}\chi = \frac{1}{2\pi}\oint \frac{\sqrt{2H-\bigl(2\pi I_z/f(s)\bigr)^{4/3}}}{\beta\bigl(v(\chi+\varepsilon t)\bigr)}\,\mathrm{d}\chi$$

and pass to the integration variable $s=\kappa\chi/\sqrt{2h_z}=\kappa\chi(2\pi I_z/f(s))^{-2/3}$:

$$I_\chi = \frac{1}{2\pi\kappa}\oint \beta^{-1}\left(\frac{v}{\kappa}\,s\left(\frac{2\pi I_z}{f(s)}\right)^{2/3}+v\varepsilon t\right) \times\sqrt{2H-\left(\frac{2\pi I_z}{f(s)}\right)^{4/3}}\left(\frac{2\pi I_z}{f(s)}\right)^{2/3}\left(1-\frac{2sf'(s)}{3f(s)}\right)\mathrm{d}s\,.$$

The dependence of the energy H on the time εt is determined from the equation $I_\chi(H,\varepsilon t)=\text{const}$. If a particle is deep inside the region of regular trajectories (far from the uncertainty curve), its quasiadiabatic invariant I_z is close to its maximum value $I_{z,\max}=2\pi(2H)^{3/4}f_{\max}$. Using the dimensionless quasiadiabatic invariant $I'=I_z/I_{z,\max}$, we obtain

$$I_\chi \approx \frac{H}{\pi\kappa\langle\beta\rangle}\oint\sqrt{1-\left(\frac{I'f_{\max}}{f(s)}\right)^{4/3}} \times\left(\frac{I'f_{\max}}{f(s)}\right)^{2/3}\left(1-\frac{2sf'(s)}{3f(s)}\right)\mathrm{d}s\,,$$

where $\langle\beta\rangle$ is the mean value of β taken outside the integrand. Such an operation can be performed because the range of s is sufficiently small (the value of I' is close to unity) and, consequently, β varies weakly in the integrand. Therefore, the invariant I_χ is a function of two variables: I' and $H/\langle\beta\rangle$. As a result, from the relations $I_\chi=\text{const}$ and $I_z=\text{const}$, we obtain an expression that describes the increase in energy with β: $H\sim\kappa\beta$. It is appropriate here to point to the analogy with the betatron acceleration of magnetized particles, for which the particle energy component perpendicular to the magnetic field increases linearly with the magnetic field because of the magnetic moment conservation (see Refs [12, 92]). However, it must be noted that in the case of each concrete particle, the relation obtained is valid during a limited period of time. As the energy increases, the particle approaches the uncertainty curve, and the approximations used become inapplicable.

We now obtain the relation for the time t^* in which a particle reaches the uncertainty curve. The time t^* is determined by matching the value of the quasiadiabatic invariant at the initial moment, $I_\chi(H_0,\varepsilon t_0)$ (H_0 is the particle energy at the initial moment), to its value on the uncertainty curve $I_\chi(H^*,\varepsilon t^*)$ (H^* is the energy corresponding to the uncertainty curve). The quantity H^* can be obtained from the relation

$$I_z=\frac{1}{2\pi}\,(2H^*)^{3/4}f(1)=\frac{8}{3\pi}\,(2H^*)^{3/4}\,.$$

Hence, $H^*=(1/2)(3\pi I_z/8)^{4/3}=(1/2)(\kappa x^*)^2$.

We consider the case where the parameter v is quite small, and changes in the quantity $(\kappa\chi,\ \beta p_\chi)$ during a single turn in the $\beta(v(x+\varepsilon t))$ plane can be neglected:

$$2\pi I_\chi=\oint\frac{p_\chi\beta}{\beta}\,\mathrm{d}\chi=\frac{1}{\langle\beta\rangle\kappa}\oint p_\chi\beta\,\mathrm{d}\kappa\chi=\frac{S}{\langle\beta\rangle\kappa}\,,$$

where S is the area bounded by the corresponding trajectory in the $(\kappa\chi,\beta p_\chi)$ plane. Hence, we can find an expression for t^*:

$$\beta(v\varepsilon t^*)=\beta(v\varepsilon t_0)\,\frac{S^*}{S_0}\,, \tag{19}$$

where S_0 is the area within the trajectory at the initial moment, S^* is the area within the trajectory at the moment when the trajectory reaches the uncertainty curve (for any given trajectory, S_0 is a quantity uniquely defined by the energy and the invariant I_z at the initial moment). Thus, we have determined the time required for the particle to leave the acceleration mode corresponding to its motion before crossing the separatrix.

We note that because the motion before crossing the separatrix involves an increase in the energy $H\sim\kappa\beta$, reaching the separatrix signifies that the particle has attained the energy $H/H_0\approx S^*/S_0$, where H_0 is the initial energy.

5.1.2 Acceleration of particles crossing the separatrix. In its motion in the region in which crossing of the uncertainty curve occurs, a particle regularly crosses the separatrix. As a result, jumps of the quasiadiabatic invariant I_z occur periodically (see Section 4.1 and Appendix A). The quantity I_χ also experiences jumps, synchronized with the jumps of I_z: $\Delta I_\chi=(\partial I_\chi/\partial I_z)\,\Delta I_z$. Consequently, the behavior of a particle at long times depends on the ratio of the jump values and the drift in the phase plane of slow variables.

As was noted in Section 3.2, the time required for the quasiadiabatic invariant I_z to undergo a change of the order of unity due to diffusion is $\sim 1/\kappa^3$. The time of slow drift in the phase plane due to the electric field is determined by the quantity $1/v\varepsilon$. Therefore, the particle dynamics depend on the relation $\delta=\kappa^3/v\varepsilon$. If $\delta\ll 1$, the drift time is much shorter than the diffusion time, and the dynamics of the particle are determined by the drift (jumps in the invariant represent background phenomena in this case). If $\delta\gg 1$, the diffusion of particles in the space of invariants becomes the main process.

In this section, we consider the limit in which jumps of the invariant can be neglected. In this case, the problem can be integrated as this was done above: averaging over z-oscillations yields a Hamiltonian with 1.5 degrees of freedom, and, if the smallness of ε is used, the problem becomes completely integrable. But analytic expressions for the increase in energy with time can be obtained only if $I_z\ll 1$. Small values of I_z correspond to trajectories leading from the $z=0$ plane. Hence, particles on such trajectories spend most of their time far from the $z=0$ plane [i.e., particle motion corresponds to motion in one of the separatrix loops (Figs 4b, c)].

The coordinates of the bottoms of potential wells of the two inner regions in the (z, p_z) plane are $\pm\sqrt{2\kappa\chi}$ (the minima of the potential energy $U = (1/2)(\kappa\chi - (1/2)z^2)^2$).

We expand Hamiltonian (18) around the position of the bottom of one of the potential wells. For this, we introduce a variable equal to the deviation of the coordinate z from the value $-\sqrt{2\kappa\chi}$ and let $\tilde{z} = z + \sqrt{2\kappa\chi}$ denote this new variable. Expanding the Hamiltonian in $\tilde{z}$ yields the expression

$$H = \frac{1}{2}p_\chi^2\beta^2 + \frac{1}{2}p_z^2 + \kappa\chi\tilde{z}^2 .$$

The obtained Hamiltonian describes a system representing a harmonic oscillator with the variable frequency $\omega(\chi) = \sqrt{2\kappa\chi}$. Then the Hamiltonian of fast motion represents the harmonic oscillator energy:

$$h_z = \frac{1}{2}p_z^2 + \frac{1}{2}\tilde{z}^2\omega^2(\chi) .$$

The quasiadiabatic invariant can also be written as

$$I_\chi = \frac{1}{\pi}\int_0^{\chi_{\max}} \frac{1}{\beta}\sqrt{2H - I_z\sqrt{8\kappa\chi}}\,\mathrm{d}\chi .$$

Here, the lower integration limit is set equal to zero, although, strictly speaking, we must integrate not from zero but from a certain value $\chi_{\min}$ determined by the condition $p_\chi(\chi_{\min}) = 0$. But we see from Fig. 6a that the area inside the curve $I_z = \text{const}$ for $I_z \ll 1$ is mainly determined by the region of large χ.

We now introduce the variable $\chi' = \sqrt{2\kappa\chi}\,I_z/H$. Then

$$I_\chi = \frac{\sqrt{2}\,H^{5/2}}{\pi\kappa I_z^2}\int_0^{\chi'_{\max}} \frac{\chi'}{\beta}\sqrt{1-\chi'}\,\mathrm{d}\chi' .$$

Introducing the mean value of β for a single turn in the plane of slow variables, $\langle\beta\rangle$, we obtain

$$\frac{\sqrt{2}\,H^{5/2}}{\pi\kappa I_z^2\langle\beta\rangle} = \text{const} .$$

Hence follows the acceleration law for particles with small I_z: the energy of such particles increases as $H \sim (\kappa\beta)^{2/5}$. This law is similar to the relation obtained in the guiding center theory for the acceleration of adiabatic particles with distant reflection points [92, 95].

We note that a semianalytic expression for the dependence of the particle energy H/H_0 on the magnetic field β can be obtained for an arbitrary value of the invariant I_z.

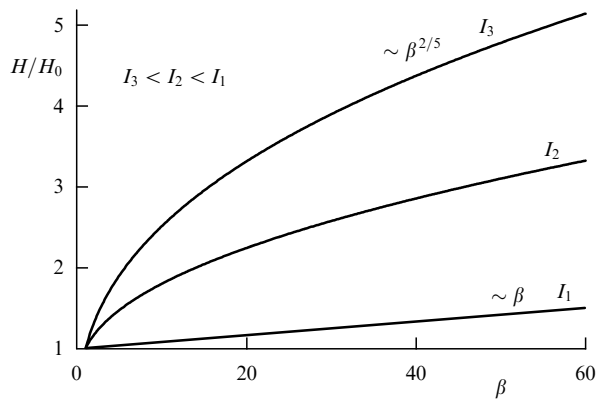

Figure 26. Dependence of the particle energy on β for different values of I_z. (From Ref. [92].)

This expression is an integral relation for I_z, H/H_0, and β. For each I_z, we then obtain a certain function H/H_0 depending on β. An example of such dependences [92] is shown in Fig. 26.

5.2 Resonance effect with the electric field taken into account

As was noted in Section 3.3, for certain values of the parameter κ, a population of resonance particles in the current sheet exists for which the total jump of the quasiadiabatic invariant is zero. Such particles enter the current sheet along the magnetic field lines, experience a half-turn in the field B_z, and leave the current sheet with the same gyrorotation phase value with which they entered it.

We now examine the mechanism of resonance particle acceleration in a current sheet due to the above effect. We adopt the current sheet model with $B_z = B_z(x/L_x)$, but assume that the gradient $\partial B_z/\partial x$ can be neglected on the scale of an ion trajectory in the plane of slow variables. Therefore, we formally consider a set of systems in each of which $B_z \approx \text{const}$. Then, using the argument x corresponds to a trajectory belonging to one configuration or another with its own B_z value. As in Section 4.1, we consider B_z to decrease, as $|x|$ increases, according to a power law. Furthermore, we take into account that a field $B_x \sim z$ can increase linearly only up to the boundaries of the current sheet (until $|z| < L_z$). When $|z| > L_z$, the increase in $B_x(z)$ becomes saturated, $B_x = B_0\,\mathrm{sign}(z)$. Therefore, it is essentially important in the problem considered that particles on transient trajectories exist. The acceleration of precisely such particles is considered in this section.

One of the principal quasistationary mechanisms of charged-particle acceleration in the current sheet of Earth's magnetotail is the acceleration by the 'dawn–dusk' field $E_y \simeq \text{const}$ [34, 96, 97]. Quasiadiabatic ions experiencing a half-turn in the field B_z cover a distance equal to two gyroradii along the field E_y. If a particle does not leave the current sheet because of a jump of the quasiadiabatic invariant, it subsequently loses nearly all its energy gain while making another half-turn in the field B_z at a certain distance from the $z = 0$ plane. By contrast, the resonance particle leaves the current sheet with all the energy it gained and moves along the field lines (Fig. 27).

If the initial energy of particles approaching the current sheet is low compared with the gain in energy, it can be neglected. Then the velocity with which the particle moves in the $z = 0$ plane is approximately cE_y/B_z. The gyroradius of such a particle is c^2E_ym/qB_z^2, while the energy gained is $W \approx 2c^2E_y^2m/B_z^2$. Here, an analogy can be drawn with the elastic interaction of a particle with a moving wall (the current sheet) [98]: in the rest frame of the wall (current sheet), the particle impinges on the current sheet with the velocity $V_x = -cE_y/B_z$ and leaves it with the velocity $V_x = cE_y/B_z$. In the laboratory frame, in which the wall (current sheet) moves with the velocity V_x, the increment of the particle velocity $\Delta V = 2cE_y/B_z$ just corresponds to the velocity of the particle at the final moment; the corresponding energy increment is $W = m(\Delta V)^2/2 = 2c^2E_y^2m/B_z^2$. Therefore, the energy gained is inversely proportional to the square of the quantity $B_z(x/L_x)$.

Because such a coherent acceleration can only be observed in regions with $x = x_N$, where x_N is determined by the relation $\kappa^{-1}(x_N) = N/C_0$ [see formula (10)], it is possible to determine the resonance values of the magnetic field $B_z(x_N/L_x)$. For

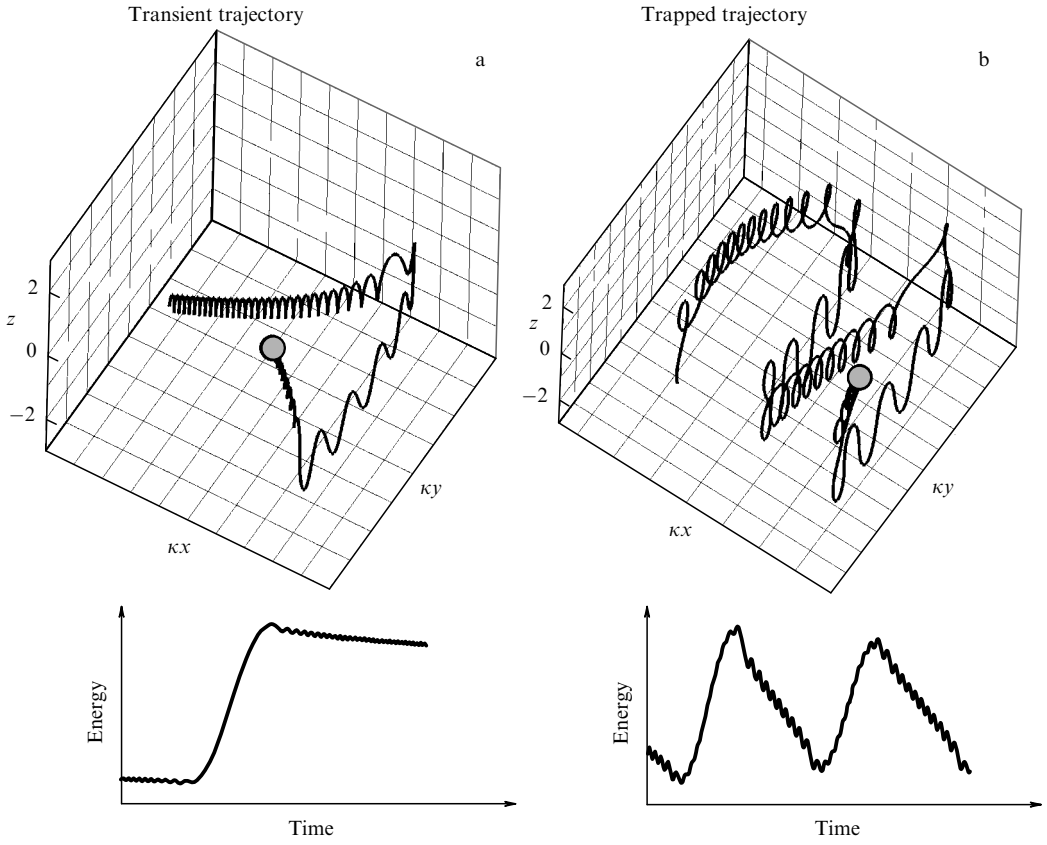

Figure 27. Trajectories of two particles starting from the boundary of the current sheet. (a) Trajectory of a transient particle that leaves the current sheet. (b) Trajectory of a particle captured from a transient orbit to a trapped orbit because of a jump of the quasiadiabatic invariant.

this, we use the definition of κ, taking into account that the particle energy is $W \sim B_z^{-2}$:

$$\kappa = \frac{B_z}{B_0}\sqrt{\frac{L}{\rho_0}} \sim B_z \sqrt[4]{W^{-1}} \sim B_z^{3/2}\,.$$

From the last equation, using the relation $\kappa \sim 1/N$, we obtain an expression for the resonance values of the magnetic field: $B_z(x_N/L_x) \sim N^{-2/3}$. The corresponding resonance energies are $W_N \sim B_z^{-2}(x_N/L_x) \sim N^{4/3}$ [52, 99]. Thus, a system of resonance regions arises along Earth's magnetotail, and as the distance from Earth increases (B_z decreases), the energy gained by particles in these regions increases as $B_z^{-2}(x_N)$ (Fig. 28a).

The existence of a chain of resonance regions results in specific phenomena observed in Earth's magnetotail. Solar-wind protons arrive in the distant magnetotail from a source in the plasma mantle (Fig. 28b). The proton flux from the mantle simultaneously reaches several different resonance regions in the current sheet, where the protons gain different energies corresponding to the number of each of these regions. Beams of accelerated particles then leave the neutral plane of the current sheet and move along magnetic field lines in the plasma sheet boundary layer (PSBL). In the PSBL, the accelerated particles are observed by spacecraft devices as a single or multiple, almost monoenergetic beams [102, 103]. The problem of observing these beams and of their properties is discussed in review [104].

Beams of particles accelerated in different resonances and therefore having different energies then approach the dipole field region. The field lines thicken in this region (the magnetic field strength increases). When crossing the field lines in this region from top down (or, vice versa, from bottom up), a spacecraft may have time to register the whole 'comb' of ion beams accelerated in different resonances along the tail nearly simultaneously. In its motion, when the spacecraft crosses a successive field line, it observes a flow of accelerated particles from the resonance corresponding to this line. As a result, a chain of resonances can show up clearly in the energy–time diagram (Fig. 29a).

The choice of a certain model of the magnetic field in Earth's magnetotail allows reconstructing the considered effect of resonance acceleration. In Refs [52, 107], a two-dimensional model [73] was used in which the tracing of particles was performed for a given electrostatic field E_y. As a result, in the region of assumed observation of energetic dispersion structures, the authors of Refs [52, 107] numerically revealed a chain of resonances in very good agreement with the predictions of analytic theory.

The simulation of particle dynamics in magnetic fields in the framework of global simulation of the structure and dynamics of the magnetosphere by methods of magnetic hydrodynamics is more complicated, but also closer to real conditions. This approach was realized by the authors of Ref. [106] in order to simulate measurements of the chains of resonances observed in experiments. As a result, the structure of accelerated beams obtained from the data of satellite observations was successfully reproduced with good precision (Fig. 29b).

In the framework of analytic theory, an expression was obtained for the energy of accelerated particles depending on the resonance number, $W_N \sim N^{4/3}$. This relation is indepen-

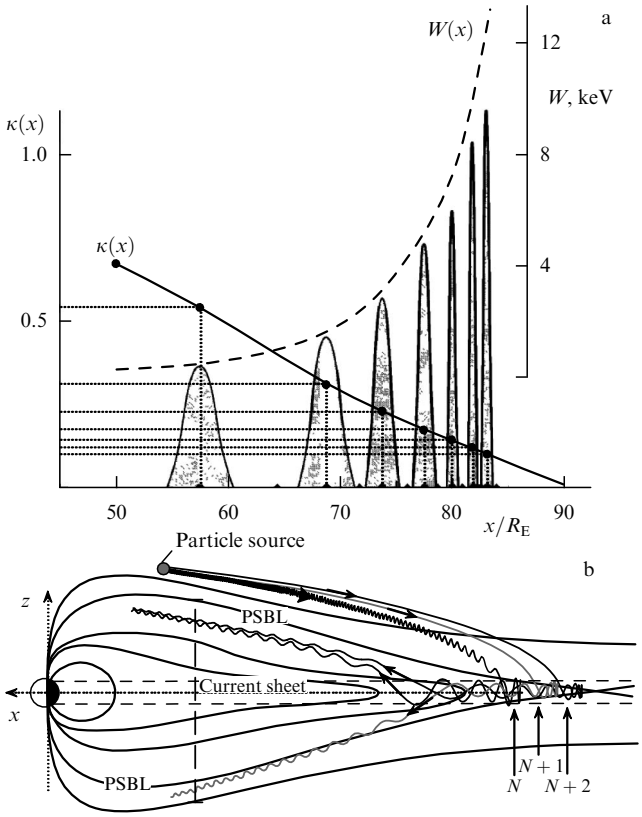

Figure 28. (a) Schematic view of resonance regions in Earth's magnetotail and the corresponding energies W (R_E is Earth's radius) (From Ref. [100].) (b) Schematic of the acceleration and dynamics of ions in the current sheet in Earth's magnetotail. The dashed line shows the observation region of dispersion structures. The vertical arrows schematically indicate the Nth, $(N+1)$th, and $(N+2)$th resonance regions, in which $\kappa \sim 1/N$. (From Ref. [101].)

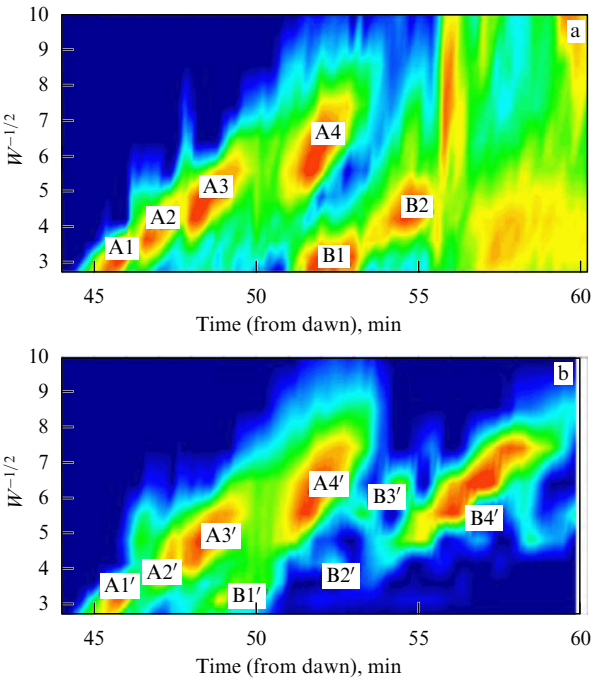

Figure 29. (In color online.) (a) Energy flux of particles with pitch angles 0–60°, observed by the satellite Cluster-1. The chain of resonances A1–A4 and B1, B2 observed by the satellite mission Cluster-1. (From Ref. [105].) (b) Simulated flux of particle energy. Chains of resonances A1′–A4′ and B1′–B4′ obtained by numerical simulation. (From Ref. [106].)

dent of the concrete magnetic field model and can be verified both by numerical simulations and by experimental observations. For this, the dependence of the observed (or simulated) energies $\ln W_N$ on the resonance number $\ln N$ is constructed. The obtained proportionality coefficient, both for the results of numerical simulation in the framework of various models of the magnetic field of Earth's magnetotail and for experimental data, turns out to be close to 4/3 (Fig. 30).

A natural generalization of the theory of resonance acceleration is a nonlinear model in which the current of accelerated particles modulates the magnetic field of the magnetosphere [108]. In the framework of this model, it has been possible to demonstrate that the mechanism of resonance acceleration is quite stable with respect to perturbations of the magnetic field $B_z(x/L_x)$, while nonlinear effects provide an additional specific local dispersion of the energy of resonance beams (differing from the average dispersion of the entire structure). This locally nonlinear effect can also be observed in experimental data (see review [104]).

Moreover, it is shown in Ref. [109] that the coefficient of the linear dependence of $\ln W$ on $\ln N$ can be affected by the ambipolar electric field E_z related to the difference in character of the motions of ions and of electrons in the current sheet.

5.3 Acceleration in the vicinity of X- and O-lines

We now consider charged particle acceleration in configurations with X- and O-lines based on the quasiadiabatic theory, following Refs [40, 78, 82]. Particle dynamics in the configurations considered in the absence of an electric field are described in Section 4.2.

We note that the process of particle acceleration immediately on the X-line (in the region of zero magnetic field) cannot be described in the framework of the considered quasiadiabatic theory. For investigating the energy gain on the X-line, an approach is used that is based on the expansion of the equations of motion in a series in the vicinity of the zero line, neglecting terms of higher orders of smallness. Within this approach, it is possible to obtain the energy of accelerated particles as a function of the system parameters [110–114]. A generalization of this approach to the case of a nonzero field B_y was proposed in Refs [115, 116]. The results obtained are in good agreement with those of numerical simulations [117–119]. But it follows in the framework of this approach that when $E_y = \text{const}$, a particle can be found in the immediate vicinity of the region of zero magnetic field only during a limited time interval (motion in the vicinity of an X-line is unstable with respect to deviations along the x axis; see Refs [110, 118, 120, 121]). When a particle leaves the immediate vicinity of the X-line, it continues its motion along the x axis. A characteristic example of particle trajectories in the vicinity of an X-line is presented in Fig. 31, which shows that the particle can cross the $z = 0$ plane before it approaches the region of zero magnetic field, $x = 0$. After crossing the $z = 0$ plane, the particle moves along the magnetic field lines; here, the particle can either return to the same half-plane from which it arrived (the light trajectory) or go in the opposite direction (the trajectory shown by the dashed line). The dynamics of such particles resemble particle dynamics in the current sheet with $B_z(x/L_x)$. Accordingly, the process of particle acceleration

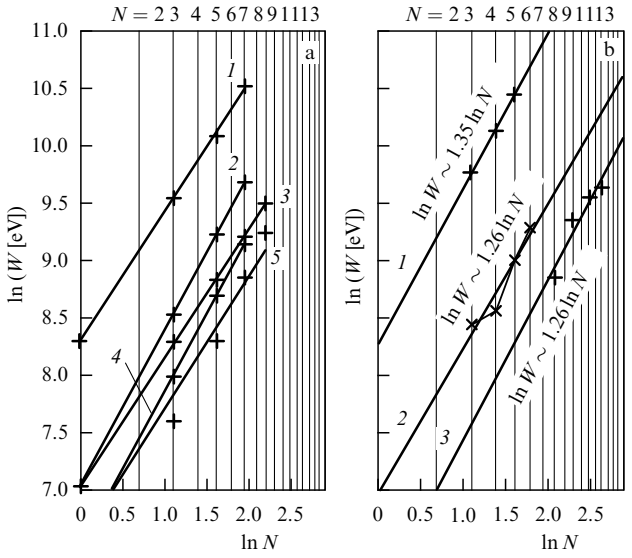

Figure 30. (a) Dependence of energy on the resonance number N obtained by numerical simulation for different configurations of the magnetic field of the current sheet and electric field intensities (see details in Ref. [52]). (b) Results of different observations by spacecraft devices Cluster-1 and Interball (data shown by X's and the corresponding dependence 2 are taken from Ref. [105]). (From Ref. [52].)

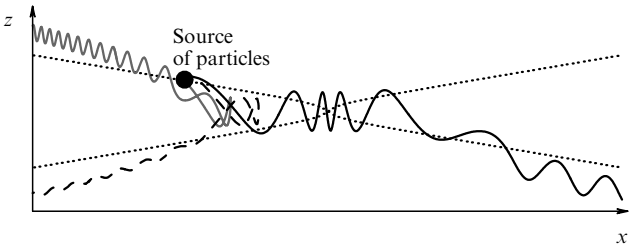

Figure 31. Three possible trajectories (dark, light, and dashed curves) of particles in the (z, x) plane in a system with an X-line. The dotted line shows the magnetic separatrix $\pm x/L_x = z/L_z$.

in the geometry considered is related to the electric field E_y applied to the set of X-lines (O-lines). Under the action of the field E_y, particles are accelerated and leave the X-line (O-line) simultaneously, moving along x in the direction of the increasing magnetic field B_z. As a result, the acceleration mechanism described in Section 5.1 is actually realized, but with specific properties of the magnetic field configuration with X-lines (O-lines). The energy gain in the course of motion is precisely the subject of our investigation.

Similarly to Section 5.1, we introduce a field E_y in the system by means of a vector potential. Here, we define the dimensionless parameter $\varepsilon = cE_y/v_0B_0$ that determines the field amplitude E_y. We introduce a slow time $\tau = \varepsilon t + p_y$ and represent Hamiltonian (13) in the form

$$H = \frac{1}{2}\,p_x^2 + \frac{1}{2}\,p_z^2 + \frac{1}{2}\left(\pm\frac{1}{2}\,\lambda^2 x^2 - \frac{1}{2}\,z^2 - \tau\right)^2 . \qquad (20)$$

The sign of $\lambda^2 x^2$ in the right-hand side of (20) is determined by the geometry of the system: the plus for the X-line and the minus for the O-line. We determine the hierarchy of time scales in the system with Hamiltonian (20). If $\lambda \ll 1$, then motion in the (z, p_z) plane proceeds much faster than motion in the $(\lambda x, p_x)$ plane. We assume that $\varepsilon \ll \lambda$ and that the evolution of the system with time proceeds more slowly than the motion of particles in the $(\lambda x, p_x)$ plane.

With the field E_y, the Hamiltonian of fast motion in Section 4.2 becomes

$$h_z = \frac{1}{2}\,p_z^2 + \frac{1}{2}\left(\pm\frac{1}{2}\,\lambda^2 x^2 - \frac{1}{2}\,z^2 - \tau\right)^2 ,$$

and, as was noted in Section 5.1, motion in the (z, p_z) plane is identical to motion characteristic of the current sheet (see Section 3.1). As a result, we can introduce the quasiadiabatic invariant I_z (see Section 3.1) and use its dimensionless equivalent $I = 3\pi I_z/8(2H)^{3/4}$:

$$I = \left(\frac{h_z}{H}\right)^{3/4} \bar{f}(k) = \left(\frac{h_z}{H}\right)^{3/4} \times \begin{cases} 2(1-k^2)\,K(k) + 2(2k^2-1)\,E(k)\,, & k < 1\,, \\ 2(1-k^2)\,kK\left(\dfrac{1}{k}\right) + (2k^2-1)\,kE\left(\dfrac{1}{k}\right), & k > 1\,. \end{cases}$$

Here,

$$k^2 = \frac{1}{2}\left(1 + \frac{\pm(1/2)\,\lambda^2 x^2 - \tau}{\sqrt{2h_z}}\right).$$

Expressing h_z in terms of I_z and substituting in (20), we obtain the Hamiltonian of slow motion

$$H = \frac{1}{2}\,p_x^2 + h_z\left(I_z, \pm\frac{1}{2}\,\lambda^2 x^2 - \tau\right).$$

In the case of a frozen time τ, the problem becomes integrable. The corresponding phase portraits are presented in Section 4.2. As noted in Section 4.2, particle trajectories can be divided into two groups: those that cross the uncertainty curve (and, consequently, cross the separatrix) and those that do not cross the uncertainty curve. The equation for the uncertainty curve in the $(\lambda x, p_x)$ plane for a system with an X-line (O-line) has the form

$$p_x = \pm\sqrt{2H - \left(\pm\frac{1}{2}\,\lambda^2 x^2 - \tau\right)^2}\,.$$

As in the case of a current sheet with $B_z(x/L_x)$ (see Section 5.1), to describe the system dynamics at times $1/\varepsilon$, we need, besides I_z, one more invariant I_x corresponding to the area of the trajectory in the plane of slow variables. In the notation introduced, I_x (which is the same invariant as I_χ introduced in Section 5.1, but written for $\chi = \lambda^2 x^2$ and with the integration variable k) takes the form

$$I_x = \alpha\frac{2\sqrt{2}}{\pi}\,I\int_{k_a}^{k_b}\frac{Q(k)}{\bar{f}^2(k)}\,\frac{\pm\left(2H\left(I/\bar{f}(k)\right)^{4/3} - 1\right)}{2k^2 - 1 + \tau\left(\bar{f}(k)/I\right)^{2/3}}\,\mathrm{d}k\,.$$

Here, α is a constant parameter defined below,

$$Q(k) = \begin{cases} kK(k)\,, & k < 1\,, \\ K(k^{-1})\,, & k > 1\,, \end{cases}$$

and the upper integration limit is determined from the condition

$$\frac{\bar{f}^{4/3}(k_b)}{2H} = I^{4/3}\,.$$

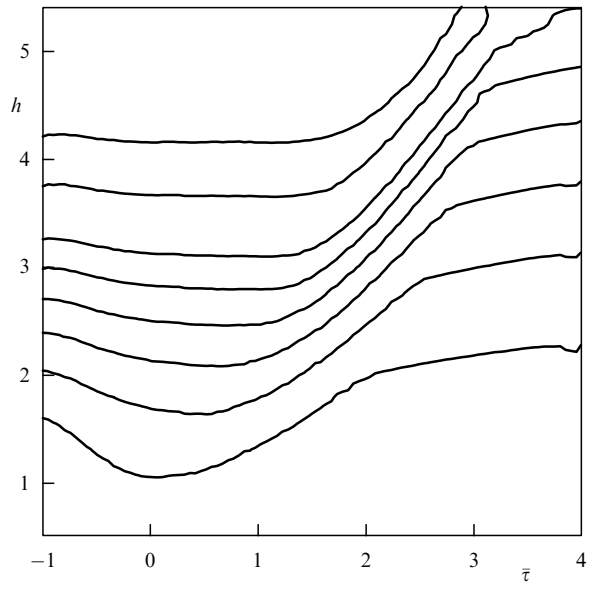

Figure 32. Phase trajectories in the $(h, \bar{\tau})$ plane for a system with an X-line. Each curve corresponds to a particle trajectory with its own quasiadiabatic invariant $\bar{I}_x$.

The lower integration limit depends on whether the trajectory crosses the $x = 0$ axis. If the trajectory does not cross the $x = 0$ axis, then $\bar{f}^{4/3}(k_a)/2H = I^{4/3}$ and $\alpha = 1$, and if it does cross the $x = 0$ axis, then $\alpha = 2$ and

$$-\tau = \left(\frac{I}{\bar{f}(k_a)}\right)^{2/3}(2k_a^2 - 1)\,.$$

As in Section 5.1, we consider the regime $\lambda^3/\varepsilon \ll 1$. In this regime, jumps of the quasiadiabatic invariants can be neglected, and we can consider the set of equations $I_z = \text{const}$, $I_x = \text{const}$. Here, the invariant I_z serves as a parameter, while the conservation of $I_x = I_x(I_z, H, \tau)$ allows finding trajectories in the (H, τ) plane.

We now introduce the normalized quasiadiabatic invariant $\bar{I}_x = I_x/I$ and the new variables

$$x = \bar{x}I^{1/3}\,, \quad p_x = \bar{p}_x I^{-1/3}\,,$$

$$H = hI^{4/3}\,, \quad h_z = \bar{h}_z I^{4/3}\,,$$

$$\tau = \bar{\tau}I^{2/3}\,,$$

$$\bar{k}^2 = \frac{1}{2}\left(1 + \frac{(1/2)\,\lambda^2\bar{x}^2 - \bar{\tau}}{\sqrt{2\bar{h}_z}}\right),$$

in which the relation for h and $\bar{\tau}$ becomes

$$\bar{I}_x = \frac{\alpha\sqrt{8}}{\pi}\int_{\bar{k}_a}^{\bar{k}_b}\frac{Q(\bar{k})}{\bar{f}^2(\bar{k})}\left[\frac{\pm(2h\bar{f}^{4/3}(\bar{k}) - 1)}{2\bar{k}^2 - 1 + \bar{\tau}\bar{f}^{2/3}(\bar{k})}\right]^{1/2}\mathrm{d}\bar{k}\,.$$

Here, the plus sign corresponds to X-lines and the minus corresponds to O-lines. Solving the equation $\bar{I}_x(h, \bar{\tau}) = \text{const}$, we can obtain trajectories in the $(h, \bar{\tau})$ phase plane. In the case of an X-line, these trajectories are presented in Fig. 32, whence we see how the particle energy increases with time $\bar{\tau}$.

6. Statistical consequences of the conservation of the quasiadiabatic invariant: description of an ensemble of trajectories

In Sections 3–5, we addressed the problems of particle dynamics and obtained sets of trajectories corresponding to the quasiadiabatic approximation $I_z = \text{const}$ for different systems. Moreover, we demonstrated that taking the jumps ΔI_z into account leads to diffusion of the quasiadiabatic invariant.

However, not only individual particle trajectories are of interest, because the properties of a self-consistent system that depend directly on the particle distribution over trajectories are also important. In this section, we show how the theory of quasiadiabatic dynamics considered in Sections 3–5 permits describing the formation of distribution functions in the central region of the current sheet and at its boundaries. We also discuss problems of a self-consistent formation of the current sheet due to currents carried by transient particles. We demonstrate that particle scattering and transitions from transient trajectories to quasi-trapped trajectories underlie the evolution process of the current sheet.

6.1 Distribution function of trapped particles at the center of a current sheet

We consider the problem of the particle distribution at the center of a current sheet within the approximation $I_z = \text{const}$. As was shown in Section 3.1, the value of the quasiadiabatic invariant I_z determines the trajectory of a particle in the plane of slow variables. Trajectories most significantly elongated along the κx axis correspond to small values of I_z. However, Fig. 6a, with a set of trajectories in the $(\kappa x, p_x)$ plane, was plotted for a system with a magnetic field $B_x \sim z$ without taking the loss cone into account. In a real current sheet, the magnetic field B_x does not increase to infinity with the distance from the $z = 0$ plane but takes constant values that can be described by the simple analytic model

$$\frac{B_x}{B_0} = \begin{cases} \dfrac{z}{L_z}\,, & |z| \leqslant L_z\,, \\ \operatorname{sign} z\,, & |z| > L_z\,. \end{cases}$$

Hence, trajectories that deviate from the $z = 0$ plane at a sufficiently large distance fall into the region with a constant magnetic field and never return to the system. Precisely these are transient trajectories. In the case of a current sheet with concrete parameters, a value of I_z^* can be found for which all particles with $I_z < I_z^*$ are transient.

The position of a particle in the half-plane of slow variables (for $p_x > 0$) is characterized by three parameters: the particle energy H, the normalized value of the quasiadiabatic invariant I, and the quantity $k = k(\kappa x, p_x)$ (with $k^2 = (1/2)(1 + \kappa x/\sqrt{2h_z})$) determining the position of the particle on the trajectory. With these parameters, it is possible to determine the particle coordinates averaged over fast oscillations, projected onto the $z = 0$ plane, and expressed in dimensionless form [40, 122]:

$$\begin{aligned} \kappa\langle x\rangle &= \left(\frac{I}{\bar{f}(k)}\right)^{2/3}(2k^2 - 1)\,, \\ \kappa\langle y\rangle &= \sqrt{1 - \left(\frac{I}{\bar{f}(k)}\right)^{4/3}}\,. \end{aligned} \tag{21}$$

Here, $\bar{f}(k) = 3f(s)/8$, and the function $f(s)$ is presented in Section 3.1. We define I^* such that the particle does not leave the current sheet when $I > I^*$. On the average, particles leaving the current sheet move along the magnetic field lines:

$$\langle z\rangle^2 = 2\kappa\langle x\rangle\,.$$

We define the boundary of the current sheet as the location where the magnetic field tends to a constant value. The boundary thus defined is described by the following relation in dimensionless variables: $z^2_{\text{boundary}} = 1/\sigma = \sqrt{L_z/\rho_0}$. Hence, a particle reaches the boundaries of the current sheet $\langle z\rangle = \pm\sqrt{\sigma}$ when $\kappa\langle x\rangle_{\text{esc}} = \sigma/2$. Particles that leave the current sheet can be considered transient. The largest possible value of $\langle x\rangle_{\text{turn}}$ for each trajectory is determined by the turning point $p_x = 0$. If $\langle x\rangle_{\text{turn}} > \langle x\rangle_{\text{esc}}$, the particle is transient. It follows from the definition of $\langle y\rangle$ that $\langle y\rangle = 0$ at $p_x = 0$. Then the value of k corresponding to the turning point ($p_x = 0$) is found from the relation

$$\bar{f}(k_{\text{turn}}) = I\,.$$

We thus obtain the following expression for $\langle x\rangle_{\text{turn}}$:

$$\kappa\langle x\rangle_{\text{turn}} = 2k^2_{\text{turn}} - 1\,.$$

The condition $\langle x\rangle_{\text{turn}} > \langle x\rangle_{\text{esc}}$ implies that

$$2k^2_{\text{turn}} - 1 > \frac{1}{2}\,\sigma\,.$$

If the current sheet is sufficiently thick ($\sigma \gg 1$), we can use the function $\bar{f}(k)$ for $k \gg 1$: $\bar{f}(k) \approx 3\pi/16k$. We then obtain the condition for a trajectory to be transient:

$$I < I^* \sim \frac{3\pi\sqrt{\sigma}}{8}\,.$$

If the quantity I^* is known, then, from the general particle distribution function, we can single out its part that corresponds to particles trapped in the current sheet. For this, for example, we define an isotropic Maxwell distribution function with a thermal velocity v_0 at the center of the current sheet. We then represent this function as a distribution not over velocities but over values of the quasiadiabatic invariant I (Fig. 33a).

We divide the phase space into two regions, those occupied by particles on transient trajectories ($I < I^*$) and on trapped trajectories ($I > I^*$). In our problem, the region with $I < I^*$ plays the role of the loss cone in the ordinary guiding center theory: particles from this region have small pitch angles and are 'spilled out' from the magnetoplasma configuration. We modify the resulting distribution function as follows: we set its value in the phase space region where $I < I^*$ to zero and return the remaining part to velocity space. The distribution function obtained as a result of this operation and expressed as a function of longitudinal and transverse velocities (at the center of the current sheet $v_\parallel = v_z$) is presented in Fig. 33b. As can be seen from the figure, the part of the distribution function corresponding to small transverse velocities at the center of the current sheet vanishes. Hence, unlike the usual loss cone of magnetized particles, which forms about a magnetic field line, the loss cone for quasiadiabatic distributions is asymmetric in the direction perpendicular to the magnetic field.

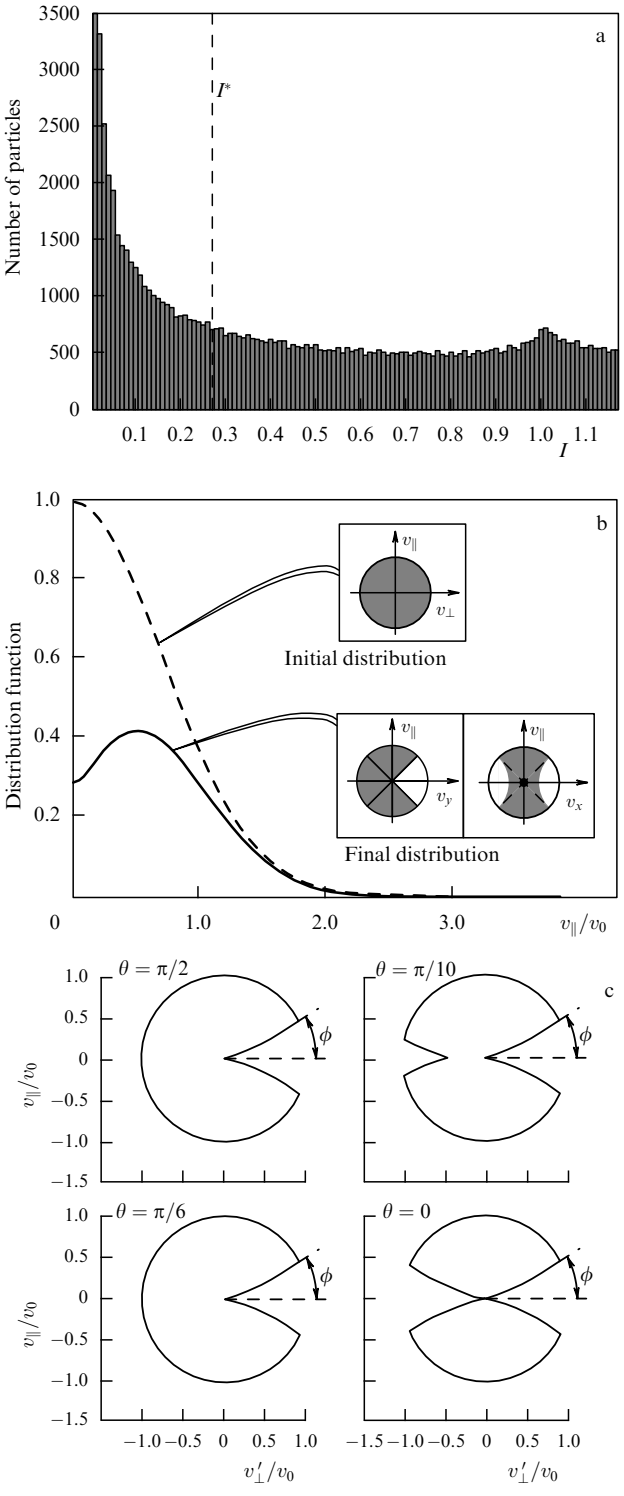

Figure 33. (a) The isotropic Maxwell particle distribution function as a function of the quasiadiabatic invariant. (b) Distribution function with the phase space cut out for $I < I^*$. (c) Cross sections of the distribution function for values 0, $\pi/10$, $\pi/6$, $\pi/2$ of the angle θ between the cross section plane rotated about the $v_\parallel$ axis and the $v_\parallel - v_x$ axis. The velocity $v'_\perp$ corresponds to the component that in the rotated coordinate system is perpendicular to the z axis. (From Ref. [122].)

We also plot the structure of phase space for different cross sections of the obtained distribution function (Fig. 33c). Each cross section is formed by the plane $v_\parallel - v'_\perp$ for different values of the angle θ between the plane of the cross section

rotated about $v_\parallel$ (i.e., about the z axis) and by the plane $v_\parallel - v_x$, where $v'_\perp$ is the velocity component that in the rotated system is perpendicular to the z axis. Hence, θ is the angle between the components $v'_\perp$ and v_x. We see from Fig. 33c that the shapes of projections of the distribution function resemble spheres with the sector corresponding to positive v_y cut out. Therefore, particles with positive v_y must leave the current sheet and form the distribution of transient particles (see Section 6.2).

6.2 Distribution function of transient particles at the center of a current sheet

While particles on quasi-trapped orbits in the current sheet form a distribution function with a characteristic anti-loss cone, the distribution of transient particles must exhibit significant asymmetry along the y direction.

The transient particles penetrate the current sheet in moving from the boundaries of the sheet, perform a half-turn in the neutral plane about B_z, and leave the current sheet. As a result, in the (p_y, p_x) plane, these particles describe a semicircle in the vicinity of the $z = 0$ plane. Because $B_z > 0$ and the particles enter the current sheet with $p_x < 0$, this semicircle occupies the region with $p_y > 0$. The corresponding particle distribution was obtained in Refs [123, 124]. As can be seen from Fig. 34a, the distribution of transient particles at the center of the current sheet has the shape of a semicircle. The thickness of this semicircle is equal to the thermal velocity v_0 of the initial distribution.

To obtain a similar distribution function in the analytic approach, we use the following procedure (see Refs [125, 126] for the details). The distribution at the boundary of the current sheet is chosen in the form of a shifted Maxwell distribution,

$$F \sim \exp\left[-\frac{(v_\parallel - v_\mathrm{D})^2 + v_\perp^2}{v_0^2}\right],$$

where $v_\parallel$ and $v_\perp$ are the parallel and perpendicular components of the particle velocity. We introduce the parameter $\varepsilon = v_0/v_\mathrm{D}$ determining the flux anisotropy of the distribution function. Because the magnetic field at the boundary of the current sheet is constant, $B_x = \pm B_0$ and $B_z = \mathrm{const}$, an analytic expression for the quasiadiabatic invariant I_z can be obtained. A particle oscillates in a constant magnetic field with a gyrofrequency ω_0, and its velocity is $v_z = v_\perp \cos(\omega_0 t)$. Performing the change $\mathrm{d}z = v_z\,\mathrm{d}t$, we calculate the integral I_z:

$$2\pi I_z = \oint v_z\,\mathrm{d}z = v_\perp^2 \oint \cos^2(\omega_0 t)\,\mathrm{d}t = \frac{\pi v_\perp^2}{\omega_0}\,. \qquad (22)$$

We next use the energy conservation law $v_\parallel^2 + v_\perp^2 = v^2$. As a result, the distribution function F can be expressed in terms of the integrals of motion:

$$F \sim \exp\left[-\frac{2\omega_0 I_z + \left(\sqrt{v^2 - 2\omega_0 I_z} - v_\mathrm{D}\right)^2}{v_0^2}\right]. \qquad (23)$$

Using the Liouville theorem, we find the distribution function at each point z inside the current sheet [125–127]. For this, we must obtain an expression for the quasiadiabatic invariant at an arbitrary point inside the sheet. We take a point in phase space with coordinates $(z_0, \kappa x_0, p_{x0}, p_{y0}, p_{z0})$. For this point,

$$2h_{z0} = p_{z0}^2 + \left(\kappa x_0 + p_{y0} - a_y(z_0)\right)^2 = v_{z0}^2 + v_{y0}^2\,,$$

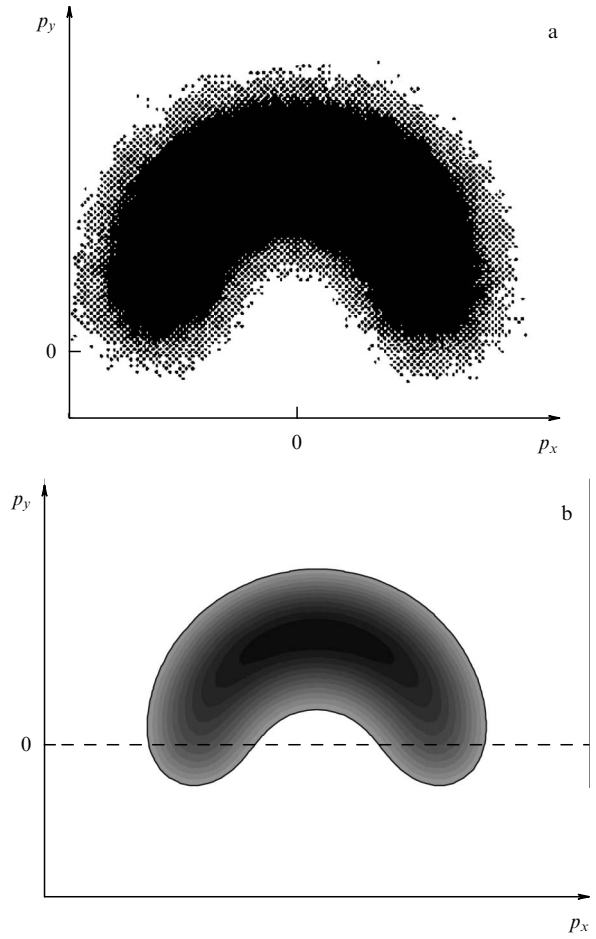

Figure 34. (a) Distribution function of transient particles obtained by numerical simulation. (From Ref. [123].) (b) Distribution function of transient particles obtained within the analytic approach. (From Ref. [30].)

where $a_y(z)$ is the dimensionless vector potential (see Section 3.1) and the constants $v_{y0} = \kappa x_0 + p_{y0} - a_y(z_0)$, $v_{z0} = p_{z0}$ are components of the particle velocity at the point $(z_0, \kappa x_0, p_{x0}, v_{y0}, v_{z0})$. We then obtain the quasiadiabatic invariant in the form

$$\begin{aligned} 2\pi I_z &= \oint \sqrt{2h_{z0} - \left(\kappa x + p_{0y} - a_y(z)\right)^2}\,\mathrm{d}z \\ &= \oint \sqrt{v_{z0}^2 + v_{y0}^2 - \left(\kappa x + p_y - a_y(z)\right)^2}\,\mathrm{d}z \\ &= \oint \sqrt{v_{z0}^2 + v_{y0}^2 - \left(v_{y0} + a_y(z_0) - a_y(z)\right)^2}\,\mathrm{d}z\,. \end{aligned} \qquad (24)$$

We next divide the phase space into elementary volumes $\mathrm{d}z\,\mathrm{d}\kappa x\,\mathrm{d}v_y\,\mathrm{d}v_z\,\mathrm{d}v_x$ and consider expression (24) to define the quasiadiabatic invariant I_z for an element of the phase volume with its center at the point $(z_0, \kappa x_0, v_{x0}, v_{y0}, v_{z0})$. Setting a certain profile $a_y(z)$ and recalculating I_z at each point z_0 for the entire volume of the (v_x, v_y, v_z) space, introduced a priori, we obtain the invariant I_z and hence the phase density $F(I_z, v)$ at the given point z_0 for the given (v_x, v_y, v_z). Thus, it is possible to find the distribution $F(p_x, p_y, p_z)$ at the center of the current sheet, where $z = 0$, by 'tracing' the distribution from the boundary of the current sheet along the transient trajectories (see Refs [125, 126]). This

distribution can be integrated over p_z to yield the distribution function in the (p_x, p_y) plane shown in Fig. 34b. As we see, the distribution function found analytically fully coincides with the result of direct numerical simulation presented in Fig. 34a.

Sickle-shaped distributions of transient particles, similar to the ones obtained in computations, are observed by spacecraft in the current sheets of Earth's magnetotail. But because the fraction of transient particles is small compared with the total density of background plasma, these distributions can be singled out only in two cases. As the current sheet is thinning, part of the background plasma is lost (the parameter σ decreases; see Section 6.1). In this case, the hot asymmetric flank of the distribution function is clearly seen to have a sickle-like shape (see Refs [128, 129]). On the other hand, we can use the fact that when crossing the current sheet, characteristics of the background plasma do not change significantly. As a result, if we subtract the distribution function at the boundary of the current sheet from the distribution function at its center, then, in the resultant residual function, sickle-like distributions of transient particles can be clearly seen whose shape is very close to that found theoretically (Fig. 35a).

We can therefore assert that the theory of quasiadiabatic particle motion in current sheets allows reconstructing the ion distribution function in the plasma layer of Earth's magnetotail with good precision.

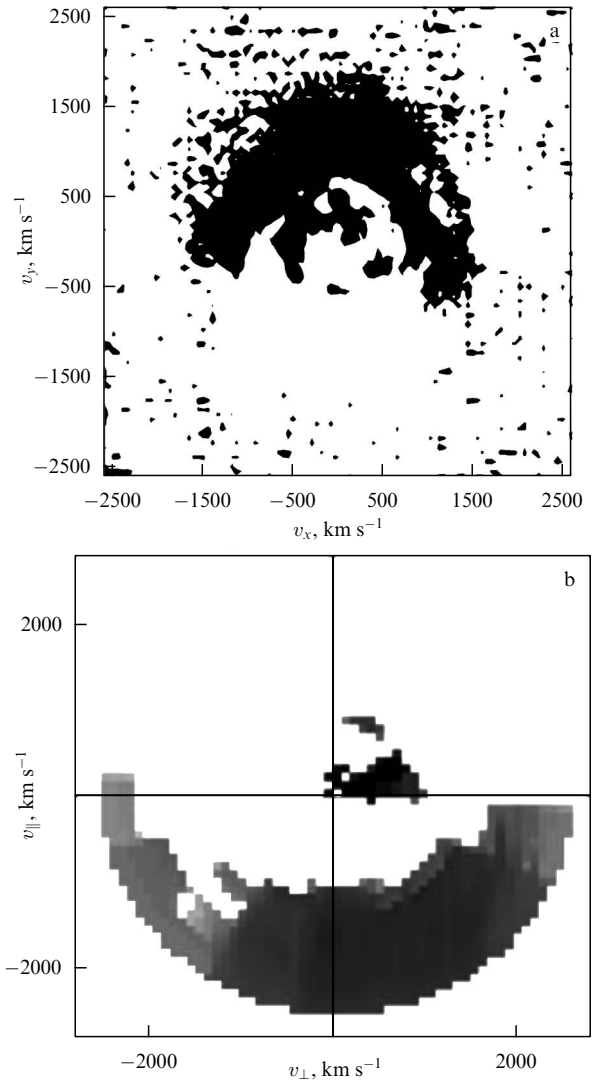

Figure 35. (a) Distribution function of transient particles measured by satellites in the current sheet of Earth's magnetotail. (From Ref. [30].) (b) Particle distribution function in the boundary region of the plasma layer. (From Ref. [32].)

6.3 Distribution function at the boundary of a current sheet

Formation of the charged particle distribution at the boundary of a current sheet (or in the boundary region of a plasma layer) is subject to the significant influence of the processes of particle acceleration by the electrostatic field E_y. Direct numerical simulations [97] and simple estimations [96] indicate that particles leaving the current sheet should form a distribution function in the velocity space with a specific 'bean-like' shape in the $(v_\parallel, v_\perp)$ space. Similar distribution functions have been repeatedly observed by spacecraft devices in the boundary region of the plasma layer [103, 108, 130, 131]. A typical example of such an observation is presented in Fig. 35b. In this section, we show, mainly on the basis of the results in Ref. [133], how that particle distribution can be obtained from velocities in the framework of the theory of quasiadiabatic dynamics.

We consider the model of a current sheet with $B_z(x/L_x)$ and $E_y = \text{const}$ discussed in Section 5.1. We are interested in particles on quasi-trapped trajectories. The projection of a typical trajectory of such a particle onto the $z = 0$ plane represents a series of open orbits linked with each other. The orbits are open because, in the field with a gradient $\partial B_z/\partial x \neq 0$, particles experience magnetic drift in the y-direction and gain energy in the field E_y. The results of numerical simulations of such a trajectory for a system with $B_z \sim 1/\sqrt{-x}$ are presented in Fig. 36.

We consider particles with initial velocities much smaller than the drift velocity at the center of the current sheet, $v_D(x_0) = cE_y/B_z(x_0/L_x)$. In this case, a particle crossing the current sheet at a coordinate x_0 moves in the central region with a velocity $v_D(x_0)$. We assume this particle to be observed at a distance $\Delta x = x - x_0$ from the point where it first crossed the current sheet. We consider the acceleration stages of the particle separately.

First, the particle, if we consider its slow motion averaged over z-oscillations, makes one fourth of a turn in the $z = 0$ plane and shifts along the y axis (the turn initiates on the y

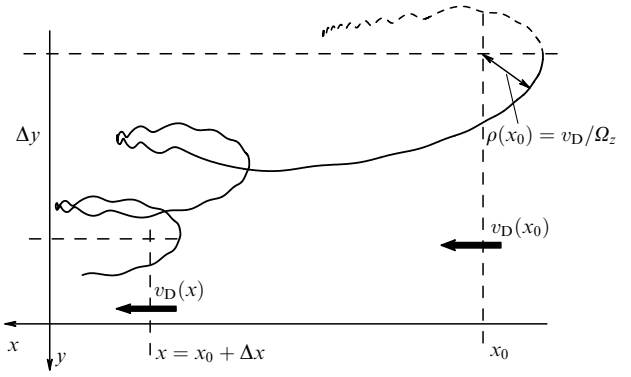

Figure 36. Trajectory of a particle in the system with Hamiltonian (18) in the case $\beta(x) \sim 1/\sqrt{-x}$.

axis) by the distance

$$\rho(x_0) = \frac{v_D(x_0)}{\Omega_z(x_0)}, \quad \Omega_z = \frac{qB_z(x_0)}{mc}.$$

Because the particle moves in a field $E_y \neq 0$, it gains the energy

$$\Delta W_1(x) = qE_y\rho(x_0) = mv_D^2(x_0).$$

This energy is half the energy a particle gains on a resonance trajectory (see Section 5.2).

The particle then moves along a quasi-trapped orbit and gains energy due to its drift in the increasing field, $\partial B_z/\partial x > 0$ (see Section 5.1). Hence, the difference between the energies at points x_0 and $x = x_0 + \Delta x$ is

$$\Delta W_2 = W(x) - W(x_0) = \frac{1}{2}\,mv_D^2(x) + W^*(x) - \frac{1}{2}\,mv_D^2(x_0) - W^*(x_0).$$

The energy $W^*(x_0)$ depends on the acceleration in the current sheet during the particle motion along E_y: $W^*(x_0) = \Delta W_1(x_0)$. In turn, $W^*(x)$ is determined by the gain in energy during the particle drift toward Earth: $W^*(x) \sim B_z^\delta(x)$, where $\delta \in [2/5, 1]$. In Refs [92, 134] (see also Section 5.1), it is shown that depending on the type of the particle trajectory, the particle energy increases in the case of convection toward Earth according to a power law with the exponent $\delta = 2/5$ (for transient particles) or $\delta = 1$ (for trapped particles). In our case, we consider δ a certain intermediate value depending on the relative number of trajectories of various types in the ensemble investigated:

$$W^*(x) = W^*(x_0)\left(\frac{B_z(x)}{B_z(x_0)}\right)^\delta = \frac{1}{2}\,mv_D^2(x_0)\,b^\delta,$$

$$b = \frac{B_z(x)}{B_z(x_0)} = \frac{v_D(x_0)}{v_D(x)}.$$

The coordinate of the particle along the y axis is determined at the observation point by relation (21) (see also Refs [40, 135]):

$$y(x) = \rho(x)\sqrt{1 - \left(\frac{I}{I^*}\right)^{4/3}},$$

where $I = I^* \sin^2\theta'$,

$$I^* = \frac{3\pi}{8}\sqrt{\frac{\rho(x)}{L_z}}.$$

The angle θ' is the pitch angle of the particle in a reference frame drifting with the velocity $v_D(x_0)$. The presence of the factor $\sin^2\theta'$ in the expression for the quasiadiabatic invariant I is explained by the quasiadiabatic invariant at the boundary of the current sheet (where $z = L_z$) being equal to $(1/2)\,v_\perp^2/\omega_0 = H\sin^2\theta'/\omega_0$ [see formula (22)]. The relation between θ' and the pitch angle θ in the rest frame is given by

$$\sin^2\theta' = \frac{v^2(x)}{v_D^2(x_0)\,b^{2+\delta}}\sin^2\theta,$$

where $mv^2 = 2W$ and we used the equation for W^*. This expression was obtained from the condition that velocities along z and y be constant in passing to the reference frame without any electric field E_y. Hence, the gain in energy resulting from a shift along the field E_y is given by

$$\Delta W_3 = qE_y\big(y(x) - y(x_0)\big).$$

The total energy increment is

$$W = \frac{1}{2}\,mv^2 = \Delta W_1 + \Delta W_2 + \Delta W_3.$$

Substituting the expressions for $\Delta W_1(x)$, ΔW_2, and ΔW_3 in the last relation, we obtain

$$v^2 = v_D^2(x)(1 + b^{2+\delta}) + v_D^2(x) \times 2b^{1+(1/2)\delta}\sqrt{1 - \left(\frac{v^2\sin^2\theta}{v_D^2(x)\,b^{2+\delta}}\right)^{4/3}}.$$

This expression defines an 'enforcement rib' for the sought particle pitch-angle distribution depending on the observation coordinate x in the approximation of a small initial particle energy. An enforcement rib is meant to be the geometric locus of points in the $(v_\parallel, v_\perp)$ plane corresponding to the largest value of phase density. Generalization to the case where the initial velocity u_0 must be taken into account is given by the formula

$$v^2 = u_0^2 + v_D^2(x)\left[1 + b^2(a-1)^2 + b^{2+\delta}a^2\right] + v_D^2(x)\,2b^{1+\delta/2}\sqrt{1 - \left(\frac{v^2\sin\theta}{v_D^2(x)\,b^{2+\delta}}\right)^{4/3}}, \qquad (25)$$

where

$$a^2 = \left(\frac{u_0\cos\theta_0}{bv_D(x)} + 1\right)^2 + \frac{u_0^2\sin^2\theta_0}{b^2v_D^2(x)},$$

and θ_0 is the pitch angle at the initial instant (at point x_0).

Figure 37 shows level lines of the proton distribution function in the boundary region of the plasma layer. Each enforcement rib corresponds to its own value of b, i.e., to a certain distance of the initial position x_0 of a particle in the current sheet from the observation point. We note that within broad limits, the positions of enforcement ribs are independent of the initial particle velocities u_0 and pitch angles θ_0 [133]. The enforcement ribs change in form as b increases (as the distance Δx increases): the greater b is, the more the enforcement ribs resemble segments of circles. In the case $\Delta x = 0$ ($b = 1$), the structure is elongated along the longitudinal direction of the velocity. For large b, the dependence on the pitch angle decreases and the enforcement ribs just become semicircles of radius R, shifted along the direction of $v_\parallel$ by the distance $v_D(x)$. The radius R is given by

$$R = v_D(x)\,b^{\delta+1} = v_D(x_0)\,b^\delta.$$

Figure 37b shows the enforcement ribs calculated by formula (25) for $v_D(x) = 100$ km s^{-1} and $u_0 = \theta_0 = 0$. The curve with $b = 9$ is quite consistent with the enforcement rib for the ion distribution function measured by a spacecraft device within the PSBL (Fig. 37c).

Small values (or vanishing) of the particle distribution function in the PSBL in the case of large pitch angles θ is explained by particles with such pitch angles not leaving the

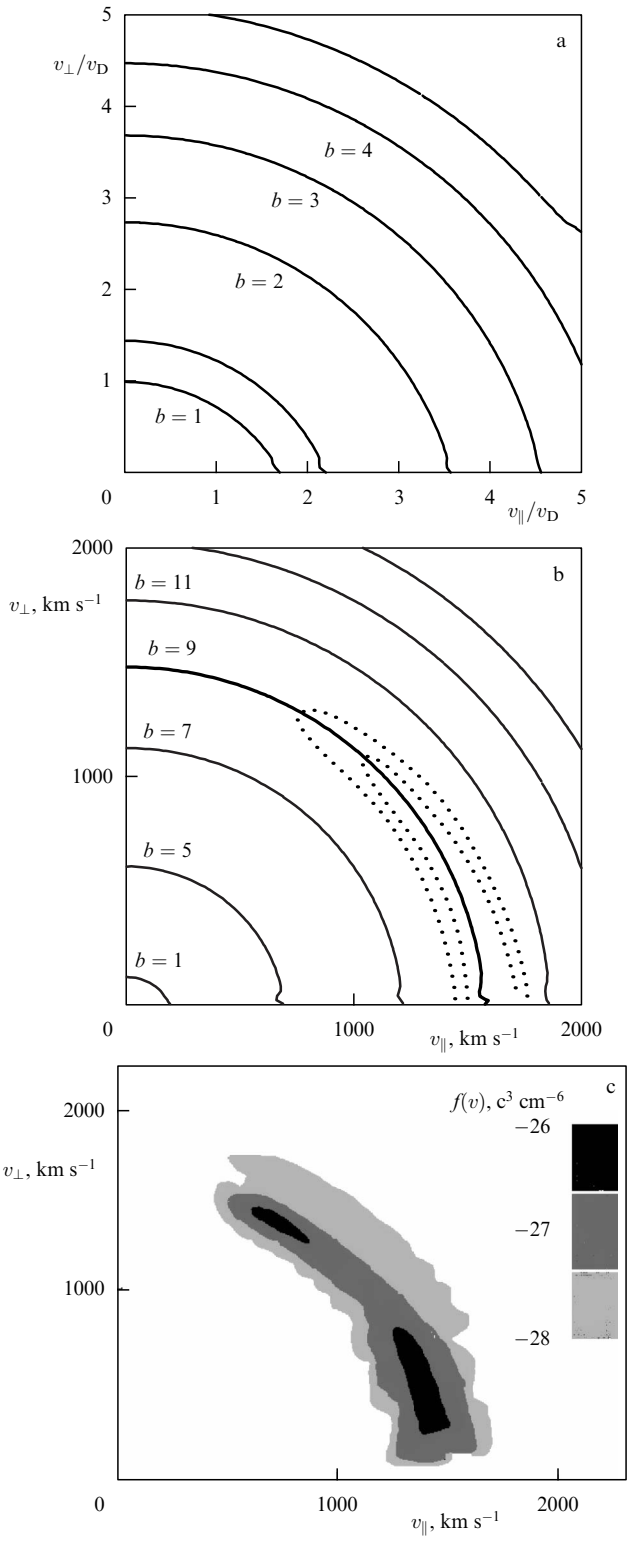

Figure 37. (a, b) Enforcement ribs of the particle distribution function in a plasma sheet boundary layer, calculated for different values of the parameter b. Figure b is similar to Fig. a with $v_D = 100$ km s^{-1}. (c) The proton distribution function measured in the plasma sheet boundary layer. (From Ref. [133].)

current sheet and not being able to take part in the formation of the distribution function in the PSBL (see Section 6.1). This effect can be obtained on the basis of the expression for v: the condition under which the radicand in formula (25) is positive determines the existence of a certain θ_{max} for each v.

In concluding this section, we can say that the results of the application of analytic methods based on the quasiadiabatic theory are in good agreement with both the results of numerical simulations and the data from direct satellite observations of ion distribution functions at the center of the plasma sheet of the magnetotail and at its boundaries.

6.4 Construction of self-consistent models of a one-dimensional current sheet

It was shown in Section 6.3 that the distribution function of transient particles can be determined at any point of the current sheet by particle tracing starting from the boundary of the system. The possibility of such tracing (i.e., analytic integrability of the equations of motion) is related precisely to the assumption of the quasiadiabatic invariant conservation. The existence of a distribution function known in the entire region (at all z) permits calculating its moments (for instance, the particle current density directed along y). Thus, it is possible to construct a self-consistent model of the current sheet, namely, a model of an equilibrium system with magnetic fields where particles move along trajectories described in the framework of the quasiadiabatic theory.

A stationary equilibrium solution for a current sheet that describes the distribution of vector and scalar potentials (and, as a consequence, of the electric and magnetic fields), as well as the distribution functions of plasma particles, must satisfy the set of Vlasov–Maxwell equations

$$\begin{aligned} &\mathbf{v}\,\frac{\partial F_\alpha}{\partial \mathbf{r}} + \frac{q_\alpha}{m_\alpha}\left(\mathbf{E} + \frac{1}{c}\,\mathbf{v}\times\mathbf{B}\right)\frac{\partial F_\alpha}{\partial \mathbf{v}} = 0\,,\\ &\operatorname{rot}\mathbf{B} = \frac{4\pi}{c}\sum_\alpha q_\alpha \int \mathbf{v} F_\alpha(\mathbf{v},\mathbf{r})\,\mathrm{d}\mathbf{v}\,,\\ &\operatorname{div}\mathbf{E} = 4\pi\sum_\alpha q_\alpha \int F_\alpha(\mathbf{v},\mathbf{r})\,\mathrm{d}\mathbf{v}\,, \end{aligned} \tag{26}$$

where $F_\alpha(\mathbf{v},\mathbf{r})$ is the particle distribution function, and m_α and q_α are the mass and charge of a particle of type α (an electron or an ion). Any function of the integrals of motion is a solution of the first equation in (26). Here, with $\mathbf{r} = x\mathbf{e}_x + z\mathbf{e}_z$, the system has two exact integrals: the total energy H and the generalized momentum $P_y = m_\alpha v_y + (q_\alpha/c)\,A_y(x,z)$.

There are a number of current sheet models in which $F_\alpha = F_\alpha(H, P_y)$ (see Refs [38, 136–140] and reviews [141–145]). But these models do not take the presence of transient particles in the real current sheet of Earth's magnetotail into account; in problems with the existence of an arbitrarily small but finite magnetic field component across the sheet, $B_z \neq 0$, a population of transient particles moving from one boundary of the sheet to another can exist. Even in the simplest problems with $B_z \neq 0$, the equations of particle motion lose their integrability, and developing a kinetic model of the sheet (i.e., finding the integrals of motion of the particles) requires introducing one more invariant of motion, whose role is taken precisely by the quasiadiabatic invariant I_z [125, 126, 146].

The class of current sheets with the conservation of I_z taken into account has a number of properties following directly from the properties of transient particle trajectories. It is shown in Refs [125, 126, 147, 148] that the main properties of current sheets associated with transient ions are as follows: (1) embedding (the plasma density profiles and the current density profiles do not coincide); (2) the fine

structure of current density profiles (for example, the existence of several local maxima of the current density, instead of one). As a result, current sheets with transient particles become metastable, i.e., for certain parameters of the system, such current sheets rapidly (sometimes even in an explosive manner [149]) undergo transition to an unstable state and are destroyed due to the development of explosive instability [62], which permits a description of the most important large-scale process developing in Earth's magnetosphere, namely, of a magnetospheric storm [25, 58, 150, 151]. Below, we discuss the main stages of the current sheet model construction taking the I_z conservation into account (we consider a thin current sheet (TCS) that exhibits relatively small space scales along the z axis), relying on the results of investigations of the self-consistent evolution of a current sheet related to jumps of the invariant I_z in Refs [46, 47, 50], and compare the models obtained with the experimental data (see Refs [22, 26, 152]). In conclusion, we present results of the development of two-dimensional models of current sheets based on a 'double' quasiadiabatic description assuming conservation of both the first (I_z) and the second (I_x) quasiadiabatic invariants.

6.4.1 Model of a one-dimensional current sheet. We formulate the basics of the one-dimensional TCS model.

1. The main carriers of current in the current sheet are ions on transient trajectories, while in the first approximation electrons can be regarded as the background ensuring the quasineutrality of the plasma (i.e., $\sum_\alpha q_\alpha \int F_\alpha(\mathbf{v}, \mathbf{r})\, d\mathbf{v} = 0$).

2. The B_z-component of the magnetic field is considered constant (not depending on the x coordinate). The component $B_y = 0$ (the validity of such an approximation is ensured by the smallness of the values of B_y in the case of many current sheets observed in the magnetotail [26, 153]).

3. The only spatially inhomogeneous component of the magnetic field is the self-consistent component $B_x(z)$, determined by the currents of transient ions.

4. Because $B_z = \text{const}$, the large-scale electrostatic field E_y persisting in Earth's magnetotail can be taken into account by passing to the de Hoffmann–Teller reference frame [154] moving uniformly along the x axis with the velocity cE_y/B_z.

5. The model takes the roles of both transient ions and of ions on quasi-trapped trajectories into account. Actually, electron currents play an important role in the formation of the current sheet structure, but because we are mainly interested in the role of quasiadiabatic ion dynamics, we only consider electrons in the simplest background approximation, when only their charge (but not current) is taken into account.

We now consider the features of particle motion on transient and quasi-trapped trajectories in the central region of the current sheet in greater detail. Figure 38 demonstrates characteristic shapes of parts of orbits of transient (dashed curve) and of quasi-trapped (solid curve) particles. As a rule, the orbits of quasi-trapped particles have a complicated serpentine-like character; therefore, at the center of a sheet, the ion velocity component along the y axis is negative, and when the particle reaches the maximum distance in the z coordinate, it is positive. By contrast, the velocity vector of a transient ion is always directed along the y axis. In the right-hand part of Fig. 38, the respective currents are shown schematically: the current of a transient ion (dashed curve) exhibits a pronounced positive maximum, while the current of a quasi-trapped ion (solid curve) is negative at the center of

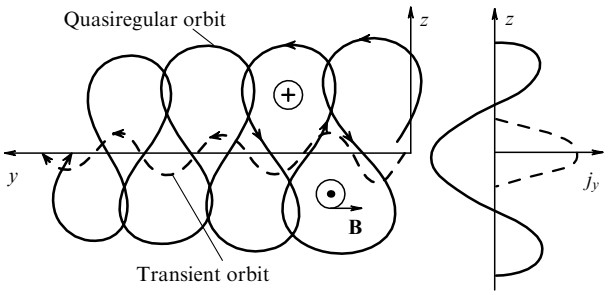

Figure 38. Parts of the orbits of two ions crossing the $z = 0$ plane. Shown are the direction of particle motion, the directions of the magnetic field component B_x, and the profiles of currents supported by each of the particles. (From Ref. [46].)

the current sheet and positive at its edges. Therefore, transient ions can be considered the main carriers of current. As regards quasi-trapped particles, whose orbits are closed, the total magnetic field supported by them is exactly equal to zero, although the local current differs from zero, and if many particles are trapped in the system, then such a current can change the structure of the sheet in an essential manner. Trajectories of both types, transient and quasi-trapped, are important for the formation of the TCS fine structure.

The TCS model assumes that impinging ion flows enter the current sheet from distant sources located at the boundaries of the system ($|z| > L_z$). Transient ions on open orbits describe semicircles in the neutral plane (a half-turn in the field B_z) (see Section 3.1). Choosing the ion distribution function at the boundary of the current sheet in the form of the Maxwell distribution with a shift velocity v_D along the magnetic field direction and representing this distribution in terms of the integrals of motion (the energy H and the invariant I_z), as was done in Section 6.2, we can find the distribution function $F(\mathbf{v})$ at each point of the current sheet (for all z).

As mentioned above, besides transient particles, particles that are on quasi-trapped trajectories exist in the current sheet. (Although the influence of jumps of the adiabatic invariant on the dynamics and properties of the system is not discussed in this section, we continue referring to closed trajectories crossing the separatrix as quasiadiabatic.) These particles do not leave the current sheet, and their distribution function cannot be found by tracing the distribution from the boundaries of the system. However, the population of particles on quasi-trapped and transient trajectories in phase space can be identified by the value of the quasiadiabatic invariant I_z^* (see Section 6.1). If $I_z < I_z^*$, then the particle is on a transient trajectory, and if $I_z > I_z^*$, then it is on a quasi-trapped trajectory. Hence, in integrating the function F over the velocity space, a distribution function differing from F must be chosen in those spatial regions where $I_z > I_z^*$. For simplicity, the distribution in the regions of phase space with $I_z > I_z^*$ is chosen in the model as the thermal Maxwell distribution $F_{tr} = n_{ts} \exp(-H/T)$, where $T = v_0^2 m/2$ is the ion temperature in the current sheet and $n_{ts} = Kn_0$ (n_0 is the transient particle density at the boundary of the current sheet and K is a free parameter characterizing the relative contribution of particles of both types). The choice of the coefficient K is determined by the necessity of taking some plasma processes into account. In a number of studies where the problem of investigating the role of plasma trapped by the

current sheet was not formulated directly [125, 126], the simplest solutions with $K = 1$ were considered, in obtaining which the distribution functions of trapped and transient particles were made to match each other with equal densities at $I_z = I_z^*$. In studying the influence of trapped plasma on the current sheet structure [49, 155], the parameter K was made to vary within a broad range of values, from $K = 0$ to $K \approx 20$.

Integrating the distribution function over velocities (or momenta p_x, p_y, p_z) with a weight coefficient v_y, we can find the particle current density $j_y(z)$. Here, $j_y(z)$ involves both the diamagnetic current and the magnetization current, due to the gradient of particle pressure, as well as the paramagnetic current resulting from the trajectories of transient particles being open (an analog of the edge current in a bounded system in which elastic reflection of particles from walls occurs) (see Refs [22, 126]). Below, the equation for the magnetic field in system (26) is written in terms of the vector potential component $\tilde{A}_y(z) = A_y - B_z x$ (see Refs [22, 148]):

$$\frac{\mathrm{d}^2 \tilde{A}_y}{\mathrm{d}z^2} + \frac{4\pi}{c} j_y(\tilde{A}_y) = 0 .$$

Here, we use the fact that the system is one-dimensional and that the current density can be represented as a function of the vector potential component $\tilde{A}_y$.

One of the key parameters of the system is $\varepsilon = v_0/v_\mathrm{D}$, which determines the relative velocity of the particle flow at the boundary of the current sheet. We see in what follows that ε also determines the depth of the emerging self-consistent current configuration.

The solution of the equation $\mathrm{d}^2\tilde{A}_y/\mathrm{d}z^2 + (4\pi/c)\, j_y(\tilde{A}_y) = 0$ can be found with the aid of an iteration procedure. At the zeroth step, a certain spatial distribution is chosen for the potential $\tilde{A}_y(z)$ and the distribution function F, and hence the current density j_y is reconstructed at each point z for this distribution. Then a new approximation for $\tilde{A}_y(z)$ is found from the current density. The iteration process continues until it converges to some function $\tilde{A}_y(z)$. Furthermore, the magnetic field B_x and the current density are determined for this function [125, 126].

The results of computations are presented in Fig. 39, where the self-consistent current density in a TCS is represented as a function of the dimensionless coordinate $\zeta = z\varepsilon^{-4/3}\omega_0/v_\mathrm{D}$ (ω_0 is the ion gyrofrequency at the boundary of the current sheet) for different values of the parameter $\varepsilon = v_0/v_\mathrm{D}$, as well as plasma density profiles for the same values of ε. Comparing Figs 39a and 39b shows that in the case of a strong flux asymmetry in the system, i.e., for small values of ε, the current and plasma density profiles exhibit a clearly expressed maximum, which smooths out as ε increases, and practically vanishes for weakly anisotropic sheets with $\varepsilon \to 10$. However, the profiles being compared also manifest an essential difference: the current density (Fig. 39a) tends to zero at the boundaries of the current sheet, while the plasma density (Fig. 39b) becomes constant, which is due to the presence of particle flows at the boundary of the system. Thus, the current sheet is embedded into a thicker plasma layer. As follows from the results of the computations presented in Fig. 39, the layer thickness is of the order of unity and its dimensional thickness is $L_z \sim \rho_0 \varepsilon^{1/3}$. Therefore, the layer thickness increases with ε up to $\varepsilon \sim 1$ ($L_z \sim \rho_0$), but in the case of weakly anisotropic layers ($\varepsilon > 1$), as shown in Ref. [126], it tends to the constant value $L_z \sim \rho_0$. Hence, all

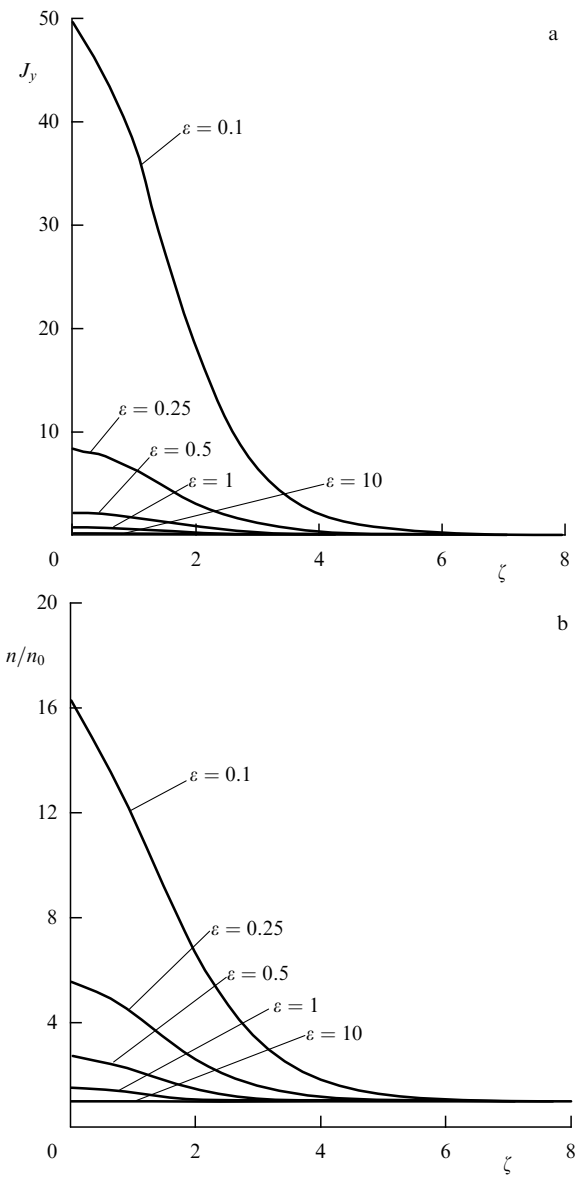

Figure 39. (a) Normalized current density $J_y = j_y/(qn_0 v_\mathrm{D} \varepsilon^{2/3})$ and (b) normalized plasma density n/n_0 as functions of the dimensionless coordinate ζ. (From Ref. [126].)

self-consistent (even weakly anisotropic) current sheets are thin: $L_z \leqslant \rho_0$.

Moreover, it is also shown in Ref. [126] that the fine structure of current density profiles in a TCS results from competition between the oppositely directed para- and diamagnetic currents. Paramagnetic currents are mainly due to transient particles (see Fig. 38) in the case of current carriers moving at the center of the current sheet (a half-turn about B_z), while diamagnetic currents are caused by the drift motion of ions even before they cross the neutral $z = 0$ plane. The main drift currents are the magnetization current, the gradient current, and the drift current due to the curvature of magnetic field lines [156]. A small contribution to the negative current density can also be made by quasi-trapped ions (see Fig. 38), but if $K = 1$, then their concentration in the system is small and, consequently, their role is insignificant. Diamagnetic currents are always much smaller than the paramagnetic ones, but at the edges of the current sheet, diamagnetic

currents can manifest themselves as weak maxima of the magnetic field at the periphery of the current sheet. The role of diamagnetic currents increases in weakly anisotropic sheets with large values of the parameter ε (see Refs [125, 126] for the details).

6.4.2 Jumps of the quasiadiabatic invariant and evolution of the current sheet during finite time intervals. The self-consistent equilibrium solution constructed in Section 6.4.1 is approximate. The accuracy of the quasiadiabatic model of a current sheet is determined by the accuracy of the conservation of quasiadiabatic invariants of motion (see Appendix A). During time intervals significantly exceeding the period of ion motion in the plane of slow variables $(\kappa x, p_x)$, ions can accumulate on quasi-trapped trajectories owing to jumps ΔI_z of the quasiadiabatic invariant (see Section 3.2).

In current sheets with $\varepsilon \ll 1$, the sheet thickness is close to the Larmor radius, and therefore the parameter κ is small, which leads to small values of the relative jumps of the invariant, $\Delta I_z/I_z \ll 1$. Here, the region of phase space occupied by quasi-trapped trajectories is small, and hence the effects of plasma accumulation in this region become insignificant [126, 155]. Jumps of the quasiadiabatic invariants, on the contrary, are significant in TCSs with $\varepsilon \sim 1$, where the phase space region occupied by quasi-trapped trajectories is already large, and jumps of the invariants of motion also increase compared with such jumps in the case $\varepsilon \leqslant 1$. The particle distribution function can therefore change in time very slowly (compared to the slow motion of particles in the $(\kappa x, p_x)$ phase plane) [47, 50]. An increase in the concentration of quasi-trapped particles causes a redistribution of the current density in the sheet, and the maximum of the current density then splits at the beginning into two maxima displaced to the periphery of the current sheet [46]. Such an evolution of the sheet can be regarded as a sequence of quasistatic equilibrium states or a relatively slow diffusion process in the space of invariants of motion I_z. As shown in Section 3.2, the particle distribution function in this approximation can be found from the solution of the diffusion equation with the diffusion coefficient $D_{II} \sim \kappa^2(1 - I^{4/3})/\tau_c$, where I is the dimensionless quasiadiabatic invariant and $\tau_c = 2\pi/(qB_z/mc)$ is the period of particle motion in the $(\kappa x, p_x)$ plane (the period of oscillations in the field B_z).

The assumption that the system undergoes fast relaxation to the equilibrium permits using the distribution function profiles obtained at different time instants as the distributions corresponding to quasiequilibrium configurations that the system passes in the course of its evolution. We can therefore assume that at each instant, the right-hand sides of Eqns (26) contain 'snapshots' of the distribution function undergoing evolution and obtained by solving the diffusion equation.

Successive changes in the current density profile resulting from the accumulation of particles on quasi-trapped trajectories inside the TCS at the instant $\tau = t/\tau_c$ for a characteristic configuration of the current sheet in Earth's magnetotail are depicted in Fig. 40. The accumulation of particles on quasi-trapped trajectories can be seen to lead to a trough in the current density profile at the center of the sheet. The accumulation time characteristic of quasi-trapped particles in the current sheet of Earth's magnetotail has been estimated to be 10–60 min [50], which is in agreement with the lifetime of the thin current sheet determined from the results of satellite observations.

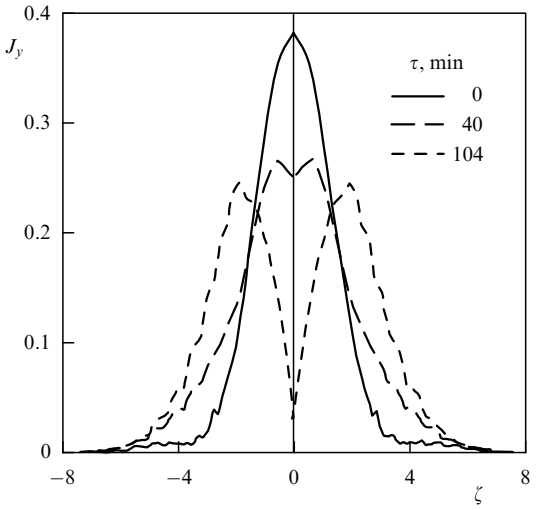

Figure 40. Three current density profiles in a current sheet undergoing evolution at instants when no trapped particles are present in the sheet ($\tau = 0$), a small concentration of particles is present ($\tau = 40$ min), or there are many particles ($\tau = 104$ min). (From Ref. [46].)

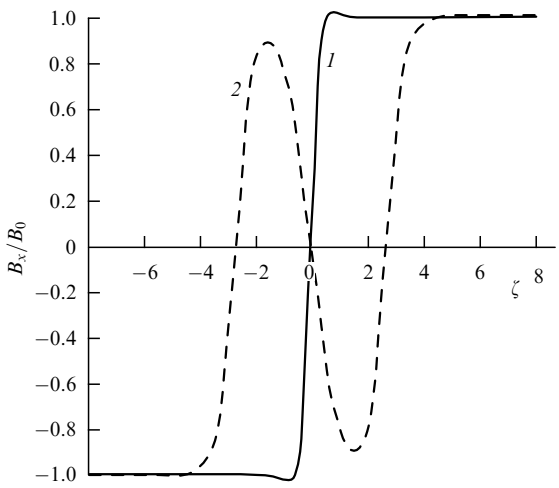

Figure 41. Two self-consistent stationary profiles of the normalized magnetic field B_x in a simple TCS with a single maximum in the current density (curve *1*) and in a triply split TCS (curve *2*). (From Ref. [49].)

The problem of the limits of plasma accumulation close to the TCS is discussed in Ref. [155], where it is shown that upon reaching a negative minimum in the current density, the current sheet can be destroyed and equilibrium may no longer exist. For this reason, the accumulation process of particles on quasi-trapped trajectories was termed 'ageing' of the current sheet. However, it must be noted that in another study [49], the possibility was revealed of the existence of 'exotic' triply split current equilibria, in which a high concentration of trapped plasma is observed with a characteristic three-layer configuration such that a negative current is observed at the center of the sheet and a positive current is observed at its edges (Fig. 41). Such a configuration, unlike the doubly split one, is stable with respect to small external perturbations of the magnetic field, although the value of the threshold density of particles on quasi-trapped trajectories does exist, an excess of which leads to the destruction of the triple current sheet.

The relation between the doubly and triply split equilibrium states is still unclear, because it has not been possible to achieve smooth transition from the first to the second and vice versa. It can only be asserted that three types of equilibria have been found as solutions of the set of Vlasov–Maxwell equations: an unsplit state, a doubly split state, and a triply split state. In a current sheet where the plasma exhibits a weak flux anisotropy ($\varepsilon \sim 1$), because of diffusion in the space of quasiadiabatic invariants, an unsplit equilibrium current sheet can undergo the transition to a split state that experiences slow evolution toward a triply split equilibrium. The rate of this evolution turns out to be variable: it increases with time, because the increase in the concentration of ions on quasitrapped trajectories leads to the formation of a 'smoothed out' magnetic field profile with a large value of the parameter κ, which in turn provides further enhancement of particle scattering (in accordance with the expression for the diffusion coefficient $D \sim \kappa^2$) and particle capture in the vicinity of the current sheet. Thus, the mechanism of the 'ageing' process implies a positive feedback between the 'depth' of the minimum in the current profile at the center of the current sheet and the diffusion coefficient $D \sim \kappa^2$, which may result in a very fast explosive evolution of the system at the final stages of its existence [46, 50].

6.4.3 Asymmetry of the current sheet and multicomponent systems. Nonsymmetric TCSs are quite often registered in Earth's magnetotail [153]: they have also been revealed by the satellite Mariner-10 during its flight through the magnetosphere of Mercury [157]. The most natural source of asymmetry in a current sheet may be the asymmetry of plasma flows crossing the current sheet [158, 159], or the presence of a nonzero magnetic field component B_y in the current sheet [160, 161]. Below, we consider the influence of the first mechanism in a current sheet with $B_y = 0$, assuming for simplicity that the only source of plasma at the boundary of the system is located in the northern hemisphere, and no sources exist in the southern hemisphere [157]. Ions penetrating the current sheet from the boundaries of the system, describing a half-circle about the field B_z in the neutral $z = 0$ plane, can start moving in the opposite direction toward the source ('reflection') or can undergo transition to the side of the current sheet opposite the source ('refraction'). Particle reflection and refraction processes depend essentially on the phase difference between crossings of separatrices at the entrance to and the exit from the sheet (see Sections 3.1, 3.3). This phase difference is determined by the parameter κ (actually, the ratio of the frequencies of slow and fast motions), i.e., it ultimately depends on parameters of the sheet (L_z, B_z/B_0) and on the particle energy. The probabilities of reflection and of refraction, averaged over the distribution, are the same for ions, with the exception of a group of particles with resonance energy values for which the phase difference $\delta\xi$ is zero, i.e., the jump in the quasiadiabatic invariant of motion at the entrance is compensated by the jump of an equal magnitude at the exit (see Section 3.3). Such particles experience either only reflection (even resonances) or only refraction (odd resonances) upon interaction with the current sheet [162].

Figure 42 outlines a model of a one-dimensional TCS in which the ion distribution function in the sheet contains particles with resonance energies; the structure of the sheet can then be determined by the dominance of either the reflection or refraction of particles arriving from the only

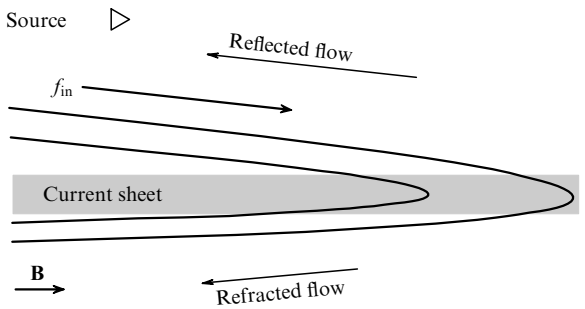

Figure 42. Schematic of the distribution of incident, reflected, and refracted plasma flows in the vicinity of TCSs. (From Ref. [159].)

source located in the region $z > 0$. The free parameter $r \leqslant 1$ describes the probability of particle reflection in the direction toward the source; the particle refraction coefficient is, accordingly, $1 - r$. Hence, $r = 0$ corresponds to total refraction of the plasma flux through the current sheet, i.e., to the symmetric case. The value $r = 1$ corresponds to total ion reflection toward the source, i.e., to the maximum asymmetry of the system.

We write the distribution function F of transient ions in a layer for $z > 0$ and $z < 0$ in terms of the distribution function of transient particles at the boundary of the sheet F_0:

$$F_{|z>0} = \begin{cases} F_0\,, & v_{\|} < 0\,, \\ rF_0\,, & v_{\|} > 0\,, \end{cases}$$

$$F_{|z<0} = \begin{cases} (1-r)\,F_0\,, & v_{\|} < 0\,, \\ 0\,, & v_{\|} > 0\,, \end{cases}$$

where $v_{\|}$ is the velocity component along the direction of the magnetic field. It is also assumed that upon interaction of the ions with the current sheet, the form of the distribution function does not change and no particle or energy losses exist. The directions of the plasma flows before and after the interaction with the TCS are shown in Fig. 42.

Self-consistent Vlasov–Maxwell equations (26) with the distribution function F were solved numerically and, as a result, equilibrium solutions were found for the parameter r ranging from 0 to 1 and a fixed $\varepsilon = 1$ [159]. The plasma density profiles for five values of the reflection coefficient r are shown in Fig. 43a. Analysis of partial currents reveals that the paramagnetic currents due to the half-turn of ions in the neutral plane about the field B_z tend to support the symmetry of current density profiles. The asymmetry of the current sheet is determined only by diamagnetic currents depending on the density distribution of plasma particles. Because the incident and reflected flows are added on the side of the source, the plasma density is higher there than on the opposite side (the case $r = 0$ is an exception). Figure 43b shows how, owing to diamagnetic negative currents, the current density profile becomes flatter on the side of the source, while its amplitude decreases. The shift of a nonsymmetric current sheet as a whole occurs in accordance with the condition that the pressure be balanced across the sheet, when an increase in the coefficient r is accompanied by an increase in the plasma density on the side of the source and a decrease on the opposite side.

The one-dimensional quasiadiabatic TCS model also permits studying other effects, for example, the influence of a multicomponent plasma on the structure of the current

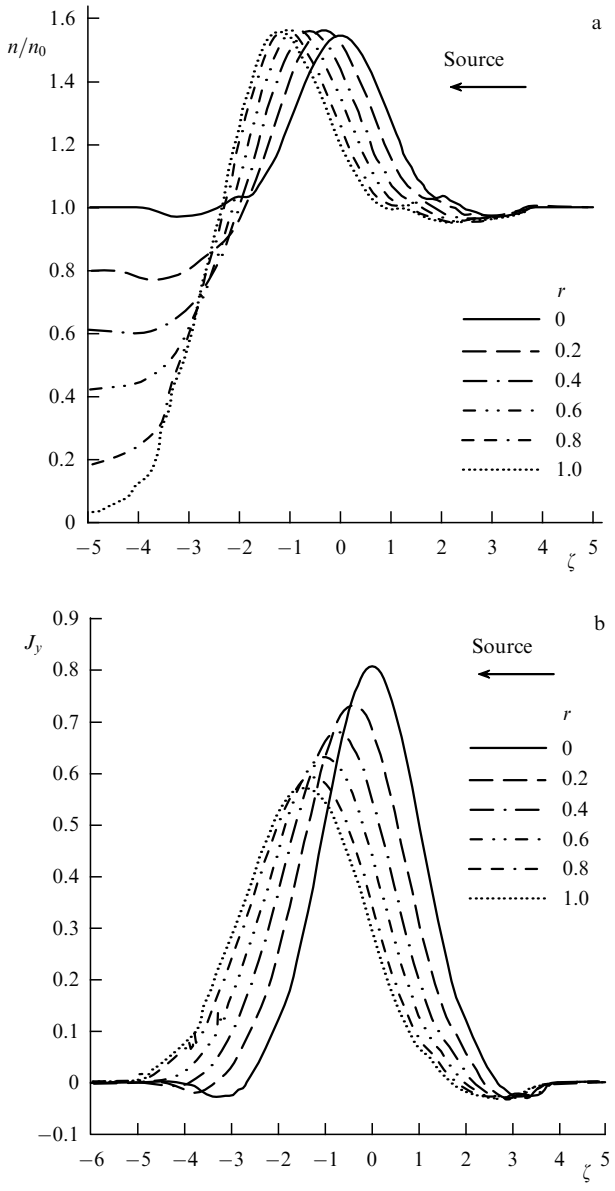

Figure 43. Plasma density (a) and current density (b) as functions of the dimensionless coordinate for values of the reflections coefficient r varying from 0 to 1 in steps of 0.2. The location of the plasma source is shown ($\zeta > 0$). (From Ref. [159].)

sheet. In Ref. [163] (see also review [22]), the results are presented of self-consistent solutions for a current sheet whose plasma contains not only protons but also heavy oxygen ions. It is shown that the orbits of transient heavy ions lead to the current sheet thickening severalfold, because of the larger Larmor radii of heavy ions. Moreover, the current due to oxygen ions dominates at the periphery of the current sheet, while the proton current dominates at its center. The results reveal the formation of a structure with multiple embeddings resembling a Russian doll: a relatively thin proton layer of the thickness of the order of the proton gyroradius is embedded into a relatively thick oxygen current sheet (of the order of several proton gyroradii), and the entire current sheet is in turn embedded into an even broader plasma sheet (whose thickness is only limited by the size of the model; in a real magnetosphere, it can reach several hundred proton gyroradii).

6.4.4 Comparison with experimental data. Owing to satellite missions of the past two decades (Interball, Cluster, and THEMIS (Time History of Events and Macroscale Interactions during Substorms)), it has become possible to obtain unprecedented detailed information on current sheets in Earth's magnetotail [17, 129, 152, 153, 164], which allows performing a comprehensive comparison of observational data with theoretical models.

A comparison of satellite data and results based on current sheet models taking the invariant I_z into account has revealed the broad possibilities provided by these models in describing experimental data [26, 147]. In the framework of TCS models, it has been possible to describe the 'embedding' property of the observed current sheets. Success has been achieved in showing that for the absolute majority of current sheets observed in Earth's magnetotail, the decrease in the current density j_y occurring as the magnetic field $|B_x|$ increases with the distance from the $z = 0$ ($B_x = 0$) plane is significantly more rapid than the decrease in the plasma density $n_p(z)$ [165]. That is, the profile $j_y(z)$ is embedded, as it were, in a wider profile $n_p(z)$. Embedding is a natural property of TCSs with a population of transient particles, which permits describing experimentally observed current density profiles in the framework of the model considered [22, 26, 31, 152, 166].

Another universal property of the TCS constructed with the conservation of the quasiadiabatic invariant I_z taken into account has been confirmed with the aid of satellite observations. Theoretical TCS models based on the quasiadiabatic description of the motion of plasma particles predict that the sheet thickness (spatial scale of the profile of $j_y(z)$) must be of the order of the gyroradius of transient ions in the field B_0. This estimate has been confirmed [30, 31] for most of the current sheets observed in Earth's magnetotail.

The first experimental data on the observation of bifurcation of the current sheet in Earth's magnetotail were published in Ref. [63] in 1996. Subsequent satellite missions confirmed this configuration of the magnetic field with a local minimum in the density of j_y at the center of the sheet ($z = 0$) [64, 153]. The theoretical description of bifurcated current sheets based on quasiadiabatic models fully explains the diversity of such structures, observed in experiments [46, 167]. It must be noted that the role of dynamic processes in the formation of bifurcated current sheets has still not been fully investigated. On the one hand, there is a series of observations of bifurcated current sheets performed over a long period of time [168]. On the other hand, a number of authors have indicated that the bifurcation of a current sheet can be caused by its vertical oscillations in space [63, 169, 170]. Such oscillations are typically associated with various instabilities developing in current sheets possessing a significant store of free energy (see Refs [171–74] and review [22]).

6.5 Models of two-dimensional current sheets

The model of a one-dimensional current sheet can be used in describing the most recent available results of satellite observations. But a zero (or small) value of the gradient $\partial B_z/\partial x$ in the magnetotail is a temporary manifestation of specific conditions for a certain interval of x values, rather than an inherent property of the system. With the exception of cases where thin current sheets with $L_x/L_z \approx 25$ are formed [175], the magnetotail is usually characterized by the ratio $L_x/L_z \sim 5$ and a relatively large gradient $\partial B_z/\partial x$ [176, 177]. It must also be noted that local regions are sometimes observed

with a reversed gradient $\partial B_z/\partial x < 0$ [178–181]. The problem of how the gradient $\partial B_z/\partial x$ influences the structure of a current sheet therefore deserves a separate investigation.

The idea of a current sheet model with $B_z(x/L_x)$ was proposed in a relatively simple form in Ref. [93] and realized numerically in Refs [182–184]. The description of ion dynamics in the framework of the quasiadiabatic theory discussed in this review is based on the results in Sections 4.1 and 5.1, where the possibility is shown of describing particle motion with the conservation of the first, I_z, and the second, I_x, quasiadiabatic invariants.

We specify a certain profile of the magnetic field $B_z(x/L_x)$ in the region $x \in [x_0, x_1]$. At the boundary $x = x_0$, we set the ion distribution function to correspond to the distribution function of particles arriving in the distant magnetotail from sources in the mantle (Fig. 28b). This function must be represented as a function of the invariant I_z and of the total energy H at $x = x_0$, $F_0(I_z, H)$. The function F at $x = x_0$ can be written as $F_0(p_x, I_z)$. Then, using the initially fixed profile $B_z(x/L_x)$, it is possible to find the expression for the second quasiadiabatic invariant $I_x = I_x(H, I_z)$, which plays the main role in the problem considered (see Section 5.1):

$$I_x = \frac{\sqrt{8}}{2\pi} \int_{x_-}^{x_+} \sqrt{H - h_z(I_z, \kappa x')}\, \mathrm{d}x' .$$

Here, the energy h_z of fast motion can be expressed in terms of I_z and κx, as in Section 3.1. Because $H = h_z(I_z, \kappa x_0) + (1/2)\, p_x^2$, we obtain the expression

$$I_x = \frac{1}{\pi} \int_{x_-}^{x_+} \sqrt{p_x^2 + 2h_z(I_z, \kappa x_0) - 2h_z(I_z, \kappa x')}\, \mathrm{d}x' ,$$

where the integration limits $x_\pm$ are determined from the condition that the integrand vanish. Thus, $F_0(p_x, I_z)$ can be expressed in terms of the invariants I_x and I_z: $F_0(I_x, I_z)$ at $x = x_0$.

The presence of the field E_y leads to particle convection toward Earth (in the direction of increasing x). The distribution function $F(I_x, I_z, x)$ can therefore be obtained by projecting the function $F_0(I_x, I_z)$, as is done in Section 6.4 for a one-dimensional current sheet. That is, having specified the profile $B_z(x/L_x)$, we can determine the function $F(I_x, I_z, x)$ at each point $x \in [x_0, x_1]$. Subsequently, integrating $v_y F(I_x, I_z, x)$ over velocities, we find the current density

$$j_y(x) \sim \int v_y F(I_x, I_z, x)\, J(I_x, I_z)\, \mathrm{d}I_z\, \mathrm{d}I_x ,$$

where $J(I_x, I_z)$ is the Jacobian of the transition from $\mathrm{d}\mathbf{p}$ to $\mathrm{d}I_z\, \mathrm{d}I_x$ and the velocity component v_y must be expressed in terms of the invariants I_z and I_x. Using $j_y(x)$, it is possible to determine the profile $B_z(x/L_x)$ and then to repeat the procedure. This iteration process stops when the profile $B_z(x/L_x)$ ceases to undergo changes from one iteration to another.

The technique considered permits obtaining self-consistent profiles of the magnetic field $B_z(x/L_x)$ and moments of the ion distribution function along x in a system averaged over particle oscillations in the field B_x [93].

There is also a more complicated approach, which generally permits obtaining practically all the characteristics of a two-dimensional configuration with quasiadiabatic ions. In developing the methods for current sheet simulation that

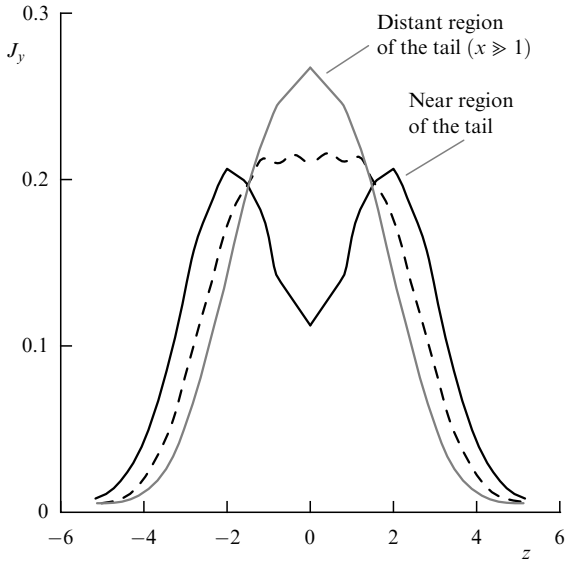

Figure 44. Profiles of current densities for different values of the x coordinate. The coordinate z is normalized to the ion Larmor radii.

were considered in Section 6.4, the function of quasi-trapped ions can be represented as $F_{\mathrm{trap}} \sim K \exp\left(-(H + \omega_0 I_x)/T\right)$, where K is a parameter characterizing the relative density of quasi-trapped particles, and H and T are the total energy and temperature. The quantity K is a free parameter in the problem because the sources of plasma with quasi-trapped and transient particles are conventionally independent. Quasi-trapped ions can occupy the current sheet not only because transient particles are scattered and trapped but also because of the convection from the far region of the tail to the near region in the two-dimensional problem. Transient ions do not experience multiple oscillations in the plane of slow variables and have no time to be shifted along the x direction due to the inhomogeneity of the magnetic field. Therefore, the motion of ions can be considered locally one-dimensional and the same distribution functions that were used in Section 6.4 can be applied for their description. We therefore describe transient ions using the distribution function F_{trans} in (23).

Because we are only interested in the role of quasiadiabatic particle dynamics, we take electrons into account only as a cold background supporting the charge neutrality of the system. Solving the two-dimensional equation for the magnetic field components B_x and B_z,

$$\frac{\partial B_x}{\partial z} - \frac{\partial B_z}{\partial x} = \frac{4\pi q}{c} \int v_y \left(F_{\mathrm{trans}}(|\mathbf{v}|, I_z) + F_{\mathrm{trans}}(|\mathbf{v}|, I_x)\right) \mathrm{d}\mathbf{v} ,$$

with the proper boundary conditions allows examining the two-dimensional current density distribution in the current sheet. Cross sections of the current density profiles for different x are shown in Fig. 44. As can be seen from the figure, for large x values (far from Earth), the current density is bell-shaped (the solid thin curve), which suggests that the current of transient ions is dominant, while the concentration of quasi-trapped ions is small compared with the concentration of transient particles. In approaching Earth, the concentration of quasi-trapped ions and their local current become more and more significant; redistribution of the current density across the sheet occurs, in the course of which its maximum in the neutral plane is replaced by a

minimum. At small x (the thick solid curve), the thickening and splitting of the current density profile become noticeable and reach a maximum at the edge of the current sheet closest to Earth (it is interesting to compare Fig. 44 and Fig. 40: the only difference between them is that the density of quasi-trapped particles increases in time in Fig. 40, but increases in space in Fig. 44).

The influence of the longitudinal inhomogeneity on the structure of the current sheet is therefore the cause of an important difference between the dynamics of quasiadiabatic transient and trapped ions. Transient ions are the main carriers of current, and they can carry a practically one-dimensional current density distribution in the current sheet. Their distribution function can only depend on the quasiadiabatic invariant of fast motion, I_z, and the total energy. By contrast, owing to the conservation of the invariant I_x, quasi-trapped ions are redistributed within the current sheet, and hence their density increases in the direction of the increase in the B_z component. Consequently, the roles of the particles carrying the main current are interchanged. This is manifested in the thickening of the current density profile and in its splitting as the observer approaches Earth.

7. Conclusion

We have performed a detailed analysis of the quasiadiabatic dynamics of charged particles in systems with a weak magnetic field, in which the spatial scale of the field inhomogeneity is much smaller than the particle gyroradius. We have shown that owing to the existence of a small parameter in such systems, it is possible to introduce a quasiadiabatic invariant, which is analogous to the magnetic moment. Moreover, in the case of two-dimensional systems, it is possible to introduce a second quasiadiabatic invariant similar to the longitudinal invariant of bounce oscillations of magnetized particles. The conservation of quasiadiabatic invariants for long periods of time is not possible due to the existence of random jumps of the invariant, related to crossing of the separatrix in the plane of fast motion. Exceptions are represented by populations of particles for which jumps of the invariants in the case of two successive crossings of the separatrix compensate each other due to the resonance effect, and populations of particles that are on regular trajectories not crossing the uncertainty curve.

The existence of quasiadiabatic invariants permits describing the dynamics of charged particles in one-dimensional and two-dimensional current sheets. We have examined a number of important applications corresponding to configurations of the magnetic field that are most often encountered in the course of describing magneto-plasma structures in a space environment. For example, we have described the dynamics of charged particles in current sheets with a longitudinal inhomogeneity of the magnetic field $B_z = B_z(x)$ with a magnetic field shear $B_y \neq 0$, in bifurcated sheets with two maxima of the current density, and in sheets involving X- and O-lines. Based on the constructed picture of particle dynamics, various mechanisms of effective particle acceleration in current sheets were considered, which can be described analytically using the assumption that quasiadiabatic invariants are conserved.

We have shown how the use of the quasiadiabatic invariant allows integrating trajectories of an ensemble of particles in a current sheet and reconstructing the distribution function at the boundary and in the central region. The analytic results obtained are in good qualitative and quantitative agreement with the results of direct satellite measurements. This makes the quasiadiabatic theory a powerful and effective tool for constructing magneto-plasma equilibrium states (current sheets) and investigating their evolution and acceleration of particles interacting with them.

The authors are grateful to the referee for the valuable comments. The work was supported by the RFBR grants 11-02-01166-a, 12-02-91158-GFEN-a, and 13-01-00251, and by the grant N.Sh. 623.2012.2. The work of A.I.N. was supported by the grant NSh-2519.2012.1. The work of D.L.V was supported by an NSF grant (SVET-0900177).

8. Appendices

A. Transitions across a separatrix and jumps of the quasiadiabatic invariant in Hamiltonian systems with fast and slow motions

In this Appendix, the general theory of jumps of the quasiadiabatic invariant is presented for transitions across the separatrix in Hamiltonian systems. We consider Hamiltonian systems with fast and slow motions that have two degrees of freedom: one corresponds to fast motion and the other one to slow motion. For fixed values of the slow variables, the phase portrait of fast motion is assumed to be divided by separatrices into three regions. When the slow variables change, the phase points cross the separatrix.

The value of the quasiadiabatic invariant 'action' is constant along the trajectory in the leading approximation until the trajectory reaches a separatrix. On the separatrix, the 'action' experiences a standard geometric jump related to the difference between the areas inside the trajectory in one of the loops of the separatrix and those in the external region. This approximation is called quasiadiabatic. Below, following Ref. [185], we obtain a formula for the next term in the asymptotic formula for changes in the 'action' in transition across the separatrix. The calculated correction to the quasiadiabatic approximation turns out to be a quantity of the order of $\kappa \ln \kappa$ in general, where κ is a small parameter characterizing the relation between the rates with which slow and fast variables change. If certain symmetry conditions are satisfied, this correction is of the order of κ. Such symmetry conditions are satisfied, for example, in the problem of the motion of a charged particle (ion) in the parabolic model of Earth's magnetotail.

The above correction to the quasiadiabatic approximation is related to particle motion in the vicinity of the separatrix. It is therefore called a jump of the quasiadiabatic invariant at a separatrix crossing (it is sometimes termed a dynamic jump, in order to distinguish it from a geometric jump). Although this jump of the quasiadiabatic invariant is small, it is essential for the dynamics of the system. Adding jumps for multiple crossings of the separatrix leads to diffusion of the quasiadiabatic invariant in the corresponding space.

The particular case of systems with fast and slow variables considered here is represented by Hamiltonian systems with a single degree of freedom, whose Hamiltonians depend on slowly varying parameters. Formulas for the change in the adiabatic invariant due to a crossing of the separatrix were obtained for such systems independently in Ref. [44] and in Refs [186, 187], while in the particular case of a pendulum in a slowly changing gravitational field (or a

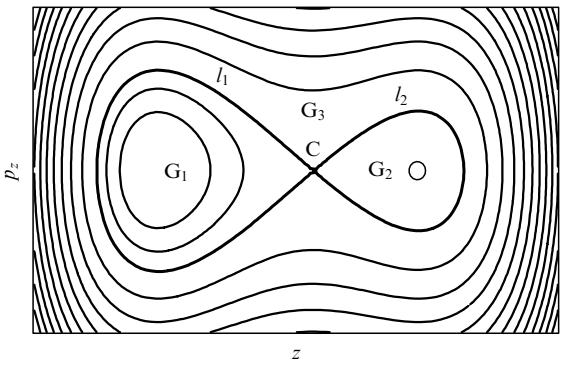

Figure 45. Schematic view of a phase portrait of fast motion.

charged particle in an electrostatic wave of slowly changing amplitude), the formulas were first obtained in Ref. [188]. Formulation of the problem of the behavior of an adiabatic invariant crossing a separatrix traces back to studies collected in books [1, 2].

A.1 Basic equations

We consider a Hamiltonian system with the Hamiltonian $H = H(p_z, z, p_x, \kappa x)$, where z and x are coordinates and p_z and p_x are their conjugate momenta. The equations of motion are given by

$$\dot{p}_z = -\frac{\partial H}{\partial z}\,,\ \dot{z} = \frac{\partial H}{\partial p_z}\,,\ \dot{p}_x = -\kappa\frac{\partial H}{\partial \kappa x}\,,\ \kappa\dot{x} = \kappa\frac{\partial H}{\partial p_x}\,.$$

The variables p_z and z are termed fast, and the variables p_x and κx, slow. The Hamiltonian system for p_z and z, when p_x, $\kappa x = \text{const}$ is called fast, or nonperturbed. We assume that the phase portrait of the nonperturbed system is similar to the one shown in Fig. 45.

The separatrices l_1 and l_2 passing through the saddle point C divide the portrait into regions G_1, G_2, and G_3. The areas of the regions G_1, G_2 and $G_1 \cup G_2$ are denoted by $S_v = S_v(p_x, \kappa x)$, $v = 1, 2, 3$. We let $h_c(p_x, \kappa x)$ denote the value of the Hamiltonian at the saddle point C and set $E = H - h_c$. Then, $E = 0$ at the point C and on the separatrices, and $E > 0$ in G_3 and $E < 0$ in $G_{1,2}$. We assume that the following quantities are different from zero (for definiteness, positive):

$$\Theta_v = \{S_v, h_c\} \equiv -\oint_{l_v} \{E, h_c\}\,\mathrm{d}t\,.$$

Here and below, $\{,\}$ are Poisson brackets in terms of κx and p_x:

$$\{f, g\} = f'_{\kappa x} g'_{p_x} - f'_{p_x} g'_{\kappa x}\,.$$

A.2 Quasiadiabatic approximation

Motion in each of the G regions can be described using the quasiadiabatic approximation. We let I denote the variable action of the fast system. In the quasiadiabatic approximation, the condition $I = \text{const}$ is satisfied along the trajectory (which is equivalent to the action I being a quasiadiabatic invariant) in each of the G_i regions, and a change in the variables p_x and κx is described by a Hamiltonian system with the Hamiltonian $\kappa\Phi(I, p_x, \kappa x)$, where p_x and κx are conjugate variables and Φ is the function H expressed in terms of I, p_x, and κx:

$$\dot{p}_x = -\kappa\frac{\partial \Phi}{\partial \kappa x}\,,\quad \kappa\dot{x} = \kappa\frac{\partial \Phi}{\partial p_x}\,.$$

Such a system is termed slow. Solutions of a slow system can land on the curve $\Phi(I, p_x, \kappa x) = h_c(p_x, \kappa x)$ corresponding to the separatrix of the fast system. This curve is called the uncertainty curve [189]. Crossing the separatrix leads to probabilistic phenomena [190, 191], which can be described in the quasiadiabatic approximation as follows.

Let motion start at $t = 0$ from a point $M_0(p_{z0}, z_0, p_{x0}, \kappa x_0)$, and $(p_{z0}, z_0) \in G_3(p_{x0}, \kappa x_0)$. In the region G_3, the action is assumed to be constant until the instant of reaching the separatrix: $I = I^- = \text{const}$. A change in p_x and κx is described by the solution $Y_3(\tau), X_3(\tau)$, $\tau = \kappa t$ of the system with the Hamiltonian $\kappa\Phi(I^-, p_x, \kappa x)$ and the initial conditions $(p_{x0}, \kappa x_0)$. The instant t_* of reaching the separatrix is determined from the relation $S_3(Y_3(\tau_*), X_3(\tau_*)) = 2\pi I^-$, $\tau_* = \kappa t_*$. The quantities $p_{x*} = Y_3(\tau_*)$ and $\kappa x_* = X_3(\tau_*)$ can be determined by solving the set of equations $S_3(\kappa x_*, p_{x*}) = 2\pi I^-$, $h_c(p_{x*}, \kappa x_*) = H(p_{z0}, z_0, p_{x0}, \kappa x_0)$.

After crossing the separatrix, the point can continue motion either in region G_1 or in region G_2. In the course of motion in region G_i, $i = 1, 2$, the action is again assumed to be constant: $I = S_i(p_{x*}, \kappa x_*)/(2\pi)$. Hence, in the quasiadiabatic approximation, in crossing the separatrix, the action experiences a jump related to the difference in geometry between phase trajectories in the G_i regions (a geometric jump).

A change in the slow variables is described by the solution $Y_i(\tau)$, $X_i(\tau)$ constructed for the G_i region of the slow system with the initial condition $Y_i(\tau_*) = p_{x*}$, $X_i(\tau_*) = \kappa x_*$.

Capture in one region or another is considered a random event. For a point M_0, the probability of being trapped in the G_i region is given by (see Refs [42, 44])

$$P_i = \frac{\Theta_i(p_{x*}, \kappa x_*)}{\Theta_3(p_{x*}, \kappa x_*)}\,,\quad i = 1, 2\,.$$

A.3 Improved quasiadiabatic invariant

The following quantity is called the improved quasiadiabatic invariant:

$$\begin{aligned} J &= J(p_z, z, p_x, \kappa x) = I + \kappa u(p_z, z, p_x, \kappa x)\,,\\ u &= \frac{1}{4\pi}\int_0^T \left(\frac{\partial H}{\partial p_x}\int_0^t \frac{\partial H}{\partial \kappa x}\,\mathrm{d}t'\right)\mathrm{d}t\\ &\quad -\frac{1}{4\pi}\int_0^T \left(\frac{\partial H}{\partial \kappa x}\int_0^t \frac{\partial H}{\partial p_x}\,\mathrm{d}t'\right)\mathrm{d}t\,. \end{aligned} \tag{27}$$

The integrals in (27) are calculated along the phase trajectory of the fast system passing through the point (p_z, z), T is the period of motion along this trajectory, t is the motion time counted from the instant of passing through point (p_z, z), and J is the improved first approximation in the averaging method [9]. When motion occurs far from the separatrices in times of the order of $1/\kappa$, I remains constant with a precision $\sim\kappa$, and J with a precision $\sim\kappa^2$. The derivation of formula (27) is given in Ref. [185].

The main idea underlying the calculation of the dynamic jump in the quasiadiabatic invariant is as follows. In motion far from the separatrix, the improved quasiadiabatic invariant changes by a quantity $\sim\kappa^2$, while the dynamic jump is a quantity $\sim\kappa\ln\kappa$ or, in the symmetric case (when $\Theta_1 = \Theta_2$ and

$S_1 = S_2$), $\sim \kappa$. Therefore, the dynamic jump is related to motion in the vicinity of the separatrices, and for its calculation we can use asymptotic expansions in the vicinities of separatrices.

A.4 Asymptotic expansions for nonperturbed motion in the vicinity of separatrices

In the asymptotic expansions given below, a, b_i, and g_i are smooth functions of p_x and κx.

The following expansion is valid for the period $T = T(h, p_x, \kappa x)$ of motion along the trajectory $E = h$ lying in the region G_i, $i = 1, 2, 3$:

$$T = -a_i \ln|h| + b_i + O\big(h \ln|h|\big)\,, \tag{28}$$

$$a_1 = a_2 = a\,,\ a_3 = 2a\,,\ b_3 = b_1 + b_2\,. \tag{29}$$

In accordance with the formula $T = 2\pi\,\partial I/\partial h$, the following expansion is valid for the action I on the trajectory considered:

$$2\pi I = S_i - a_i\, h \ln|h| + (b_i + a_i)\, h + O\big(h^2 \ln|h|\big)\,. \tag{30}$$

From the identity

$$\oint_{l_i} \frac{\partial E}{\partial \alpha}\,\mathrm{d}t = -\frac{\partial S_i}{\partial \alpha}\,,\quad \alpha = p_x\,,\ \kappa x\,,$$

we obtain

$$\oint_{E=h} \frac{\partial E}{\partial \alpha}\,\mathrm{d}t = -\frac{\partial S_i}{\partial \alpha} + O\big(h \ln|h|\big)\,,\quad \alpha = p_x, \kappa x\,, \tag{31}$$

$$\oint_{E=h} \left(\frac{\mathrm{d}E}{\mathrm{d}t}\right)_{\mathrm{tot}} \mathrm{d}t = -\kappa\Theta_i + \kappa O\big(h \ln|h|\big)$$

in the region G_i. The integrand in the last formula is the total derivative of the function E.

Let $C\sigma\eta$ be the set of principal coordinates for the saddle point C. The axes of this system are the bisectors of the angles between the separatrix segments entering the point C and leaving it. The axis $C\sigma$ is directed toward the interior of G_2. The $C\eta$ axis is directed toward the interior of G_3, such that the coordinate system $C\sigma\eta$ is right-handed.

The following formulas represent asymptotic expansions for function u (27):

(a) if the point (p_z, z) lies inside the region G_i, $i = 1, 2$ close to C on the $C\sigma$ axis, then the following expansion holds for the function u:

$$2\pi u = g_i + O\big(\sqrt{|h|}\ln|h|\big)\,,\quad h = E(p_z, z, p_x, \kappa x); \tag{32}$$

(b) if the point (p_z, z) lies inside the region G_3 close to C on the positive part of the $C\eta$ axis, then

$$2\pi u = \frac{1}{2}\,a(\Theta_2 - \Theta_1)\,\ln h + \frac{1}{2}\,(\Theta_1 b_2 - \Theta_2 b_1) + \frac{1}{2}\{S_2, S_1\} + g_3 + O(\sqrt{h}\,\ln h)\,, \tag{33}$$

where $g_3 = g_1 + g_2$.

A.5 Calculation of a change in the quasiadiabatic invariant

Far from the separatrices, the improved quasiadiabatic invariant changes only by a quantity $O(\kappa^2)$. Therefore, an order-of-magnitude change of κ is gained in a small vicinity of the separatrices, and to calculate it we can use the asymptotic expansions presented in A.4. This method, which is similar to the stationary phase method of calculating integrals, is represented below.

Let a phase point start motion at $t = 0$ in the region G_3, with $I = I^-$, $J = J^-$, and $u = u^-$; when $\tau = \tau^+ = K$, let this point lie in region G_i, $i = 1, 2$ with $I = I^+$ and $J = J^+$. We now introduce the following notation: τ_*, p_{x*}, and κx_* are the values of slow time and slow variables calculated in the quasiadiabatic approximation upon reaching the separatrix (we assume that $\tau_* < \tau^+$); t_*^- is the instant at which the phase point lands for the last time on the positive $C\eta$ axis close to the saddle C; t_*^+ is the instant at which the phase point lands for the first time on the $C\sigma$ axis close to C; $h_*^\pm$, $J_*^\pm$, $p_{x*}^\pm$, and $\kappa x_*^\pm$ are E, J, y, x values on the trajectory at $t = t_*^\pm$, $\xi = h_*^-/(\kappa\Theta_3)$, and $\xi_i = |h_*^+|/(\kappa\Theta_i)$. Here, Θ_j (and, in what follows, a, b_j, g_j, $\partial S_j/\partial\kappa x$, $\partial S_j/\partial p_x$, $j = 1, 2, 3$) are calculated at $\kappa x = \kappa x_*$, $p_x = p_{x*}$. The initial point is assumed not to belong to an exceptional small-measure set for which the phase point passes at a small distance ($\ll \kappa$) from the saddle point C and therefore moves in its vicinity for an untypically long time. Hence, $\kappa t_*^\pm = \tau_* + O(\kappa \ln \kappa)$.

The purpose of further calculations is to express J^+ in terms of J^-, ξ_i in the leading approximation.

A.5.1 Approaching the separatrix. When $0 \leqslant t \leqslant t_*^-$, the projection of a phase point onto the (p_z, z) plane describes coils close to nonperturbed trajectories. It can be verified that in the case of motion in the region $E > h > \kappa$, the quantity J changes by $O(\kappa^2/h)$. In particular, in the region $E > \sqrt{\kappa}/|\ln\kappa|$, the value of J changes by $O(\kappa^{3/2}\ln\kappa)$. After the arrival of the moving point in the region $0 < E < \sqrt{\kappa}/|\ln\kappa|$, we determine the instants when it successively crosses the $C\eta$ ray near the point C. These instants are numbered starting from the last one: $t_*^- = t_0 > t_1 > \ldots > t_N > 0$. We let h_n, τ_n, I_n, J_n, p_{xn}, κx_n denote the values of E, τ, I, J, p_x, κx at $t = t_n$. We introduce an arbitrary positive small constant $k < 1$, which is independent of κ. If $\xi > k\sqrt{\kappa}$, then the following formulas hold:

$$h_{n+1} = h_n + \kappa\big[\Theta_3 + O(\sqrt{h_{n+1}})\big]\,, \tag{34}$$

$$\tau_{n+1} = \tau_n + \kappa\,\frac{1}{2}\,a\,\ln h_n + \kappa a \ln(h_n + \Theta_1\kappa) + \kappa\,\frac{1}{2}\,a\,\ln h_{n+1} - \kappa b_3 + \kappa O(\sqrt{h_{n+1}})\,,$$

$$S_3(p_{xn}, \kappa x_n) = S_3(p_{x0}, \kappa x_0) + \Theta_3(\tau_n - \tau_0) + O(h_{n+1}^2 \ln^2 h_{n+1}) + O(\kappa\sqrt{h_{n+1}})\,. \tag{35}$$

In the formula for τ_{n+1}, it is taken into account that the point passes close to the saddle C three times, with the respective values of E close to h_n, $h_n + \Theta_1\kappa$, and h_{n+1}.

In calculating the asymptotic form of the change in J, we only use the leading terms of expansions (34), (35) (not involving the symbol O), and we do not present the derivation of the estimates of residual terms for simplicity.

The change in the improved quasiadiabatic invariant is represented as

$$J_*^- - J^- = (J_*^- - J_N) + (J_N - J^-)\,.$$

The second term in the right-hand side is of the order of $O(\kappa^{3/2}\ln\kappa)$. In calculating the first term, we use the leading

terms of expansions (30), (32), (33) for J_N and J_*^-. We determine the quantities h_N, $S_3(p_{xN}, \kappa x_N)$ entering the expansion for J_N with the aid of the leading terms of expansions (34), (35).

It can be shown that using the leading terms of the expansions permits obtaining the asymptotic form of $J_* - J^-$ up to $O(\kappa^{3/2} \ln \kappa)$.

We perform the necessary calculations. Let h_n' and τ_n' be the values of h_n and τ_n calculated using the leading terms in (34). We set $\vartheta_{ij} = \Theta_i/\Theta_j$ and obtain

$$
\begin{aligned}
&h_n' - h_*^- = n\Theta_3\kappa\,,\\
&\tau_N' - \tau_0 = \sum_{n=0}^{N-1}(\tau_{n+1}' - \tau_n')\\
&\quad = \kappa\biggl[- Nb_3 + a\sum_{n=0}^{N-1} \ln\,(h_*^- + n\Theta_3\kappa)\biggr]\\
&\quad = -\kappa N b_3 + a\kappa\sum_{n=0}^{N-1} \ln\,(h_*^- + n\Theta_3\kappa)\\
&\quad + a\kappa\sum_{n=0}^{N-1} \ln\,(h_*^- + n\Theta_3\kappa + \Theta_1\kappa)\\
&\quad + \frac{a}{2}\,\kappa \ln\,(h_*^- + N\Theta_3\kappa) - \kappa\,\frac{a}{2}\ln h_*^-\\
&\quad = -N\kappa b_3 + \kappa a\biggl[2N \ln\,(\Theta_3\kappa) + \ln\frac{\Gamma(\xi+N)}{\Gamma(\xi)}\\
&\quad + \ln\frac{\Gamma(\xi+N+\vartheta_{13})}{\Gamma(\xi+\vartheta_{13})} + \frac{1}{2}\ln\,(\xi+N) - \frac{1}{2}\ln\xi\biggr]\\
&\quad = N\kappa\bigl(-b_3 + 2a\ln\,(\Theta_3\kappa)\bigr) + \kappa a\biggl[\ln\frac{\sqrt{2\pi}}{\Gamma(\xi)}\\
&\quad + \left(\xi+N-\frac{1}{2}\right)\ln\,(\xi+N)\ - (\xi+N) + \ln\frac{\sqrt{2\pi}}{\Gamma(\xi+\vartheta_{13})}\\
&\quad + \left(\xi+N+\vartheta_{13}-\frac{1}{2}\right)\ln\,(\xi+N+\vartheta_{13}) - (\xi+N+\vartheta_{13})\\
&\quad + \frac{1}{2}\ln\,(\xi+N) - \frac{1}{2}\ln\xi\biggr] + O\left(\frac{\kappa}{N}\right)\\
&\quad = N\kappa\bigl(-b_3 - 2a + 2a\ln\,(\Theta_3\kappa)\bigr)\\
&\quad + \kappa a\biggl[\ln\frac{2\pi}{\Gamma(\xi)\Gamma(\xi+\vartheta_{13})}\\
&\quad + 2\left(\xi+N+\vartheta_{13}-\frac{1}{4}\right)\ln\,(\xi+N)\ - 2\xi - \frac{1}{2}\ln\xi\biggr]\\
&\quad + O(\kappa^{3/2}\ln\kappa)\,.
\end{aligned}
\tag{36}
$$

Here, $\Gamma(\cdot)$ is Euler's gamma function and the Stirling asymptotic formula is used for Γ.

Substituting the obtained expressions into the expansions for I and u in (30) and (33), we finally obtain

$$
\begin{aligned}
2\pi(J_*^- - J^-) = 2\kappa a\Theta_3\biggl[&-\frac{1}{2}\ln\frac{2\pi}{\Gamma(\xi)\,\Gamma(\xi+\vartheta_{13})} + \xi\\
&+\left(-\xi+\frac{1}{2}\,\vartheta_{23}\right)\ln\xi\biggr] + O(\kappa^{3/2}\ln\kappa)\,,\quad \vartheta_{ij} = \Theta_i/\Theta_j\,.
\end{aligned}
\tag{37}
$$

Comment. The estimate of the residual term in (37) turns out to be much better than in intermediate formulas at $E = h_N$. This is because the residual terms in asymptotic expansions are constrained by relations providing the quasiadiabatic invariance at large h.

In the leading approximation, formula (37) permits obtaining the relation between $S_i(p_{x*}^-, \kappa x_*^-)$, J^-, and $\xi\,(i = 1, 2)$, which is needed in what follows. The following relations hold:

$$
\begin{aligned}
S_j(p_{x*}^-, \kappa x_*^-) - S_j(p_{x*}, \kappa x_*) &= \frac{\partial S_j}{\partial p_x}\,(p_{x*}^- - p_{x*})\\
&+ \frac{\partial S_j}{\partial \kappa x}\,(\kappa x_*^- - \kappa x_*) + O(\kappa^2\ln^2\kappa)\,,\\
h_*^- = -\frac{\partial h_c}{\partial p_x}\,(p_{x*}^- - p_{x*}) &- \frac{\partial h_c}{\partial \kappa x}(\kappa x_*^- - \kappa x_*) + O(\kappa^2\ln^2\kappa)\,.
\end{aligned}
\tag{38}
$$

The last relation follows from the definition of p_{x*} and x_* and the energy integral $H = h_c(p_{x*}, \kappa x_*)$. Regarding the first relation for $j = 3$ in (38) and the second relation as a linear system for $p_{x*}^- - p_{x*}$ and $\kappa x_*^- - \kappa x_*$, solving it, and substituting the result in the first relation for $j = 1, 2$, we obtain

$$
\begin{aligned}
S_i(p_{x*}^-, \kappa x_*^-) - S_i(p_{x*}, \kappa x_*) &= \{S_i, S_3\}\,\frac{h_*^-}{\Theta_3}\\
&+ \vartheta_{i3}\bigl(S_3(p_{x*}^-, \kappa x_*^-) - S_3(p_{x*}, \kappa x_*)\bigr)\\
&+ O(\kappa^2\ln^2\kappa)\,,\quad i = 1, 2\,.
\end{aligned}
\tag{39}
$$

The expansions presented in Section A4 permit expressing $S_3(p_{x*}^-, \kappa x_*^-)$ in terms of J_*^- and ξ; formula (37) expresses J_*^- in terms of J^-, ξ. Therefore, (39) permits expressing $S_i(p_{x*}^-, \kappa x_*^-)$ in terms of J^-, ξ.

A.5.2 Crossing the separatrix. In a single turn in the vicinity of the separatrix l_i at a distance of the order of κ from it, the value of the function E changes by the quantity $-\kappa\Theta_i + O(\kappa^{3/2})$. Therefore, $\xi \in (0, 1+k\sqrt{\kappa})$, $k = \text{const} > 0$. If $\xi \in (k\sqrt{\kappa}\,,\ \vartheta_{23} - k\sqrt{\kappa}\,)$, then after crossing the separatrix, the point is trapped in G_2, while if $\xi \in (\vartheta_{23} + k\sqrt{\kappa}, 1 - k\sqrt{\kappa})$, it is trapped in G_1. Below, we consider the first case for definiteness. When $t_*^- \leqslant t \leqslant t_*^+$, the projection of the phase point onto the (p_z, z) plane describes a curve close to the separatrix l_2. The following relations are satisfied:

$$
\begin{aligned}
&h_*^+ = h_*^- - \Theta_2\kappa + O(\kappa^{3/2})\,,\\
&t_*^+ = t_*^- - \frac{1}{2}\,a\ln h_*^- - \frac{1}{2}\,a\ln|\,h_*^+| + b_2 + O(\kappa\ln^2\kappa)\,,\\
&S_2(p_{x*}^+, \kappa x_*^+) = S_2(p_{x*}^-, \kappa x_*^-) + \Theta_2\kappa(t_*^+ - t_*^-) + O(\kappa^{3/2})\,.
\end{aligned}
$$

These relations, together with the expansions in Section A.5.1, allow expressing J_*^- and ξ in terms of $S_2(p_{x*}^-, \kappa x_*^-)$, ξ_2.

A.5.3 Moving away from the separatrix. Arguments similar to those presented in Section A.5.2 when applied to motion in the region G_i, $i = 1, 2$ lead to the relation

$$
\begin{aligned}
2\pi(J^+ - J_*^+) = \kappa a\Theta_i\biggl[&-\ln\frac{\sqrt{2\pi}}{\Gamma(\xi_i)} + \xi_i\\
&+\left(\frac{1}{2} - \xi_i\right)\ln\xi_i\biggr] + O(\kappa^{3/2}\ln\kappa)\,.
\end{aligned}
\tag{40}
$$

We note that formulas (37) and (40) hold for any number of degrees of freedom of slow motion.

A.5.4 The final formula. In Section A.5.3, the quantity J^+ is expressed in terms of J_*^+ and ξ_i. The formulas in Section A.5.2 permit expressing J_*^+ and ξ in terms of $S_i(p_{x*}^-, \kappa x_*^-)$ and ξ_i. In turn, the formulas in Section A.5.1 allow expressing $S_i(p_{x*}^-, \kappa x_*^-)$ in terms of J^-, ξ. As a result, we can express J^+ in terms of J^- and ξ_i : in the case of arrival in the region G_i, if $k\sqrt{\kappa} < \xi_i < 1 - k\sqrt{\kappa}$, then

$$
\begin{aligned}
2\pi J^+ &= S_i(p_{x*}, \kappa x_*) + \vartheta_{i3}\bigl(2\pi J^- - S_3(p_{x*}, \kappa x_*)\bigr) \\
&+ \kappa a \Theta_i \left(\xi_i - \frac{1}{2}\right)\bigl[\ln(\kappa\Theta_i) - 2\vartheta_{i3}\ln(\kappa\Theta_3)\bigr] \\
&- \kappa a \Theta_i \ln \frac{(2\pi)^{3/2}}{\Gamma(\xi_i)\,\Gamma\bigl(\vartheta_{i3}(1-\xi_i)\bigr)\,\Gamma(1-\vartheta_{i3}\xi_i)} \\
&+ \kappa\Theta_i\left(\frac{1}{2} - \xi_i\right)(b_i - \vartheta_{i3}b_3) + \kappa(g_i - \vartheta_{i3}g_3) \\
&+ \kappa\vartheta_{i3}\left(\frac{1}{2} - \xi_i\right)\{S_i, S_3\} \\
&+ O\bigl(\kappa^{3/2}\bigl(|\ln\kappa| + (1-\xi_i)^{-1}\bigr)\bigr)\,. \qquad (41)
\end{aligned}
$$

The quantity $\xi_i \in (0, 1)$ is a function of the initial conditions, and its value can experience a change of the order of unity when there is a small change, of the order of κ, in the arguments. Therefore, in dealing with an individual jump, it is expedient to treat ξ_i as a random quantity. For a given initial point $M_0(p_{z0}, z_0, p_{x0}, \kappa x_0)$, the probability of the event $\xi_i \in (\alpha, \beta) \subset (0, 1)$ is, by definition,

$$
Q_{i,(\alpha,\beta)} = \lim_{\delta\to 0}\,\lim_{\kappa\to 0}\frac{\text{mes}\;U_{i,(\alpha,\beta)}^{(\delta)}}{\text{mes}\;U_i^{(\delta)}}\,,
$$

where $U_i^{(\delta)}$ is a set of points in the δ-neighborhood of M_0 that are to be captured in the region G_i, and $U_{i,(\alpha,\beta)}^{(\delta)}$ is the set of points from $U_i^{(\delta)}$ for which $\xi_i \in (\alpha, \beta)$, and mes(...) is the phase volume. It can be shown (see the derivation of a similar relation in Ref. [192]) that $Q_{i,(\alpha,\beta)} = \beta - \alpha$.

It follows that the distribution of ξ_i is uniform on (0, 1). The quantity J^+ is also treated as random, and formula (41) determines its conditional distribution under the condition that the points are trapped in the region G_i.

If the initial and final points of a trajectory are chosen such that $u = 0$ at these points, then we can substitute the quantity $I^\pm$ for $J^\pm$ in (41); the second term in the right-hand part of (41) then vanishes.

A.5.5 Formulas for changes in the quasiadiabatic invariant in other transitions. Above, it was assumed that $\Theta_1 > 0$, $\Theta_2 > 0$. If the signs of Θ_i are different, other transitions occur between the regions. For example, let $\Theta_1 > 0$, $\Theta_2 < 0$, and $\Theta_3 > 0$. Then the probability of points from G_2 and G_3 to arrive in the region G_1 is unity. The change in J in the transition from G_3 to G_1 is given by formula (41), with $k\sqrt{\kappa} < \xi_i < 1 - \vartheta_{31} - k\sqrt{\kappa}$. The change in J in the transition from G_2 to G_1 in the case $k\sqrt{\kappa} < \xi_2 < 1 - k\sqrt{\kappa}$ is described by the formula

$$
\begin{aligned}
2\pi J^+ &= S_1(p_{x*}, \kappa x_*) + \vartheta_{12}\bigl(2\pi J^- - S_2(p_{x*}, \kappa x_*)\bigr) \\
&+ \kappa a(1-\xi_2)\bigl(\Theta_2\ln(\kappa\Theta_1) - \Theta_1\ln|\kappa\Theta_2|\bigr) \\
&- \kappa a\Theta_1\ln\frac{2\pi(1-\xi_2)\sqrt{-\vartheta_{21}}}{\Gamma(\xi_2)\,\Gamma(\vartheta_{31} - \vartheta_{21}\xi_2)} \\
&+ \kappa(1-\xi_2)(\Theta_1 b_2 - \Theta_2 b_1) + \kappa(g_1 - \vartheta_{12}g_2) \\
&- \kappa(1-\xi_2)\{S_1, S_2\} + O\bigl(\kappa^{3/2}\bigl(|\ln\kappa| + (1-\xi_2)^{-1}\bigr)\bigr)\,, \\
\xi_2 &= \frac{h_*^-}{\kappa\Theta_2}\,. \qquad (42)
\end{aligned}
$$

Here, h_*^- is the value of E at the last arrival on the Cσ axis in the region G_2 close to the saddle point C.

The formulas for other transition options are obtained from (41) and (42) by altering the direction of time and the region labels. The method for obtaining formula (41) is general and permits calculating changes in the quasiadiabatic invariant for other types of the phase portrait divided into regions by separatrices. The essential assumptions underlying this derivation are the nondegeneracy of singular saddle points and nonzero rates of change of the areas of regions in the quasiadiabatic approximation. In what follows, we everywhere use the notation ξ for the quantity $1 - \xi_i$.

A.6 Jump of the quasiadiabatic invariant in the problem of charged particle motion in the parabolic model of Earth's magnetotail

The motion of a charged particle in the parabolic model of Earth's magnetotail is described by Hamiltonian (4). The fast variables are z and p_z, and the slow variables are κx and p_x. Phase portraits of fast motion for $\kappa x > 0$ and $\kappa x < 0$ are shown in Figs 4a and b. When $\kappa x > 0$, the portrait of fast motion has separatrices on it. A jump of the quasiadiabatic invariant in the case of transition across the separatrix from the region G_3 into G_1 or G_2 is given by formula (41). Owing to the symmetry of the problem under the change $z \to -z$ in (41), we can set $S_1 = S_2 = S_3/2$, $\Theta_1 = \Theta_2 = \Theta$, $b_1 = b_2$, $g_1 = g_2$, and $\vartheta_{i3} = 1/2$. Then Eqn (41) gives

$$
\begin{aligned}
J^+ &= \frac{1}{2}\,J^- - \frac{\kappa a\Theta}{2\pi}\ln(2\sin\pi\xi) \\
&+ O\bigl(\kappa^{3/2}\bigl(|\ln\kappa| + (1-\xi)^{-1}\bigr)\bigr)\,. \qquad (43)
\end{aligned}
$$

In passing from (41) to (43), reflection and duplication formulas for the gamma function are used. The coefficient a in (43) is equal to $1/\sqrt{\kappa x}$. For the areas of the regions G_i, we have

$$
S_{1,2} = \frac{8}{3}\,(\kappa x)^{3/2}\,.
$$

Consequently, $\Theta = (\partial S_{1,2}/\partial\kappa x)\,p_x = 4p_x\sqrt{\kappa x}$. As a result, in the leading approximation we obtain

$$
J^+ = \frac{1}{2}\,J^- - \frac{2\kappa p_x}{\pi}\ln(2\sin\pi\xi)\,. \qquad (44)
$$

For the transition from $G_{1,2}$ to G_3, we similarly find

$$
J^+ = 2J^- - \frac{4\kappa p_x}{\pi}\ln(2\sin\pi\xi)\,. \qquad (45)
$$

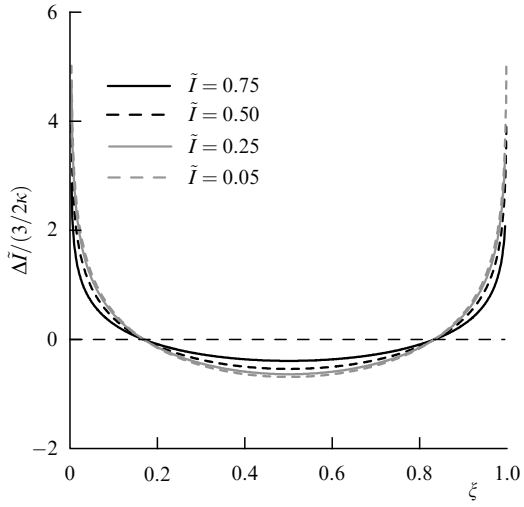

Figure 46. Dependence of $\Delta\tilde{I}$ on ξ for several values of $\tilde{I}$.

Applying formula (27) for the improved quasiadiabatic invariant, it is not difficult to verify that for both $z = 0$ and $p_z = 0$, we have $u = 0$ and, consequently, $J = I$.

Therefore, if at the instant $t_\pm$ the phase point has $z = 0$ or $p_z = 0$, then we can substitute the quantity $I^\pm$ for $J^\pm$ in formulas (44) and (45).

A.7 Jump of the quasiadiabatic invariant as a function of the fast phase

The jump in the quasiadiabatic invariant, ΔI_z, in the problem of charged particle dynamics with Hamiltonian (4) is described by an expression following from formulas (44) and (45):

$$\Delta I_z = -\frac{2}{\pi}\,\kappa p_x^*\,\ln\left(2\sin\pi\xi\right).$$

We now introduce the dimensionless quasiadiabatic invariant $\tilde{I} = 3\pi I_z/8(2H)^{3/4}$, use the formula relating the area inside a separatrix loop and the value of κx^*, and take into account that $p_x^* = \pm[2H - (\kappa x^*)^2]^{1/2}$. We can then write

$$\Delta\tilde{I} = -\frac{3}{2}\,\frac{\kappa\,\operatorname{sign} p_x^*}{(2H)^{1/4}}\,\sqrt{1-\tilde{I}^{4/3}}\,\ln\left(2\sin\pi\xi\right). \tag{46}$$

From formula (46), the jump in the invariant is seen to exhibit a logarithmic divergence in the vicinity of $\xi = 0$ and $\xi = 1.0$ (Fig. 46).

Relation (46) for a jump in the quasiadiabatic invariant as a function of ξ has been repeatedly verified by direct numerical integration of the original Hamiltonian system for concrete problems. For a mathematical pendulum with slowly changing parameters (a system with 1.5 degrees of freedom), formula (46) was verified by numerical simulation in Ref. [193], and for a charged particle in the magnetic field of a current sheet, in Refs [194, 195].

B. Jumps of the quasiadiabatic invariant in the case of its small initial values

It must be noted that in deriving formulas (44) and (45) for a jump of the quasiadiabatic invariant, the existence of a single small parameter κ in the system was assumed. These relations are therefore inapplicable when the values of the quasiadiabatic invariant are small ($\tilde{I} \leqslant \kappa$). Obtaining formulas for a jump of the quasiadiabatic invariant in this case requires a separate analysis.

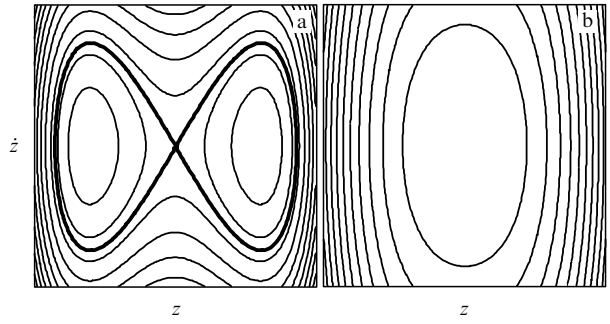

Figure 47. Phase portrait of the system with the Hamiltonian $H = (1/2)(\dot{z})^2 + (1/2)(z^4 - \kappa\dot{x}^* t z^2)$ for (a) $\kappa\dot{x}^* t > 0$ and (b) $\kappa\dot{x}^* t < 0$.

We obtain an expression for a jump of the quasiadiabatic invariant, ΔI_z, in the case of small values of the invariant I_z itself (of the order of κ or less) [196]. We write the Hamiltonian equations for Hamiltonian (4):

$$\begin{aligned}\dot{p}_z = \ddot{z} &= -z\left(\frac{1}{2}\,z^2 - \kappa x\right),\\ \dot{p}_x = \ddot{x} &= \kappa\left(\frac{1}{2}\,z^2 - \kappa x\right).\end{aligned} \tag{47}$$

Particles with a small I_x cross the uncertainty curve at approximately $x = 0$. For such particles, in the vicinity of the point of crossing the uncertainty curve (and, consequently, the separatrix), we can write $\kappa x \approx \kappa\dot{x}^* t$, where $\dot{x}^* = p_x^*$ is the momentum at the instant of crossing the separatrix. Hence, the first equation of system (47) becomes $\ddot{z} = -(1/2)\,z^3 + z\kappa\dot{x}^* t$, where $\kappa\dot{x}^* t$ is the slow time. The Hamiltonian of this system has the form $H = (1/2)(\dot{z})^2 + (1/2)(z^4 - \kappa\dot{x}^* t z^2)$. The phase portrait of this Hamiltonian for a frozen $\kappa\dot{x}^* t$ is presented in Fig. 47 for $\kappa\dot{x}^* t > 0$ and $\kappa\dot{x}^* t < 0$. For $\kappa\dot{x}^* t > 0$, the phase portrait has two separatrix loops and an external region, as does the phase portrait in Fig. 5b.

We now change the variables as $w = z(1/2)(\kappa\dot{x}^*)^{-1/3}$, $r = t(\kappa\dot{x}^*)^{1/2}$. Then the first equation of system (47) becomes

$$\frac{\mathrm{d}^2 w}{\mathrm{d}r^2} = rw - 2w^3. \tag{48}$$

Equation (48) is the second Painlevé equation and no longer involves a small parameter. The asymptotic form of the solution of Eqn (48) was found in Ref. [197]. As $r \to -\infty$,

$$w(r) = \alpha_-(-r)^{-1/4}\sin\left[\frac{2}{3}\,(-r)^{3/4} + \frac{3}{4}\,\alpha_-^2\,\ln(-r) + \varphi_-\right], \tag{49}$$

and as $r \to +\infty$,

$$w(r) = \pm\sqrt{\frac{r}{2}} \pm \alpha_+(2r)^{-1/4} \times \cos\left(\frac{2\sqrt{2}}{3}\,r^{3/4} - \frac{3}{2}\,\alpha_+^2\,\ln r + \varphi_+\right). \tag{50}$$

Here, (α_-, φ_-) and (α_+, φ_+) are related to the action–angle variables for solutions in the limit as $r \to \pm\infty$:

$$\alpha_+^2 = \frac{1}{\pi} \ln \frac{1+|p|^2}{2|\mathrm{Im}\,(p)|}\,,$$

$$\varphi_+ = -\frac{\pi}{4} + \frac{7}{2}\,\alpha_+^2 \ln 2 - \arg\Gamma(\mathrm{i}\alpha_+^2) - \arg\,(1+p^2)\,,$$

$$p = \sqrt{\exp\,(\pi\alpha_-^2) - 1}$$

$$\times \exp\left\{\mathrm{i}\left[\frac{3\alpha_-^2}{2} \ln 2 - \frac{\pi}{4} - \arg\Gamma\left(\frac{\mathrm{i}\alpha_-^2}{2}\right) - \varphi_-\right]\right\},$$

Γ is the gamma function, and $\arg(\ldots)$ is the argument of a complex number.

Just as in Section 3.1, it is possible to introduce a quasiadiabatic invariant I_w as the area, normalized to 2π, bounded by the particle trajectory. In the asymptotic regimes $r \to \pm\infty$, we then obtain the values for the quasiadiabatic invariant:

$$I_w^{\pm} = \frac{1}{2}\,\alpha_{\pm}^2\,.$$

The quantities I_w^- and I_w^+ coincide in the leading approximation with the value I_w of the quasiadiabatic invariant before and after the separatrix is crossed. For the invariant I_z, we obtain

$$I_z = 4(\kappa\dot{x}^*)\frac{1}{2\pi}\oint \dot{w}\,\mathrm{d}w = 4(\kappa\dot{x}^*)\,I_w\,.$$

B.1 Jump of the quasiadiabatic invariant in the case of transition from the external region to one of the loops of the separatrix

Based on the relations obtained above, if I_w^- and φ_- are known, we can determine the value of I_w^+ as

$$I_w^+ = \frac{1}{2\pi} \ln \frac{1+|p|^2}{2|\mathrm{Im}\,(p)|}\,,$$

$$p = \sqrt{\exp\,(2\pi I_w^-) - 1}$$

$$\times \exp\left(\mathrm{i}3I_w^- \ln 2 - \frac{\mathrm{i}\pi}{4} - \mathrm{i}\arg\Gamma(\mathrm{i}I_w^-) - \mathrm{i}\varphi_-\right).$$

The jump of the quasiadiabatic invariant in crossing the separatrix is given by $\Delta I_w = 2I_w^+ - I_w^-$.

The comparison of Fig. 48, in which the dependence $\Delta I_w(\varphi_-)$ is presented, with Fig. 46 shows that in the case of small initial values of the invariant I_w^-, the behavior of the jumps $\Delta I_w(\varphi_-)$ in Fig. 48 differs essentially from the behavior of jumps in the case of moderate initial I_z values, presented in Fig. 46. The main difference consists in the absence of the region of negative jump values of the invariant at small I_w. This is because the quasiadiabatic invariant is a positive quantity. As a consequence, for small initial values of the invariant, the jump cannot be negative (the total value of the invariant and of its jump cannot be less than zero). Therefore positive jumps dominate in the case of small initial I_w values.

Straightforward verification of the formula for $\Delta I_w(\varphi_-)$ with the aid of numerical integration of the initial Hamiltonian set of equations (47) has confirmed the validity of the obtained expressions [196].

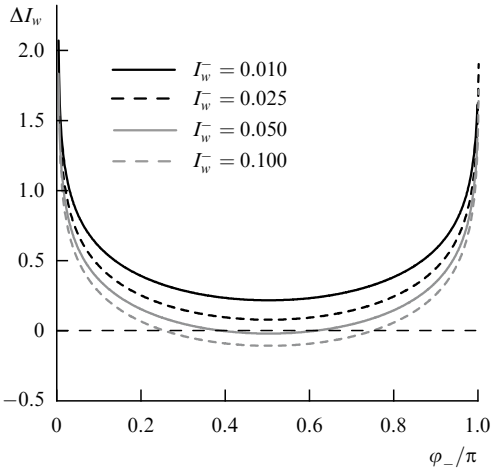

Figure 48. Dependence $\Delta I_w(\varphi_-)$ for different values of I_w^-.

It is worth noting that the expression obtained for the jump of the quasiadiabatic invariant should turn into formula (7) for moderate initial values of I_w^- (i.e., when $I_w^- \sim 1$ or $I_z \sim \kappa$). To verify this, we substitute the expression for p in the expression for I_w^+:

$$I_w^+ = I_w^- - \frac{1}{2\pi} \ln \sqrt{\exp\,(2\pi I_w^-) - 1}$$

$$- \frac{1}{2\pi} \ln \left[2\sin\left(3I_w^- \ln 2 - \frac{\pi}{4} - \arg\Gamma(\mathrm{i}I_w^-) - \varphi_-\right)\right].$$

We now introduce the new notation

$$\varphi' = 3I_w^- \ln 2 - \frac{\pi}{4} - \arg\Gamma(\mathrm{i}I_w^-) - \varphi_-\,.$$

If $I_w^- \sim 1$, we can use the asymptotic formula

$$\ln\left[\exp\,(2\pi I_w^-) - 1\right] \approx 2\pi I_w^-\,.$$

Substituting this and the expression for φ' in the formula for I_w^+, we find

$$\Delta I_w = -\frac{1}{\pi} \ln\,(2\sin\varphi')\,.$$

We now use the relation $I_z = 4\kappa p_x I_w$ and obtain

$$\Delta I_z = -\frac{4}{\pi}\,\kappa p_x \ln\,(2\sin\varphi')\,.$$

The last expression coincides exactly with the expression $\Delta J = 2J^+ - J^-$ in (44).

B.2 Jump of the quasiadiabatic invariant in the case of transition from one of the separatrix loops to the external region

We consider the jump of the quasiadiabatic invariant in the transition from a separatrix loop to the external region. We assume the quantities I_w^+ and φ_+ to be known. It is then necessary to obtain an expression for I_w^-. We write the equation for p:

$$\frac{1+|p|^2}{2|\mathrm{Im}\,p|} = g_1(I_w^+)\,, \qquad \arg\,(1+p^2) = g_2(I_w^+, \varphi_+)\,,$$

where

$$g_1 = \exp\left(2\pi I_w^+\right),$$
$$g_2 = -\varphi_+ - \frac{\pi}{4} + 7I_w^+ \ln 2 - \arg\Gamma(2\mathrm{i}I_w^+).$$

We write $|p|^2$ in terms of g_1 and g_2:

$$|p|^2 = \sin^2 g_2(g_1^2 - 1) + \left(g_1 - \cos g_2\sqrt{g_1^2 - 1}\right)^2.$$

The quantity I_w^- is expressed in terms of $|p|^2$:

$$I_w^- = \frac{1}{2\pi}\ln\left(1 + |p|^2\right).$$

Thus, we have obtained I_w^- as a function of I_w^+ and φ_+. The corresponding expression for the jump in the quasiadiabatic invariant is $\Delta I_w = I_w^+ - 2I_w^-$.

We note that in the case of a zero initial value of the quasiadiabatic invariant ($I_w^+ = 0$), we obtain $p = \pm\mathrm{i}\alpha_-^2 = \ln 2/\pi$. Then, after the separatrix is crossed,

$$I_z = \frac{2}{\pi}\,\kappa|p_x^*|\ln 2.$$

Hence, after the separatrix is crossed, particles with a zero initial value of the quasiadiabatic invariant have values of the invariant that are independent of ξ. Direct numerical integration has shown this relation to hold [196].

C. Jumps of the quasiadiabatic invariant in a system with a degenerate saddle point

We now show that in a system with a degenerate singular point, the jump of the quasiadiabatic invariant ΔI_z is of the order of $\kappa_{\mathrm{bif}}^{3/4}$ (the particle dynamics for such a system are discussed in Section 4.3). In order to derive the formula for the jump ΔI_z, we use the same approach that was expounded in Appendix A for a system with a nondegenerate singular point. Because the jump is of the order of $\kappa_{\mathrm{bif}}^{3/4}$ and the change in the invariant occurs far from the separatrix $\sim\kappa_{\mathrm{bif}}$, we assume that the main part of the change in the quasiadiabatic invariant is related precisely to motion close to the separatrix. We consider particle motion in the plane of fast variables (z, p_z) for the system described by Hamiltonian (15). A slow change in $\kappa_{\mathrm{bif}}x$ leads to a change in the energy of fast motion, h_z, and, as a result, to the crossing of the separatrix.

Let a particle be primarily outside the region bounded by the separatrix (the external region) (Fig. 49). Owing to a decrease in the energy h_z, the particle approaches the separatrix and at an instant t^* crosses it. Then the particle leaves the separatrix and enters one of the two loops (an internal region). This motion can be represented as a sequence of turns of the particle in the (z, p_z) plane. In the external region, the particle covers the distance between successive crossings of the $z = 0$ axis in a half-period. We choose a point on the $z = 0$ plane as the initial point for counting these half-turns. In the case of a particle moving inside the internal region, we assume the starting point for counting turns to be a point on the $p_z = 0$ axis close to the saddle point, and we count the numbers of complete turns. The values of slow variables are assumed to be equal to their values at the initial turn (half-turn) points and are marked by the respective period (half-period) number n. The first turn in the internal region corresponds to $n = -1$, and all the turns in this region have negative numbers ($n < 0$). The first half-turn in the external region corresponds to $n = N$. In the external region,

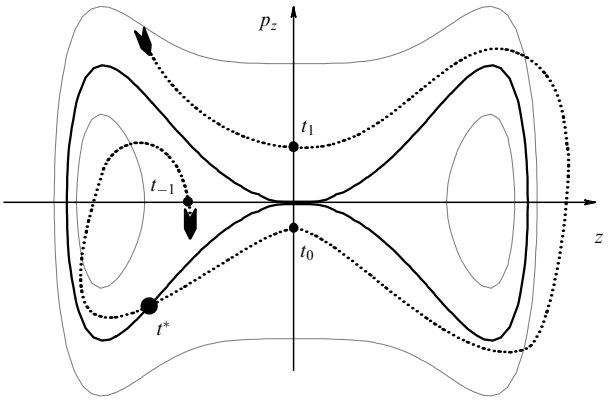

Figure 49. Schematic image of trajectory in the (z, p_z) plane.

the number of half-turns therefore varies from $n = N$ to $n = 0$, and in the internal region, from $n = -1$ to $n = -N$.

We introduce the variable

$$h = h_z - \frac{(\kappa_{\mathrm{bif}}x)^2}{2} = H - \frac{p_x^2 + (\kappa_{\mathrm{bif}}x)^2}{2}$$

on the separatrix $h = 0$. The quantity h^* corresponds to the value of h at the initial point of the half-period during which the particle crosses the separatrix (the number of this half-period $n = 0$). We set $h_n = h^* + n\kappa_{\mathrm{bif}}\Theta$, where $\Theta = \{S, h_c\}$ and $h_c = p_x^2/2 + (\kappa_{\mathrm{bif}}x)^2/2$ is the value of H at the saddle point ($\Theta = \{S,\ h_c\}$ is the rate at which the area bounded by the separatrix changes, $\{\ldots,\ldots\}$ are Poisson brackets, and $\kappa_{\mathrm{bif}}\Theta$ is the change in h along the trajectory during one turn (half-turn) near the separatrix). We calculate Θ for the values of the $\kappa_{\mathrm{bif}}x$ and p_x corresponding to the crossing of the separatrix. During motion of a particle in the external region, h decreases and the $(n+1)$th turn precedes the nth turn (in the internal region $h < 0$ and $|h|$ increases). We consider $h^*/(\kappa_{\mathrm{bif}}\Theta) \in [k, 1-k]$, where $k > 0$ is a small arbitrary positive constant (i.e., k does not depend on κ_{bif}).

To find the change in the quasiadiabatic invariant during one half-turn (complete turn), we use the relation $2\pi\partial I_z/\partial h_z = T$, where T is the period of nonperturbed motion in the plane of fast variables (for which $\kappa_{\mathrm{bif}}x = \mathrm{const}$) in the inner region (or half-period in the case of motion in the external region). Here, we use the asymptotic expansion of T and I_z. The change of the invariant I_z during a single half-turn (turn) with the number n is related to a change in the period T and of the area S bounded by the separatrix:

$$\begin{aligned} S_{n+1} - S_n &\approx \Theta(\tau_{n+1} - \tau_n), \\ \tau_{n+1} &\approx \tau_n - \frac{1}{2}\,\kappa_{\mathrm{bif}}\left(T_{n+1} + T_n\right). \end{aligned} \tag{51}$$

Here, $T_n = T_n(h_n, \kappa_{\mathrm{bif}}x)$, with the value of $\kappa_{\mathrm{bif}}x$ taken at the instant of separatrix crossing. We drop the second argument $\kappa_{\mathrm{bif}}x$ in expressions for the period in what follows to simplify writing the formulas. We use the notation $\tau = \kappa_{\mathrm{bif}}t$ for the slow time. The equation $2\pi\partial I_z/\partial h_z = T$ leads to the relation $2\pi I_z = S + \int_0^h T(h')\,\mathrm{d}h'$. Hence,

$$2\pi(I_{z,n+1} - I_{z,n}) = (S_{n+1} - S_n) + \int_{h_n}^{h_{n+1}} T(h')\,\mathrm{d}h'. \tag{52}$$

Substituting (51) in Eqn (52), we obtain

$$2\pi(I_{z,n+1}-I_{z,n})\approx\int_{h_n}^{h_{n+1}}T(h')\,\mathrm{d}h'-\Theta\kappa_{\mathrm{bif}}\,\frac{1}{2}\,(T_{n+1}+T_n)\,. \tag{53}$$

The change in I_z during a single half-turn (turn) is determined by the difference between the integral $\int_{h_n}^{h_{n+1}}T(h')\,\mathrm{d}h'$ and its approximation $(1/2)\,\Theta\kappa_{\mathrm{bif}}(T_{n+1}+T_n)$. The calculation of the jump ΔI_z therefore reduces to the problem of asymptotic calculation of the difference between the area bounded by the curve T and the approximation of this area by a trapezoid with a step $\Theta\kappa_{\mathrm{bif}}$.

To calculate ΔI_z, we must sum the changes in I_z during all the half-turns in the external region and all the turns in the internal region. We use the expansion of the Hamiltonian close to the saddle point to obtain an approximate expression for the period T.

In the vicinity of the saddle point, motion of a particle slows down and the period of oscillations in the plane of fast variables approximately corresponds to the time required for covering a small distance in the immediate vicinity of the saddle point. To calculate this time, we consider motion close to $z=0$ and neglect the term $\sim z^8$ in the expansion of h: $4h\approx 2p_z^2-\kappa_{\mathrm{bif}}\,xz^4$. The half-period of rotation in the external region $T_{\mathrm{out}}=\int\mathrm{d}z/p_z$ can be calculated as

$$\begin{aligned}T_{\mathrm{out}}(h,\kappa_{\mathrm{bif}}\,x)&\approx\sqrt{2}\int_{-d_z}^{d_z}\frac{\mathrm{d}z}{\sqrt{4h+\kappa_{\mathrm{bif}}\,xz^4}}\\&\approx\frac{\sqrt{2}}{\sqrt{4h}(\kappa_{\mathrm{bif}}\,x/4h)^{1/4}}\int_{-\infty}^{\infty}\frac{\mathrm{d}\alpha}{\sqrt{1+\alpha^4}}\\&=(2h\kappa_{\mathrm{bif}}\,x)^{-1/4}\,2^{-3/4}\,B\!\left(\frac{1}{4}\,,\,\frac{1}{4}\right).\end{aligned} \tag{54}$$

Here, d_z is a positive number, $d_z/h^{1/4}\to\infty$ as $h\to 0$. We introduce the notation $c_{\mathrm{out}}=2^{-3/4}B(1/4,1/4)$.

The period of rotation in the internal region $T_{\mathrm{in}}=\int\mathrm{d}p_z/\dot{p}_z$ can be found as

$$\begin{aligned}T_{\mathrm{in}}(h,\kappa x)&\approx\frac{1}{(\kappa_{\mathrm{bif}}\,x)^{1/4}}\int_{-d_p}^{+d_p}\frac{\mathrm{d}p_z}{\left(2p_z^2+4|h|\right)^{3/4}}\\&\approx\frac{1}{2\left(|h|\kappa_{\mathrm{bif}}\,x\right)^{1/4}}\int_{-\infty}^{+\infty}\frac{\mathrm{d}\alpha}{(\alpha^2+1)^{3/4}}\\&=\left(2|h|\kappa_{\mathrm{bif}}\,x\right)^{-1/4}2^{-5/4}\,B\!\left(\frac{1}{4},\,\frac{1}{4}\right).\end{aligned} \tag{55}$$

Here, d_p is a positive number, $d_p/h^{1/2}\to\infty$ as $h\to 0$. Thus, $T_{\mathrm{in}}=c_{\mathrm{in}}(2|h|\kappa_{\mathrm{bif}}\,x)^{-1/4}$, where $c_{\mathrm{in}}=c_{\mathrm{out}}/\sqrt{2}$.

We now consider three successive stages in the motion of a particle: approaching the separatrix, crossing the separatrix, and moving away from the separatrix. We let I_* and I_{*-1} denote the respective values of the invariant I_z on the $z=0$ axis during the last half-turn before crossing the separatrix and on the $p_z=0$ axis during the first turn after crossing the separatrix: $I_*=I_{z,0}$ and $I_{*-1}=I_{z,-1}$.

We first consider the approach of a particle to the separatrix (the energy h decreases). Substituting (54) in Eqn (53), we obtain

$$\begin{aligned}2\pi(I_{z,n+1}-I_{z,n})\approx{}&\frac{c_{\mathrm{out}}}{(2\kappa_{\mathrm{bif}}\,x)^{1/4}}\int_{h_n}^{h_{n+1}}\frac{\mathrm{d}h}{h^{1/4}}\\&-\Theta\kappa_{\mathrm{bif}}\,\frac{1}{2}(T_{n+1}+T_n)\,.\end{aligned} \tag{56}$$

We use the relation $2\pi(I_{z,N}-I_*)=\sum_{n=0}^{N-1}2\pi(I_{z,n+1}-I_{z,n})$ and Eqn (51):

$$\begin{aligned}2\pi(I_{z,N}-I_{z,*})\approx{}&-\frac{1}{2}\,\kappa_{\mathrm{bif}}\,\Theta\sum_{n=0}^{N-1}(T_{n+1}+T_n)\\&+(2\kappa_{\mathrm{bif}}\,x)^{-1/4}c_{\mathrm{out}}\,\frac{4}{3}\,(h_N^{3/4}-h^{*3/4})\,.\end{aligned} \tag{57}$$

To find the total change in I_z before the separatrix is crossed, we introduce the variable $\xi=h^*/(\kappa_{\mathrm{bif}}\,\Theta)$. In accordance with this definition, $\xi\in[k,1-k]$. Taking (51) into account, we rewrite Eqn (57) as

$$\begin{aligned}\frac{2\pi(I_{z,N}-I_*)}{(2\kappa_{\mathrm{bif}}\,x)^{-1/4}\,c_{\mathrm{out}}(\kappa_{\mathrm{bif}}\,\Theta)^{3/4}}\approx{}&-\sum_{n=0}^{N}(\xi+n)^{-1/4}\\&+\frac{4}{3}\left[(\xi+N)^{3/4}-\xi^{3/4}\right]+\frac{1}{2}\left[(\xi+N)^{-1/4}+\xi^{-1/4}\right].\end{aligned} \tag{58}$$

We now consider a half-turn with a crossing of the separatrix. At the beginning of this half-turn, the energy of the particle is $h^*=\xi\kappa_{\mathrm{bif}}\,\Theta$, and by the end of the turn, $h_{-1}=h^*-\kappa_{\mathrm{bif}}\,\Theta=(\xi-1)\,\kappa_{\mathrm{bif}}\,\Theta$. The change in the invariant I_z during this half-turn can be found as

$$\begin{aligned}\frac{2\pi(I_*-I_{*-1})}{(2\kappa_{\mathrm{bif}}\,x)^{-1/4}(\kappa_{\mathrm{bif}}\,\Theta)^{3/4}}\approx{}&-\frac{1}{2}\left(c_{\mathrm{out}}|\xi|^{-1/4}+c_{\mathrm{in}}|\xi-1|^{-1/4}\right)\\&+\frac{4}{3}\left(c_{\mathrm{in}}|\xi-1|^{3/4}+c_{\mathrm{out}}|\xi|^{3/4}\right).\end{aligned} \tag{59}$$

The change in the adiabatic invariant at the third stage can be written as

$$\begin{aligned}\frac{2\pi(I_{*-1}-I_{z,-N})}{(2\kappa_{\mathrm{bif}}\,x)^{-1/4}c_{\mathrm{in}}(\kappa_{\mathrm{bif}}\,\Theta)^{3/4}}\approx{}&-\sum_{n=-1}^{-N}|\xi+n|^{-1/4}\\&+\frac{4}{3}\left(|\xi-N|^{3/4}-|\xi-1|^{3/4}\right)\\&+\frac{1}{2}\left(|\xi-N|^{-1/4}+|\xi-1|^{-1/4}\right).\end{aligned} \tag{60}$$

In Eqn (60), we use the fact that the particle starts its motion in the internal region, having the energy $h_{-1}=(\xi-1)\,\kappa_{\mathrm{bif}}\,\Theta$.

The jump $\Delta I_z=I_{z,-N}-I_{z,N}$ can be represented as the sum of expressions (58)–(60):

$$\begin{aligned}\frac{2\pi\Delta I_z}{(2\kappa_{\mathrm{bif}}\,x)^{-1/4}(\kappa_{\mathrm{bif}}\,\Theta)^{3/4}}\approx{}&c_{\mathrm{out}}\sum_{n=0}^{N}|\xi+n|^{-1/4}\\&+c_{\mathrm{in}}\sum_{n=-1}^{-N}|\xi+n|^{-1/4}\\&-\frac{4}{3}\left(c_{\mathrm{out}}|\xi+N|^{3/4}+c_{\mathrm{in}}|\xi-N|^{3/4}\right)\\&-\frac{1}{2}\left(c_{\mathrm{out}}|\xi+N|^{-1/4}+c_{\mathrm{in}}|\xi-N|^{-1/4}\right).\end{aligned} \tag{61}$$

Therefore, the jump in the quasiadiabatic invariant takes the form

$$2\pi\Delta I_z\approx-(2\kappa_{\mathrm{bif}}\,x)^{-1/4}c_{\mathrm{out}}(\kappa_{\mathrm{bif}}\,\Theta)^{3/4}\,g(\xi)\,, \tag{62}$$

where the function $g(\xi)$ is defined as

$$g(\xi) = \lim_{N\to\infty}\Bigg[-\sum_{n=0}^{N}|\xi+n|^{-1/4} - \frac{1}{\sqrt{2}}\sum_{n=-1}^{-N}|\xi+n|^{-1/4} + \frac{4}{3}\left(\frac{1}{\sqrt{2}}\,|\xi-N|^{3/4}+|\xi+N|^{3/4}\right) + \frac{1}{2}\left(|\xi+N|^{-1/4}+\frac{1}{\sqrt{2}}\,|\xi-N|^{-1/4}\right)\Bigg]. \quad (63)$$

Expression (63) can be represented in integral form (see Ref. [84]):

$$g(\xi) = \frac{1}{\Gamma(1/4)}\int_0^\infty \left\{\frac{1+1/\sqrt{2}}{t} - \frac{\exp(-\xi t)+(1/\sqrt{2})\exp\left[-(1-\xi)\,t\right]}{1-\exp(-t)}\right\}\frac{\mathrm{d}t}{t^{3/4}}\,. \quad (64)$$

To calculate $\Theta = \{S, h_\mathrm{c}\} = (\partial S/\partial\kappa_\mathrm{bif}\,x)(\partial h_\mathrm{c}/\partial p_x)$, we use the expression

$$\frac{\partial S}{\partial\kappa_\mathrm{bif}\,x} = -\oint\frac{\partial(H-h_\mathrm{c})}{\partial\kappa x}\,\mathrm{d}t = -\frac{1}{2}\oint\frac{\partial}{\partial\kappa_\mathrm{bif}\,x}\left[p_z^2+\left(\kappa_\mathrm{bif}\,x-\frac{1}{4}\,z^4\right)^2-(\kappa_\mathrm{bif}\,x)^2\right]\mathrm{d}t = \frac{1}{4}\oint z^4\,\mathrm{d}t\,. \quad (65)$$

Replacing the integration over time by integration over the coordinate, we obtain $\partial S/\partial\kappa_\mathrm{bif}\,x = (\kappa_\mathrm{bif}\,x)^{1/4}c_2$, where $c_2 = 2^{-1/4}\,B(1/2, 3/4)$. The final expression is $\Theta = (\kappa_\mathrm{bif}\,x)^{1/4}p_x c_2$, and from Eqn (62), we find

$$2\pi\Delta I_z \approx -\kappa_\mathrm{bif}^{3/4}\,\frac{p_x^{3/4}}{(\kappa_\mathrm{bif}\,x)^{1/16}}\,\tilde{c}g(\xi)\,, \quad (66)$$

where $\tilde{c} = c_\mathrm{out}c_2^{3/4}/2^{1/4} = \pi^{5/8}2^{11/16}\sqrt{\Gamma(1/4)} \approx 6.27144 \approx 1.996\pi$, and the values of $\kappa_\mathrm{bif}\,x$ and p_x are determined at the separatrix crossing instant.

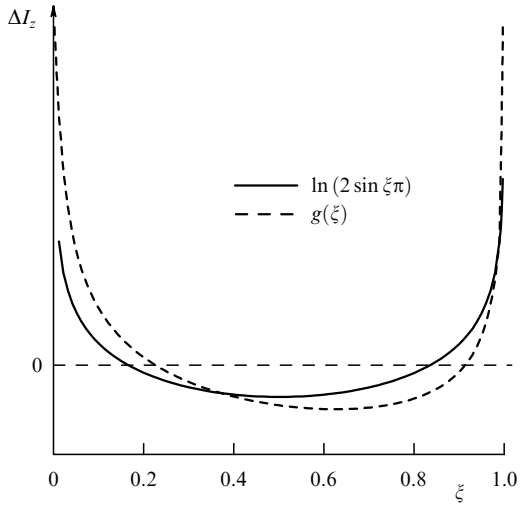

Figure 50. Dependence of the jump of the quasiadiabatic invariant on ξ for a system with a non-degenerate singular point (solid curve) and a system with a degenerate singular point (dashed curve).

The comparison of the function $g(\xi)$ with $\ln(2\sin\pi\xi)$, corresponding to a dependence of jumps of the quasiadiabatic invariant on ξ in the system with a nondegenerate singular point, is presented in Fig. 50. As seen from the figure, the function $g(\xi)$ is not symmetric with respect to $\xi = 1/2$. However, it can be noted that, as in the case of a nondegenerate singular point, the mean jump of quasiadiabatic invariant (66) is precisely equal to zero: $\langle\Delta I_z\rangle_\xi = 0$ (see Ref. [84]).

References

1. Ehrenfest P *Collected Scientific Papers* (Amsterdam: Interscience Publ., 1959)
2. Ehrenfest P *Otnositel'nost'. Kvanty. Statistika* (Relativity. Quanta. Statistics) (Moscow: Nauka, 1972)
3. Landau L D, Lifshitz E M *Mechanics* (Oxford: Pergamon Press, 1976) [Translated from Russian: *Mekhanika* (Moscow: Nauka, 1988)]
4. Størmer C *The Polar Aurora* (Oxford: Clarendon Press, 1955)
5. Alfvén H *Kungl. Svenska Vetenskapsakad. Handlingar Ser. 3* **18** (3) (1939)
6. Alfvén H, Fälthammar C-G *Cosmical Electrodynamics. Fundamental Principles* (Oxford: Clarendon Press, 1963)
7. Fälthammar C-G *Phys. Chem. Earth* **22** 599 (1997)
8. Bogoliubov N N, Zubarev D N *Ukr. Mat. Zh.* **7** 5 (1955)
9. Bogoliubov N N, Mitropolsky Y A *Asymptotic Methods in the Theory of Non-linear Oscillations* (New York: Gordon and Breach Sci. Publ., 1961) [Translated from Russian: *Asimptoticheskie Metody v Teorii Nelineinykh Kolebanii* (Moscow: Gostekhizdat, 1955)]
10. Van Allen J A, Frank L A *Nature* **183** 430 (1959)
11. Vernov S N et al. *Sov. Phys. Dokl.* **4** 154 (1959) [*Dokl. Akad. Nauk SSSR* **124** 1022 (1959)]
12. Sivukhin D V, in *Reviews of Plasma Physics* Vol. 1 (Ed. M A Leontovich) (New York: Consultants Bureau, 1965) p. 1 [Translated from Russian: *Voprosy Teorii Plazmy* Vol. 1 (Ed. M A Leontovich) (Moscow: Gosatomizdat, 1963) p. 7]
13. Northrop T G *The Adiabatic Motion of Charged Particles* (New York: Interscience Publ., 1963)
14. Chirikov B V *Sov. J. Plasma Phys.* **4** 289 (1978) [*Fiz. Plazmy* **4** 521 (1978)]
15. Zaslavskii G M, Chirikov B V *Sov. Phys. Usp.* **14** 549 (1972) [*Usp. Fiz. Nauk* **105** 3 (1971)]
16. Cary J R, Brizard A J *Rev. Mod. Phys.* **81** 693 (2009)
17. Ness N F *J. Geophys. Res.* **70** 2989 (1965)
18. Frank A G *Proc. (Trudy) Lebedev Phys. Inst.* **74** 107 (1976) [*Tr. Fiz. Inst. Akad. Nauk* **74** 108 (1974)]
19. Frank A G *Phys. Usp.* **53** 941 (2010) [*Usp. Fiz. Nauk* **180** 982 (2010)]
20. Frank A G, Bugrov S G, Markov V S *Phys. Plasmas* **15** 092102 (2008)
21. Yamada M, Kulsrud R, Ji H *Rev. Mod. Phys.* **82** 603 (2010)
22. Zelenyi L M et al. *Plasma Phys. Rep.* **37** 118 (2011) [*Fiz. Plazmy* **37** 137 (2011)]
23. Zelenyi L M, Veselovskii I S (Eds) *Plazmennaya Geliogeofizika* (Plasma Heliogeophysics) (Moscow: Fizmatlit, 2008)
24. Kirii N P et al. *Tr. Fiz. Inst. Akad. Nauk* **110** 121 (1979)
25. Zelenyi L M, in *Dinamika Plazmy i Magnitnykh Polei v Khvoste Magnitosfery Zemli* (Plasma and Magnetic Field Dynamics in the Tail of the Earth's Magnetosphere) (Itogi Nauki i Tekhniki, Ser. Issledovaniya Kosmicheskogo Prostranstva (Results of Science and Technology. Ser. Studies of Outer Space), Vol. 24) (Moscow: VINITI, 1986)
26. Artemyev A V et al. *Ann. Geophys.* **26** 2749 (2008)
27. Artemyev A V et al. *J. Geophys. Res.* **116** A09233 (2011)
28. Petrukovich A A et al. *J. Geophys. Res.* **112** A10213 (2007)
29. Petrukovich A A *J. Geophys. Res.* **116** A07217 (2011)
30. Artemyev A V et al. *J. Geophys. Res.* **115** A12255 (2010)
31. Petrukovich A A et al. *J. Geophys. Res.* **116** A00I25 (2011)
32. Büchner J *Geophys. Res. Lett.* **18** 1595 (1991)
33. Speiser T W *J. Geophys. Res.* **70** 4219 (1965)
34. Speiser T W *J. Geophys. Res.* **72** 3919 (1967)
35. Orazberdyev Kh, Trakhtengerts V Yu *Radiophys. Quantum Electron.* **16** 21 (1973) [*Izv. Vyssh. Uchebn. Zaved. Radiofiz.* **16** 30 (1973)]

36. Gray P C, Lee L C *J. Geophys. Res.* **87** 7445 (1982)
37. Alekseyev I I, Kropotkin A P *Geomagn. Aeronom.* **10** 615 (1971) [*Geomagn. Aeronom.* **10** 777 (1970)]
38. Harris E G *Nuovo Cimento* **23** 115 (1962)
39. Chen J, Palmadesso P J *J. Geophys. Res.* **91** 1499 (1986)
40. Sonnerup B U Ö *J. Geophys. Res.* **76** 8211 (1971)
41. Schindler K *J. Math. Phys.* **6** 313 (1965)
42. Arnold V I, Kozlov V V, Neishtadt A I *Mathematical Aspects of Classical and Celestial Mechanics* (Berlin: Springer, 2006) [Translated from Russian: *Matematicheskie Aspekty Klassicheskoi i Nebesnoi Mekhaniki* (Moscow: URSS, 2002)]
43. Büchner J, Zeleny L M *Phys. Lett. A* **118** 395 (1986)
44. Neishtadt A I *Sov. J. Plasma Phys.* **12** 568 (1986) [*Fiz. Plazmy* **12** 992 (1986)]
45. Büchner J, Zelenyi L M *J. Geophys. Res.* **94** 11821 (1989)
46. Zelenyi L M, Malova H V, Popov V Yu *JETP Lett.* **78** 296 (2003) [*Pis'ma Zh. Eksp. Teor. Fiz.* **78** 742 (2003)]
47. Zelenyi L M et al. *Adv. Space Res.* **30** 1629 (2002)
48. Prudnikov A P, Brychkov Yu A, Marichev O I *Integrals and Series* Vol. 1 *Elementary Functions* (New York: Gordon and Breach Sci. Publ., 1986) [Translated from Russian: *Integraly i Ryady* Vol. 1 *Elementarnye Funktsii* (Moscow: Nauka, 1981)]
49. Bykov A A, Zelenyi L M, Malova Kh V *Plasma Phys. Rep.* **34** 128 (2008) [*Fiz. Plazmy* **34** 148 (2008)]
50. Zelenyi L M et al. *Geophys. Res. Lett.* **29** 1608 (2002)
51. Chen J, Burkhart G R, Huang C Y *Geophys. Res. Lett.* **17** 2237 (1990)
52. Zelenyi L M et al. *JETP Lett.* **85** 225 (2007) [*Pis'ma Zh. Eksp. Teor. Fiz.* **85** 187 (2007)]
53. Birn J *J. Geophys. Res.* **84** 5143 (1979)
54. Burkhart G R, Chen J *J. Geophys. Res.* **96** 14033 (1991)
55. Neishtadt A, Vasiliev A *Nonlinearity* **18** 1393 (2005)
56. Neishtadt A et al. *Discrete Contin. Dyn. Syst. B* **10** 621 (2008)
57. Mihalov J D, Sonett C P *J. Geophys. Res.* **73** 6837 (1968)
58. Zelenyi L M et al. *Phys. Usp.* **53** 933 (2010) [*Usp. Fiz. Nauk* **180** 973 (2010)]
59. Galeev A A, Zelenyi L M *JETP Lett.* **22** 170 (1975) [*Pis'ma Zh. Eksp. Teor. Fiz.* **22** 360 (1975)]
60. Coppi B, Laval G, Pellat R *Phys. Rev. Lett.* **16** 1207 (1966)
61. Schindler K *J. Geophys. Res.* **79** 2803 (1974)
62. Zelenyi L M et al. *J. Atm. Solar-Terr. Phys.* **70** 325 (2008)
63. Hoshino M et al. *J. Geophys. Res.* **101** (A11) 24775 (1996)
64. Runov A et al. *Geophys. Res. Lett.* **30** 1036 (2003)
65. Israelevich P L, Ershkovich A I, Oran R *Planet. Space Sci.* **55** 2261 (2007)
66. Gosling J T, Szabo A *J. Geophys. Res.* **113** A10103 (2008)
67. Mingalev O V et al. *Plasma Phys. Rep.* **38** 300 (2012) [*Fiz. Plazmy* **38** 329 (2012)]
68. Artemyev A V *Phys. Plasmas* **18** 022104 (2011)
69. Berchem J, Russell C T *J. Geophys. Res.* **87** 8139 (1982)
70. Panov E V et al. *J. Geophys. Res.* **113** A01220 (2008)
71. Panov E V et al. *J. Geophys. Res.* **116** A12204 (2011)
72. Artemyev A V, Neishtadt A I, Zelenyi L M *Nonlin. Process. Geophys.* **20** 163 (2013)
73. Zwingmann W *J. Geophys. Res.* **88** 9101 (1983)
74. Lembege B, Pellat R *Phys. Fluids* **25** 1995 (1982)
75. Burkhart G R, Chen J *J. Geophys. Res.* **98** (A1) 89 (1993)
76. Karimabadi H, Pritchett P L, Coroniti F V *J. Geophys. Res.* **95** 17153 (1990)
77. Vainshtein D L, Zelenyi L M, Neishtadt A I *Plasma Phys. Rep.* **21** 457 (1995) [*Fiz. Plazmy* **21** 484 (1995)]
78. Vainchtein D L et al. *Nonlin. Process. Geophys.* **12** 101 (2005)
79. Birn J, Sommer R R, Schindler K *J. Geophys. Res.* **82** 147 (1977)
80. Cowley S W H *Planet. Space Sci.* **26** 1037 (1978)
81. Lemaire J, Burlaga L F *Astrophys. Space Sci.* **45** 303 (1976)
82. Vainshtein D L, Zelenyi L M, Neishtadt A I *Plasma Phys. Rep.* **22** 943 (1996) [*Fiz. Plazmy* **22** 1039 (1996)]
83. Burkhart G R et al. *Geophys. Res. Lett.* **18** 1591 (1991)
84. Artemyev A V, Neishtadt A I, Zelenyi L M *Chaos* **21** 043120 (2011)
85. Vasiliev A et al. *Physica D* **241** 566 (2012)
86. Delcourt D C, Malova H V, Zelenyi L M *J. Geophys. Res.* **109** A01222 (2004)
87. Delcourt D C, Malova H V, Zelenyi L M *Geophys. Res. Lett.* **33** L06106 (2006)
88. Neishtadt A, Treschev D *Ergodic Theory Dyn. Syst.* **31** 259 (2011)
89. Kaufmann R L, Lu C, Larson D J *J. Geophys. Res.* **99** 11277 (1994)
90. Neishtadt A, Vasiliev A *Chaos* **17** 043104 (2007)
91. Landau L D, Lifshitz E M *The Classical Theory of Fields* (Oxford: Pergamon Press, 1980) [Translated from Russian: *Teoriya Polya* (Moscow: Nauka, 1988)]
92. Zelennyi L M, Zogin D V, Büchner J *Kosmich. Issled.* **28** 430 (1990)
93. Zelenyi L M, Zogin D V, in *Fizika Kosmicheskoi Plazmy. Mezhdunar. Seminar, Kiev, 6 – 10 Iyunya 1993* (Physics of Cosmic Plasma. Intern. Seminar, Kiev, 6 – 10 June 1993) (Kiev, 1993) p. 1
94. Angelopoulos V et al. *Geophys. Res. Lett.* **20** 1711 (1993)
95. Tverskoy B A *Rev. Geophys. Space Phys.* **7** 219 (1969)
96. Cowley S W H, Shull P (Jr.) *Planet. Space Sci.* **31** 235 (1983)
97. Lyons L R, Speiser T W *J. Geophys. Res.* **87** 2276 (1982)
98. Shabanskii V P *Yavleniya v Okolozemnom Prostranstve* (Phenomena in Near-Earth Space) (Moscow: Nauka, 1972)
99. Ashour-Abdalla M et al. *J. Geophys. Res.* **98** (A4) 5651 (1993)
100. Ashour-Abdalla M et al. *J. Geophys. Res.* **100** (A10) 19191 (1995)
101. Dolgonosov M S et al. *Cosmic Res.* **45** 535 (2007) [*Kosmich. Issled.* **45** 564 (2007)]
102. Eastman T E et al. *J. Geophys. Res.* **89** 1553 (1984)
103. Grigorenko E E, Sauvaud J-A, Zelenyi L M *J. Geophys. Res.* **112** A05218 (2007)
104. Grigorenko E E et al. *Space Sci. Rev.* **164** 133 (2011)
105. Keiling A et al. *Geophys. Res. Lett.* **31** L12804 (2004)
106. Ashour-Abdalla M et al. *J. Geophys. Res.* **110** A12221 (2005)
107. Ashour-Abdalla M et al. *Geophys. Res. Lett.* **19** 617 (1992)
108. Zelenyi L M et al. *Geophys. Res. Lett.* **33** L18103 (2006)
109. Dolgonosov M S, Zimbardo G, Greco A *J. Geophys. Res.* **115** A02209 (2010)
110. Bulanov S V, Sasorov P V *Sov. Astron.* **19** 464 (1976) [*Astron. Zh.* **52** 763 (1975)]
111. Birn J et al. *Space Sci. Rev.* **173** 49 (2012)
112. Galeev A A *Space Sci. Rev.* **23** 411 (1979)
113. Litvinenko Y E *Astron. Astrophys.* **452** 1069 (2006)
114. Vekstein G E, Priest E R *Phys. Plasmas* **2** 3169 (1995)
115. Bulanov S V *Sov. Astron. Lett.* **6** 206 (1980) [*Pis'ma Astron. Zh.* **6** 372 (1980)]
116. Browning P K, Vekstein G E *J. Geophys. Res.* **106** (A9) 18677 (2001)
117. Browning P K et al. *Astron. Astrophys.* **520** A105 (2010)
118. Burkhart G R, Drake J F, Chen J *J. Geophys. Res.* **95** 18833 (1990)
119. Divin A et al. *Phys. Plasmas* **17** 122102 (2010)
120. Zelenyi L M et al. *Planet. Space Sci.* **32** 313 (1984)
121. Zelenyi L M, Lominadze J G, Taktakishvili A L *J. Geophys. Res.* **95** 3883 (1990)
122. Ashour-Abdalla M, Büchner J, Zelenyi L M *J. Geophys. Res.* **96** 1601 (1991)
123. Burkhart G R et al. *J. Geophys. Res.* **97** (A9) 13799 (1992)
124. Hamilton J E M, Eastwood J W *Planet. Space Sci.* **30** 293 (1982)
125. Sitnov M I et al. *J. Geophys. Res.* **105** (A6) 13029 (2000)
126. Zelenyi L M et al. *Nonlin. Process. Geophys.* **7** 127 (2000)
127. Kropotkin A P, Malova H V, Sitnov M I *J. Geophys. Res.* **102** (A10) 22099 (1997)
128. Ball B M et al. *J. Geophys. Res.* **110** A04208 (2005)
129. Zhou X-Z et al. *J. Geophys. Res.* **114** A03223 (2009)
130. Ashour-Abdalla M et al. *J. Geophys. Res.* **101** (A2) 2587 (1996)
131. Dubinin E et al., in *Proc. of the 3rd Intern. Conf. on Substorms, ICS-3, Versailles, France, 12 – 17 May 1996* (ESA Special Publ., Vol. 389, Eds E J Rolfe, B Kaldeich) (Paris: European Space Agency Publ. Division, 1996) p. 533
132. Grigorenko E E et al. *Planet. Space Sci.* **53** 245 (2005)
133. Zelenyi L M et al., in *Magnetospheric Research with Advanced Techniques. Proc. of the 9th COSPAR Colloquium, Beijing, China, 15 – 19 April, 1996* (COSPAR Colloquia Ser., Vol. 9, Eds R L Xu, A T Y Lui) (Amsterdam: Elsevier, 1998) p. 125
134. Lyons L R *J. Geophys. Res.* **89** 5479 (1984)
135. Ashour-Abdalla M et al. *J. Geophys. Res.* **99** (A8) 14891 (1994)
136. Fadeev V M, Kvabtskhava I F, Komarov N N *Nucl. Fusion* **5** 202 (1965)
137. Morozov A I, Solov'ev L S *Sov. Phys. JETP* **13** 927 (1961) [*Zh. Eksp. Teor. Fiz.* **40** 1316 (1961)]

138. Kan J R *J. Geophys. Res.* **78** 3773 (1973)
139. Schindler K, Birn J *J. Geophys. Res.* **107** (A8) 1193 (2002)
140. Yeh T *J. Plasma Phys.* **10** 237 (1973)
141. Balikhin M, Gedalin M *J. Plasma Phys.* **74** 749 (2008)
142. Montagna C, Pegoraro F *Commun. Nonlin. Sci. Num. Simulat.* **13** 147 (2008)
143. Roth M, de Keyser J, Kuznetsova M M *Space Sci. Rev.* **76** 251 (1996)
144. Schindler K *Physics of Space Plasma Activity* (Cambridge: Cambridge Univ. Press, 2007)
145. Yoon P H, Lui A T Y *J. Geophys. Res.* **110** A01202 (2005)
146. Kropotkin A P, Domrin V I *J. Geophys. Res.* **101** (A9) 19893 (1996)
147. Sitnov M I et al. *J. Geophys. Res.* **111** A08204 (2006)
148. Zelenyi L M et al. *Nonlin. Process. Geophys.* **11** 579 (2004)
149. Galeev A A, Coroniti F V, Ashour-Abdalla M *Geophys. Res. Lett.* **5** 707 (1978)
150. Angelopoulos V et al. *Science* **321** 931 (2008)
151. Baker D N et al. *J. Geophys. Res.* **101** (A6) 12975 (1996)
152. Artemyev A V et al. *Ann. Geophys.* **27** 4075 (2009)
153. Runov A et al. *Ann. Geophys.* **24** 247 (2006)
154. De Hoffmann F, Teller E *Phys. Rev.* **80** 692 (1950)
155. Zelenyi L M et al. *Cosmic Res.* **40** 357 (2002) [*Kosmich. Issled.* **40** 385 (2002)]
156. Frank-Kamenetskii D A *Lektsii po Fizike Plazmy* (Lectures in Plasma Physics) (Moscow: Atomizdat, 1968)
157. Zelenyi L et al. *Space Sci. Rev.* **132** 593 (2007)
158. Mingalev O V et al. *Plasma Phys. Rep.* **35** 76 (2009) [*Fiz. Plazmy* **35** 85 (2009)]
159. Malova H V et al. *Geophys. Res. Lett.* **34** L16108 (2007)
160. Malova H et al., in *8th Intern. Conf. Problems of Geocosmos, St. Petersburg, September 20–24, 2010* (Ed. V Semenov) (St. Petersburg, 2010) p. 151
161. Mingalev I et al., in *7th Intern. Conf. Problems of Geocosmos, St. Petersburg, May 26–30, 2008* (Eds V N Troyan, M Hayakawa, V S Semenov) (St. Petersburg, 2008) p. 172
162. Chen J *J. Geophys. Res.* **97** (A10) 15011 (1992)
163. Zelenyi L M et al. *Geophys. Res. Lett.* **33** L05105 (2006)
164. Nakamura R et al. *Space Sci. Rev.* **122** 29 (2006)
165. Asano Y et al. *Geophys. Res. Lett.* **32** L03108 (2005)
166. Malova Kh V et al. *Plasma Phys. Rep.* **36** 841 (2010) [*Fiz. Plazmy* **36** 897 (2010)]
167. Sitnov M I, Guzdar P N, Swisdak M *Geophys. Res. Lett.* **30** 1712 (2003)
168. Sergeev V et al. *Geophys. Res. Lett.* **31** L05807 (2004)
169. Petrukovich A A et al. *Ann. Geophys.* **26** 3669 (2008)
170. Rong Z J et al. *Planet. Space Sci.* **58** 1215 (2010)
171. Artemyev A V et al. *Plasma Phys. Rep.* **34** 771 (2008) [*Fiz. Plazmy* **34** 834 (2008)]
172. Erkaev N V et al. *J. Geophys. Res.* **114** A03206 (2009)
173. Golovchanskaya I V, Maltsev Y P *Geophys. Res. Lett.* **32** L02102 (2005)
174. Zelenyi L M et al. *Ann. Geophys.* **27** 861 (2009)
175. Artemyev A V et al. *Geophys. Res. Lett.* **38** L14102 (2011)
176. Artemyev A V et al. *J. Geophys. Res.* **117** A06219 (2012)
177. Birn J, Sommer R, Schindler K *Astrophys. Space Sci.* **35** 389 (1975)
178. Nakamura R et al. *Ann. Geophys.* **27** 1743 (2009)
179. Saito M H et al. *Geophys. Res. Lett.* **37** L08106 (2010)
180. Panov E V et al. *J. Geophys. Res.* **117** A06228 (2012)
181. Panov E V et al. *Geophys. Res. Lett.* **39** L08110 (2012)
182. Peroomian V, Zelenyi L M *Space Sci. Rev.* **95** 257 (2001)
183. Peroomian V, Ashour-Abdalla M, Zelenyi L M *J. Geophys. Res.* **105** (A8) 18807 (2000)
184. Peroomian V, Zelenyi L V, Schriver D *Adv. Space Res.* **30** 2657 (2002)
185. Neishtadt A I *J. Appl. Math. Mech.* **51** 586 (1987) [*Priklad. Matem. Mekh.* **51** 750 (1987)]
186. Cary J R, Escande D F, Tennyson J L *Phys. Rev. A* **34** 4256 (1986)
187. Tennyson J L, Cary J R, Escande D F *Phys. Rev. Lett.* **56** 2117 (1986)
188. Timofeev A V *Sov. Phys. JETP* **48** 656 (1978) [*Zh. Eksp. Teor. Fiz.* **75** 1303 (1978)]
189. Wisdom J *Icarus* **63** 272 (1985)
190. Arnol'd V I *Russ. Math. Surv.* **18** (6) 85 (1963) [*Usp. Mat. Nauk* **18** (6) 91 (1963)]
191. Lifshits I M, Slutskin A A, Nabutovskii V M *Sov. Phys. JETP* **14** 669 (1962) [*Zh. Eksp. Teor. Fiz.* **41** 939 (1961)]
192. Neishtadt A I *J. Appl. Math. Mech.* **39** 594 (1975) [*Priklad. Matem. Mekh.* **39** 621 (1975)]
193. Neishtadt A I, Pivovarov M L, Preprint Pr-1128 (Moscow: Space Res. Inst., 1986)
194. Savenkov B V, Zelenyi L M, Zogin D V *Plasma Phys. Rep.* **23** 404 (1997) [*Fiz. Plazmy* **23** 436 (1997)]
195. Zelenyi L M, Savenkov B V *Plasma Phys. Rep.* **19** 712 (1993) [*Fiz. Plazmy* **19** 1355 (1993)]
196. Vainshtein D L et al. *Plasma Phys. Rep.* **25** 299 (1999) [*Fiz. Plazmy* **25** 333 (1999)]
197. Its A R, Kapaev A A *Math. USSR Izv.* **31** 193 (1988) [*Izv. Akad. Nauk SSSR. Mat.* **51** 878 (1987)]